Università di Genova

Targeting the tumor microenvironment: a click chemistry-based surface-functionalization method and a therapeutic-loading strategy for plasma- and erythrocyte-derived extracellular vesicles

PHD IN BIOTECHNOLOGIES IN TRANSLATIONAL MEDICINE

CURRICULUM: CELLULAR AND MOLECULAR BIOTECHNOLOGIES

XXXVI cycle

COORDINATOR: Prof. Paolo Malatesta

Candidate

Maria Chiara Ciferri

Supervisor

Prof. Roberta Tasso

SUMMARY

ABSTRACT

Thanks to their role in intercellular communication and their natural ability to transport functional cargoes, extracellular vesicles (EVs) have been recently considered valuable therapeutic nanocarriers. Low immunological response, intrinsic targeting potential, especially for autologous EVs, and the capability to cross various biological barriers represent some of the advantages that make EVs an optimal alternative to synthetic nanoparticles for targeted drug delivery. In this project, we developed two methods for EV-engineering based on their loading with a medicinal cargo and their surface functionalization with a fluorescent peptide targeting the extracellular matrix antigen Extra domain B fibronectin (ED-B FN). The latter represents one of the most investigated FN variants for tumor-targeting strategies since it has been demonstrated to play a key role in tumorigenesis, angiogenesis, metastasis formation, and epithelial-to-mesenchymal transition (EMT). Two different EV populations have been considered in this study as an ideal proposal for both an autologous and heterologous context: plasma-derived EVs and artificial red blood cell-derived EVs (nanoerythrosomes, NanoEs). The EV membrane functionalization strategy has been based on the "traditional" click chemistry reaction (Huisgen cycloaddition) of an alkyne, in this case tied to EV surface, and an azide, owned by the anti-ED-B FN fluorescent peptide. The achievement of functionalization, evaluated by flow cytometry analysis, revealed that about 50% of EVs are peptide-clicked. In addition, after confirming that our membrane-engineering approach didn't affect EV identity, we observed that peptide-clicked EVs were efficiently internalized by responder cells (MDA-MB 231). We developed a strategy to load Paclitaxel into nanoparticles by sonication with an efficiency of about 0.1% for plasma-EVs and 1.5% for NanoEs (HPLC-MS analysis). In addition, either loaded plasma-EVs or NanoEs showed a significant cytotoxic effect on MDA-MB 231 cells when compared with their empty counterpart (MTT assay). Copper-free click chemistry and sonication turned out to be effective approaches for EV surface functionalization and therapeutic encapsulation, respectively. The development and standardization of these protocols lay the foundation for potential applications as new innovative targeted therapies in either an allogenic or an autologous scenario. In addition, targeting a tumor microenvironment antigen such as ED-B, which is expressed in a wide range of tumor types, would allow the development of therapies potentially relevant for different oncological applications.

INTRODUCTION

1)Nanotechnologies and nanomedicine for drug delivery

The interest in nanoscience has increased rapidly after the introduction of the nanotechnology concept, in 1959, during a lecture entitled “There’s plenty of room at the bottom”, held by the American physicist and Nobel Prize laureate Richard Feynman [1]. In the last decade, the extensive application of nanotechnologies in biomedicine for both the diagnosis and therapy of human diseases has been reported by many studies [1], [2]. In particular, the value of nanotechnology in many biology-related areas (the so-called “bio-nanotechnology”) such as drug delivery and molecular imaging has been intensively studied and offered many examples of nanopharmaceutical formulations currently on the market [1].

The idea of using nanoparticles, and in particular phospholipid vesicles, to improve the functionality of the already approved drug molecules arose about 50 years ago when Gregoriadis started speaking about putting “old drugs into new clothing” [3], [4]. According to Lipinski’s rule of five, drug-like molecules tend to be water insoluble and have moderately lipophilic characteristics [5]. Consequently, poor drug solubility is considered one of the main challenges facing conventional drug-delivery systems. However, the production of particles in the nanometer scale leads to an augmented surface/volume ratio and this contribute to increase the drug dissolution rate, thus enhancing its bioavailability [6]. At the end of the 70s of the last century, the work of Forssen EA and collaborators regarding the encapsulation of anthracyclines into liposomes to reduce their cardiotoxicity represented one of the first examples of nano-drug delivery studies [3], [7], [8] which culminated, in 1995, in the commercialization of the first FDA-approved nanodrug Doxil® [9]. Over the past few decades, 100 nanomedicine applications and products have been approved for commercialization by the US FDA underlining the important role of nanotechnology in healthcare, the so-called “nanomedicine” [10]. In comparison with conventional drug-delivery systems, drug administration using nanoparticles possesses several advantages as an enhanced permeability and retention effect which can allow passive targeting and accumulation at the pathological sites [11], an increased active concentration and bioavailability [12] and an improved safety and efficacy [13]. More importantly, different ligands or targeting agents can be attached to the nanocarrier surface, in order to direct it toward specific cells or tissues based on molecular recognition strategies [14]. Indeed, if the application of conventional therapeutic agents has limitations such as non-selectivity, undesirable side effects, low efficiency, and poor biodistribution [15], a targeted strategy is able to enhance the concentration of therapeutic agent in target locations so improving its therapeutic index, efficacy and the tolerability in biological systems[16]. Due to

their ability to carry drug molecules within their core, protecting them from the surrounding environment and vice versa, phospholipid vesicles can be considered highly appropriate for the targeted delivery of drugs.

2) Natural nanoparticles for targeted drug delivery

The discovery of new chemical entities with minimum side effects and maximum clinical benefit represents one of the most important goals in pharmaceutical research. A critical challenge associated with the use of nanoparticles (NPs) for drug delivery is the difficulty in their synthesis using conventional physic-chemical methods. In addition, according to a number of reports, the chemical synthesis of NPs can be relatively expensive, and also potentially toxic reagents might be needed for the chemical synthesis [10].

Nowadays, all commercially available NP-related therapeutics are based on the use of artificial nanoparticles, especially liposomes, with about 14 liposomal products authorized by FDA and EMA [17]. However, thanks to their potential to overcome part of the above described limitations associated with synthetic ones, naturally-derived NPs have been recently considered a valid alternative [18]. Among these, extracellular vesiscles (EVs), represent powerful candidates for their natural and intrinsic role as delivery vehicles in intercellular communication, being able to transfer bioactive molecules safely and successfully to recipient cells [18]. Low immunological response [12], targeting potential [13] and ability in crossing various biological barriers [19]–[22] represent other important advantages [23]. Similarities and differences between liposomes and natural nanoparticles have been already examined [24]–[26]. One of the most discussed aspects is that EVs can present longer clearance kinetics than artificial NPs, even if it is dependent on the different cell sources, the specific protein/lipid profiles, or the employed isolation procedures [25]. Indeed, the presence of a negatively-charged surface and their ability to avoid mononuclear phagocytic systems by exhibiting the surface protein CD47 would increase their stability in circulation compared to liposomes [27]. Nevertheless, it is probably the natural organotropism and so the intrinsic targeting ability that make EVs a unique and peculiar tool for targeted drug delivery. In particular, the asymmetrical lipid distribution and specific protein composition of the membrane have been found to justify their organotropism and homing ability [23], [28]. It has been demonstrated that cancer-derived EVs show a tissue tropism also at the early stages of neoplastic transformation [29] and the transplantation of autologous EVs can be used for cancer-specific targeting [30]. Based on this evidence, biofluids, and plasma in particular, would represent an ideal source of EVs to be functionalized for autologous targeted drug delivery or diagnostic purposes. Indeed, the addition of an “acquired” homing capacity to the natural one could result in a more efficient targeting effect. In addition, thanks to their characteristics which will be deeply described later, red blood

cell-derived extracellular vesicles (RBCEVs) would represent a valid alternative also for heterologous therapeutic use [31].

3) Extracellular vesicles (EVs)

All cells are able to secrete various types of membrane vesicles, known as extracellular vesicles (EVs), and this process has been observed to be conserved throughout evolution from bacteria to humans and plants [32]–[34] as a universally shared biological property. EVs were first observed in 1946 by Chargaff and West as procoagulant platelet-derived particles in normal plasma [35], and later described by Wolf as "platelet dust" [36]. After some independent observations in human cell cultures, bovine serum, seminal plasma and detailed ultrastructural studies about their release, the discovery that EVs contain RNAs, including microRNAs, brought to a renewed scientific interest [37]–[39], which resulted, in 2011, in the foundation of the International Society for Extracellular Vesicles (ISEV). The Scientific Society aimed at bringing together scientists from all over the world, establishing a standardization of procedures for EV isolation and characterization, that led to the periodic publication of specific guidelines [40]. According to guidelines, the generic term "extracellular vesicles" has to be used to indicate all cell-derived membranous structures belonging to a highly heterogeneous group comprising exosomes (50-150nm) and microvesicles (150-500nm, up to 1μm). Both vesicle types are characterized by a different biogenesis: exosomes are intra-luminal vesicles formed by the inward budding of the endosomal membrane during the maturation of multivesicular endosomes (MVEs) (intermediates within the endosomal system) and secreted upon fusion of MVEs with the cell surface; microvesicles directly shed from the cell plasma membrane [41] (Fig. 1).

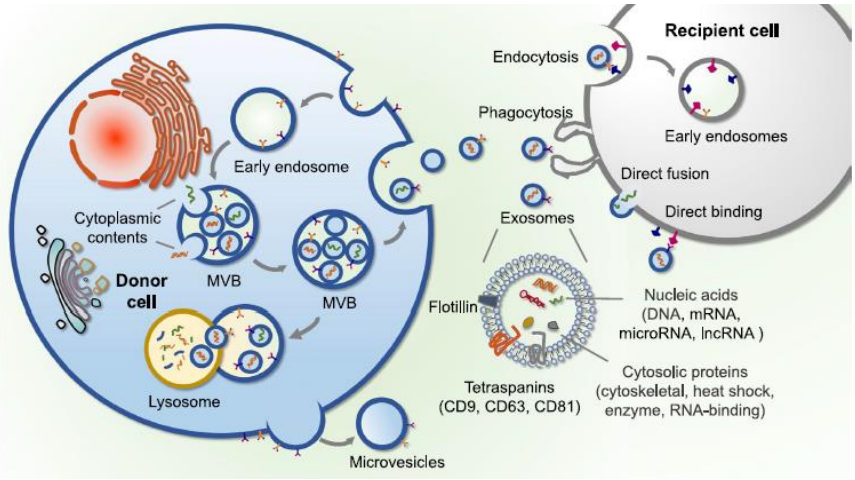

Figure 1. *Generation of exosomes and microvesicles and their interaction with a recipient cell (from: Yu D. et al. Molecular Cancer 2022, 21:56).*

Thanks to their ability to exchange components (mainly nucleic acids, lipids and proteins) between cells and to act as signaling vehicles in normal cell homeostatic as well as pathological processes [39], [42], [43], nowadays EVs are considered as more than just waste carriers.
Content, size and membrane composition of EVs are highly heterogeneous, dynamic and dependent on the cellular source, state and environmental condition. EVs contain proteins that are considered common EV-markers, that specifically reflect the vesicle localization, cellular origin and mechanism of secretion [44]–[47]. In general, EVs are highly abundant in cytoskeletal-, cytosolic-, heat shock- and plasma membrane proteins, as well as in proteins involved in their trafficking. Proteins enriched in EV sub-populations that are often used as general EV-markers include tetraspanins (CD9, CD63, CD81), major histocompatibility complex (MHC) molecules and cytosolic proteins such as specific stress proteins (heat shock proteins; HSPs), Tsg101 and the Endosomal Sorting Complex Required for Transport (ESCRT-3) binding protein Alix [39]. Overall, CD9 and CD81 belong to the top 200 most frequently identified EV proteins [39], [48].

3.1 Circulating EVs

Nowadays, EVs have been isolated and characterized from most cell types and biological fluids such as saliva, urine, nasal and bronchial lavage fluid, amniotic fluid, breast milk, plasma, serum and seminal fluid [39], [49]–[54]. Among these, blood represents an important source for EV studies not only because a blood draw is minimally invasive, but especially because EVs can be included in a liquid biopsy analysis together with other circulating components [55], [56]. Circulating EVs from patients suffering for diseases, such as cancer, can carry disease-specific molecules which gives to plasma and serum great importance in the use of EVs as biomarkers [56].
However, human plasma and serum contain a vast array of particles in addition to EVs, and especially a dominating pool of lipid particles such as chylomicrons and multiple types of lipoproteins which overlap with EVs in size or density (Fig. 2). Chylomicrons are produced after ingestion of fat-containing meals and transport lipids and cholesterol to the liver via the peripheral blood. The size of chylomicrons varies with the amount of ingested fat, ranging from 75 to 1200 nm in diameter [57]. The liver transforms the fat encapsulated in chylomicrons into very low-density lipoproteins (VLDL, 30–80 nm), which in turn can be converted into smaller types of lipoproteins (5–35 nm) such as intermediate-density lipoprotein (IDL), low-density lipoprotein (LDL), and high-density lipoprotein (HDL), for triglycerides and cholesterol transportation to and from the peripheral tissues. Lipoprotein particles are very abundant in the

circulation, and it has been observed that there are 20- to 100-fold more lipoproteins than EVs in plasma isolates [58], [59].

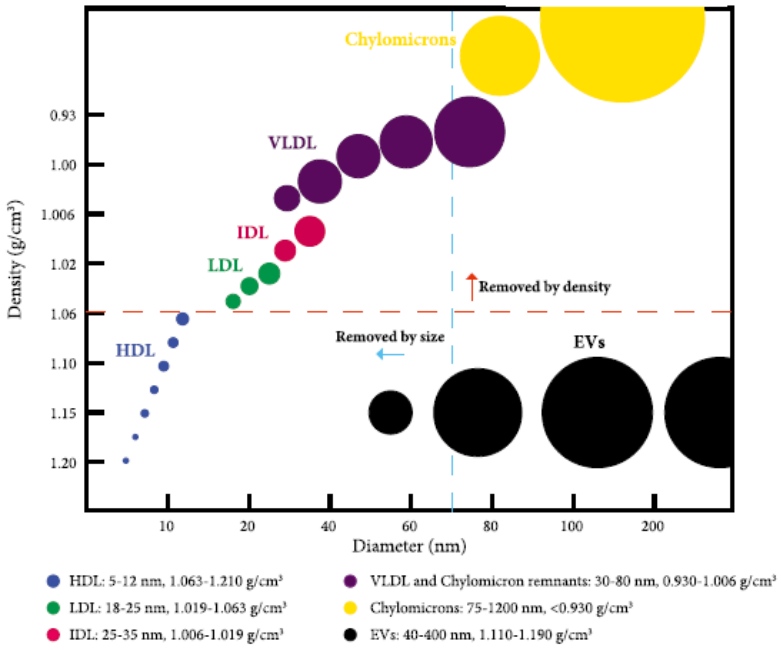

***Figure 2**. Comparison among EVs and different lipoproteins (from: Karimi N. et al., Cellular and Molecular Life Sciences 2018, 75:2873–2886).*

3.2 EV isolation and characterization methodologies

According to literature, the most employed method to isolate EVs is based on differential ultracentrifugation, which has been considered the gold standard for a long time. It is now clear that this method cannot be applied to blood EV isolation due to the complexity and heterogeneity of the starting material. Other methods have been proposed over the years, such as precipitation-, size-, affinity-, micro-, nano-, fluidic based strategies. Size exclusion chromatography (SEC) is one of the most common and used methods for the isolation of both plasma and serum EVs. Although SEC represents a fast and cheap method and allows protein, especially albumin, removal, it is ineffective in lipoprotein removal. However, the application of a iodixanol/sucrose density gradient or a sucrose cushion to the high-speed ultracentrifugation can significantly improve the purity of the EV suspension. The density (iodixanol/sucrose) gradient exploits the similarity of EV density (1.08 to 1.19 g/mL) to that of sucrose and iodixanol, which form a cushion preserving the integrity of EVs and separating high-density contaminants (1.35 g/mL). During the centrifugation, vesicles filter through the sucrose/iodixanol gradient until the point at which their density is equal to the gradient. With

the employment of the sucrose cushion, EVs are laid down on a high-density sucrose matrix with lower stress [60], [61].

According to MISEV 2018 guidelines, the best strategy for obtaining a pure blood-EV suspension would be combining two isolation methods, based on different physical principles. Therefore, a size-exclusion-based (for protein removing) combined with a density-based (for lipoprotein removing) method probably represents the most effective one for contaminant removal [56], [62].

Different techniques have been applied to quantify and characterize EVs (Fig.3): among the others, western blot (WB) and flow cytometry (FCM) for the detection of specific EV markers, dynamic light scattering (DLS) for the evaluation of EV size distribution and polydispersity, electron microscopy (TEM and SEM) for checking EV morphology, nanoparticle tracking analysis (NTA) for determining EV dimension and concentration, and tunable resistive pulse sensing (TRPS) for assessing EV concentration. [60].

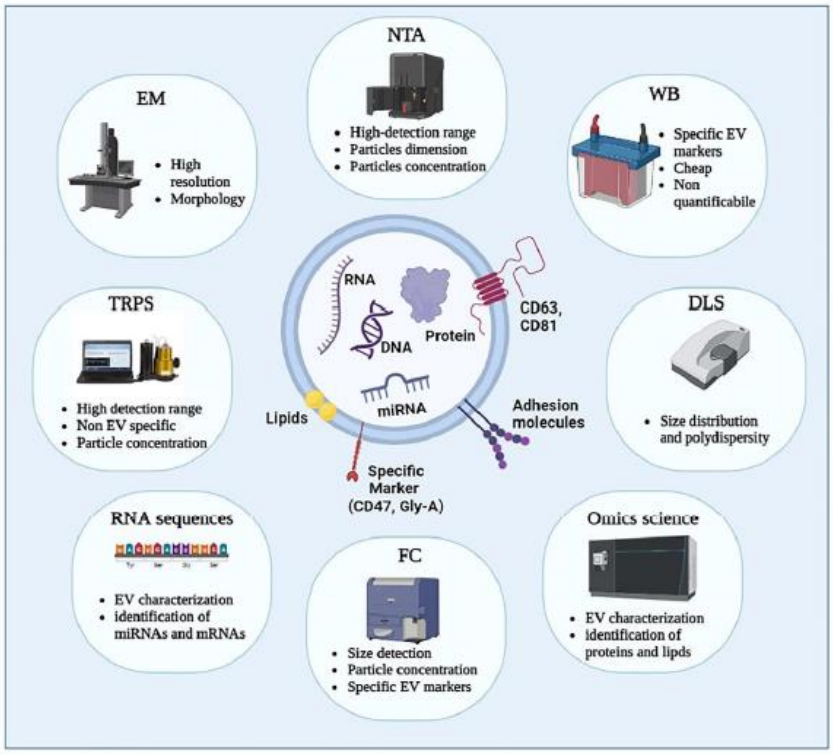

Figure 3. *EV quantification and characterization methods (from: Biagiotti S. et al., Pharmaceutics 2023, 15, 365)*

3.3 Red Blood Cell (RBC)-derived EVs

RBCs are an excellent source for EV production due to the several and unique advantages they have compared with other sources: (i) the lack of both nuclear and mitochondrial DNA [63], (ii)

their abundance, representing about 84% of all cells in the body [64], and (iii) the ease and speed of obtaining them from any human subject. Another important aspect is that RBCs have been used safely and routinely for blood transfusions over decades [63], [65].

Accordingly, RBC-derived EVs possess many benefits in health-care application which make them a simple and efficient platform for drug delivery. First of all, RBC-EVs, can be produced on a large scale without the need for cell culture, thereby reducing the cost of production and the risk of contamination [65]. Moreover, depending on preparation methods, storage solution and inter-donor variation, they are naturally released in significant amount in RBC concentrates, and so they have been "involuntary" transfused in patients together with RBCs over the years [66]. Consequently, RBCE-EVs obtained from subjects with O (positive or negative) blood group could be potentially used in an allogenic setting (Fig. 4).

In addition to the advantages above described, RBC-EVs play important functions, such as the removal of excess proteins from RBCs as transferrin receptors, acetylcholinesterase, and hemoglobin [67], [68] and a protective role to prevent RBC early clearance from circulation, clearing dangerous molecules [69], [70]. Moreover, RBC-EVs partially inherit the role of the cells from which they originate, so they are critical for communicating with endothelial cells to regulate nitric oxide and O_2 homeostasis [60], [71], [72]. Vesiculation turned out to be the most important mechanism by which RBCs eliminate waste and harmful substances accumulated throughout their lifespan [73], [74] in response to impaired signaling machineries, such as ATP depletion, calcium loading, lysophosphatidic acid exposure, oxidative stress, endotoxins, cytokines, complement, and high shear stress [75]. Interestingly, it has been proposed that RBCE-EVs include exosomes and microvesicles like other EV types. The former can be produced during the reticulocyte or erythroid precursor stage and maintained until the mature RBC stage [76]. They are generated via the typical endosomal pathway of nucleated cells after the plasma membrane has invaginated to form the early endosome which matures into the late one and evolves into multivesicular bodies [76]. On the contrary, microvesicles, which may form during the normal aging of circulating erythrocytes due to complement-mediated calcium influx, plasma membrane budding, and subsequent vesicle shedding [77], represent an integral part of RBC physiology and are linked to their maturation and aging. RBC-EVs are generally visualized as round vesicles of 100–200 nm in diameter and contain phospholipids, proteins, cholesterol, lipid, hemoglobin, and enzymes [74]. Although RBC-EVs are derived from RBCs, their membrane compositions and internal contents are not exactly the same. Indeed, specific stimulating conditions showed to play an important role for their final composition. As an example, they are reported to be different when produced naturally *in vivo*, released *ex vivo* during blood bag storage, or produced *in vitro* upon chemical treatments [78].

RBC-EVs can be identified with different EV-related markers, such as MVB formation proteins (Alix, TSG101) [79], glycoproteins (e.g., CD235a), membrane-associated proteins such as stomatin and flotillin, and especially CD47, which inhibits phagocytosis by interacting with macrophage signal regulatory protein alpha [80].

Overall, RBC-derived EVs can be divided into three categories: the naturally released vesicles, the ones released upon-stimulation, and the artificial ones. As already mentioned above, it has been reported that long-term storage in blood banking conditions can stimulate the natural production of RBC-EVs [74], [81]. Several stimuli have been shown to induce RBC-EV release even though it is not yet completely understood how the different stimuli can affect RBC-EV properties and composition. Usman and colleagues [82] proposed the *in vitro* stimulation of isolated RBCs with calcium ionophore. The possibility of isolating a large-scale amount of RBC-EVs (10^{13}–10^{14} EVs/ 200 mL of blood), the feasibility and the cost-effectiveness make this method one of the most used. Another process that induces RBC vesiculation is the induction of oxidative stress, by means of tert-butyl hydroperoxide, which leads to increased osmotic fragility and hemoglobin oxidation [83]. Artificial RBC-derived EVs are instead obtained after the application of physical stimuli as extrusion and sonication. They can be considered as RBC-membrane derived "liposomes" and they are commonly indicated as nanoerythrosomes (NanoEs).

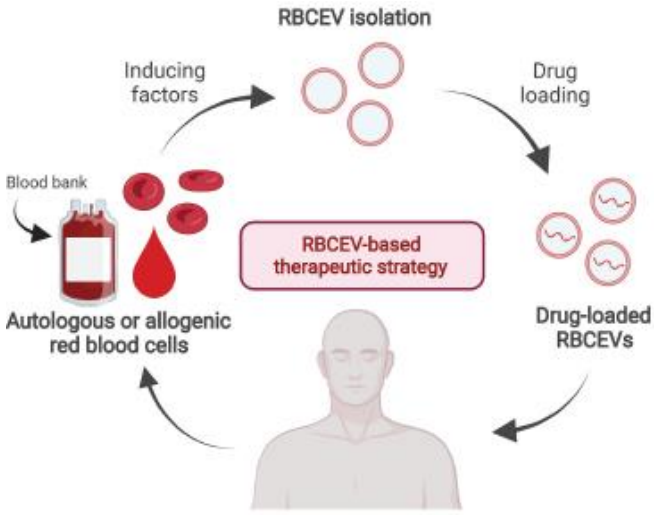

Figure 4. *A proposed strategy of drug-loaded RBC-EVs (from: Chiangjong W. et al. Frontiers in Medicine Dec 2021, Vol 8, Art 761362).*

4) EV engineering and functionalization

4.1) Surface functionalization: state of the art

There are many approaches, based on different principles, that can be used for EV-surface functionalization (Fig. 5). According to Richter and colleagues [84], these strategies can be divided into pre-isolation (also called biological) and post-isolation modifications. The first group concerns the manipulation of parent cells in order to achieve surface functionalization prior EV isolation and includes genetic, metabolic and direct parent cell membrane engineering approaches.

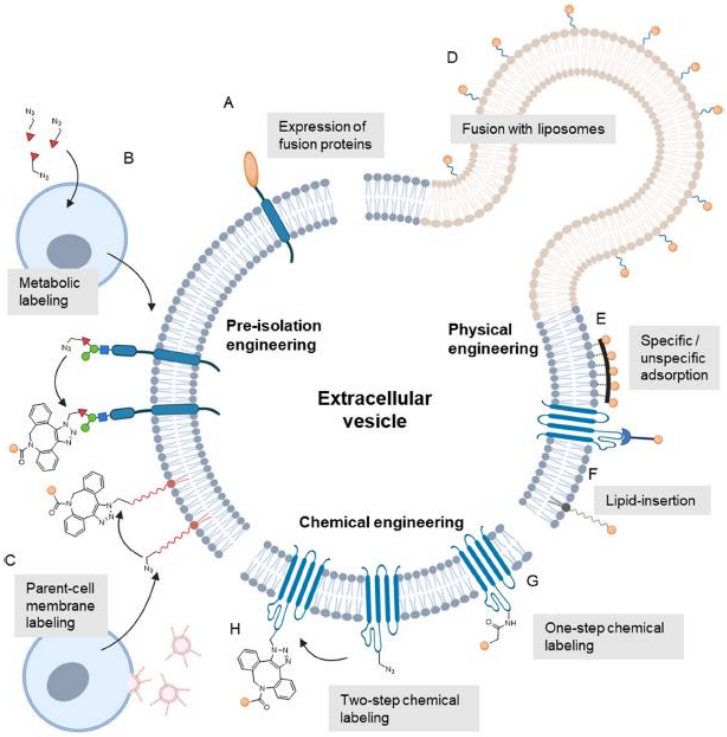

Figure 5. *Overview of EV surface engineering methods (from: Richter M et al, Advanced Drug Delivery Reviews 173, 2021, 416–426).*

In the genetic approach, cells are generally loaded with expression vectors containing chimeric genes/proteins that will be part of EVs fused with a protein of interest. The metabolic method avoids the need for genetic manipulation using the endogenous synthesis and modification processes in cells, while the direct approach is based on a direct engineering of the parent cell membrane as, for example, the fusion of liposomes with cellular membranes to exchange membrane components [85].

Post-isolation modifications include physical and chemical strategies (Table 1). The physical methods concern the application of a physical force to modify the EV surface. The physical force temporarily disrupts the lipid composition of vesicles into their constituents and after the removal of the force, vesicles spontaneously self-assemble into their natural structure [85]. The most common physical forces used for this kind of modification include sonication, extrusion, and freeze-thaw. Fusion with liposomes, insertion of lipophilic moieties into the membrane and adsorption of molecules to their surface represent the categories included in the physical modifications [84].

The chemical methods concern the direct use of chemical reagents to add functional moieties to the EV surface. Amine/carboxylic terminated phospholipid or transmembrane protein moieties present on EV membrane can be directly functionalized with different functional groups. Alternatively, functionalized phospholipids can also be incorporated in EVs by simple incubation following a hydrophobic insertion strategy [85].

Surface engineering method	Introduced moieties	Effects
Physical modification		
Fusion with liposomes		
Fusion using freeze-thaw-cycles	PEGylated and cationic lipids	Reduction / increase of interaction with cells
PEG_{8000}-mediated fusion	PEGylated lipids; cargo-encapsulation	Reduced uptake into macrophages; increased delivery of encapsulated photosensitizers
Lipid-post-insertion		
Phospholipid-insertion	PEGylated lipids and lipids modified with EGFR-binding nanobodies	Targeting of EGFR-expressing cells *in vitro*, increased circulation-time *in vivo*
Cholesterol-insertion	Cholesterol-modified siRNA to silence the huntingtin gene (a), antigen R (b) and CD45 or eGFP (c)	Silencing of target-genes
Surface adsorption		
Adsorption through a CD63-specific peptide	Peptide-bound muscle targeting peptide or morpholino oligomer against muscle-dystrophy	Targeting of muscles; functional improvement in a muscle-dystrophy mouse-model
Electrostatic adsorption	Cationized pullulan	Increased liver-uptake
Chemical modification		
One-step introduction through activated esters	Fluorescent dyes	Quantification of EV-uptake
	Biotinylated PEG-derivatives	Binding of FITC-labeled streptavidin
Two-step introduction using alkyne-azide cycloaddition	Fluorescent dyes using CuAAC	Generation of fluorescently labeled EVs
	cRGD-peptide using SPAAC	Targeting of ischemic lesions, inhibition of inflammatory responses
Two-step introduction using 6-hydrazinonicotinate acetone hydrazine and 4-formylbenzoate conjugation	Quantum dots	Generation of fluorescently labeled EVs

Table 1. *Post-isolation modifications of EVs (from: Richter M et al, Advanced Drug Delivery Reviews 173, 2021, 416–426).*

A wide variety of simple and fast chemical-based approaches can be exploited to functionalize EVs (Fig. 6). Amino groups available in lysine side chains and the N-termini of membrane-proteins represent the most abundant and suitable functional groups on the EV surface since they can be easily addressed using activated esters, such as the N-hydroxysuccinimide esters (NHS esters). While many biorthogonal reactions could potentially be employed in this setting [86], researchers have mainly focused on two-steps reaction such as azide-alkyne cycloaddition, the so-called “click chemistry”, which can be divided into copper-catalyzed alkyne–azide

cycloaddition (CuAAC) and its strain-promoted counterpart (SPAAC) [84]. The latter is considered a safer approach due to the toxicity of Cu-ions which might cause oxidative damage to EV surface-proteins. Nowadays, click chemistry represents one of most attractive and explored approaches due to its ease of synthesis with high yield and simplicity of product separation [85], [87], [88].

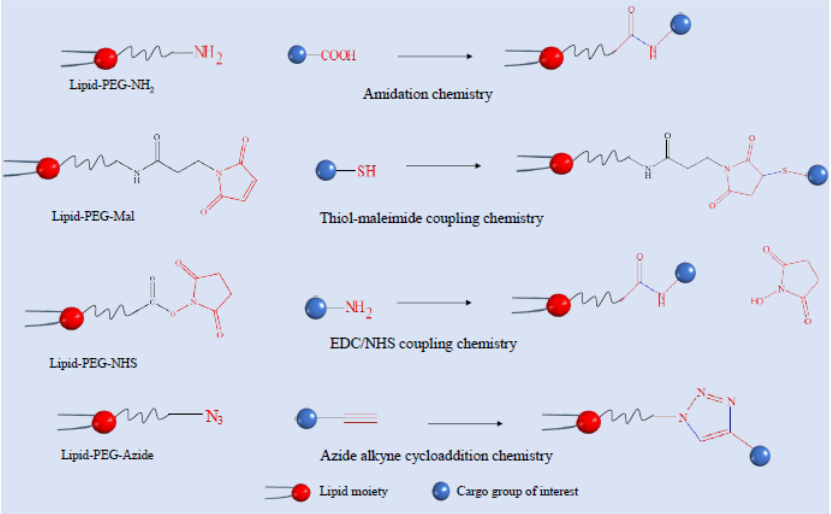

***Figure 6**. Schematic showing different chemistries for surface functionalization of EVs (from: Rayamajhi S. et al, Journal of Materials Chemistry B, Issue 21,2020).*

4.2) Click chemistry reaction for EV-surface functionalization: state of the art

Click chemistry reactions have been already proposed by different research groups as valid methods for EV surface engineering. Table 2 synthetizes part of the most recent published studies on this topic.

Type of modification	EV source	Field of application	Click chemistry reaction	Ref.
Post isolation	B16-F10, PANC-1 and HEK-293 cells	Pancreatic cancer (PC): study of the uptake properties of different EVs by PC cells	Copper-free click chemistry on isolated EVs. Alkyne-azide cycloaddition. The alkyne (DBCO-NHS) is bound to EV membrane. A fluorescent azide has been used (AlexaFluor 488-azide) to be clicked on EV surface.	[89]
Post isolation	Mouse MSCs	Bone targeting via alendronate/hydroxyapatite binding for Osteoporosis therapy	Copper-free click chemistry on isolated EVs. Alkyne-azide cycloaddition. The alkyne is bound to EV membrane. An azido-alendronate has been clicked to EV surface.	[90]
Post isolation	4T1 cells	*In vivo* Imaging	Copper-catalyzed click chemistry on isolated EVs. Alkyne-azide cycloaddition. The alkyne is bound to EV membrane. A fluorescent azide (azide-fluor 545) has been clicked to EV surface.	[91]
Post isolation	RBC-EVs	Role of the protein corona in the exogenous surface functionalization of EVs	Covalent binding *via* biorthogonal click-chemistry of the Cetuximab (CTX)- DBCO-fluorescent antibody. EVs undergo PEGylation before clicking with the functionalized CTX.	[92]
Pre isolation	MDA-MB-231 and HCT-116 cells	Inflammatory diseases involving CD44	Azide groups are generated on the cell surface via metabolic engineering. Then cell surface is clicked with DBCO-PHA (dibenzocyclooctyne-terminated PEGylated hyaluronic acid) PHA was chosen as it has shown prolonged circulation in the blood and specific binding affinity to CD44-overexpressing tissues	[93]
Pre isolation	Human lung adenocarcinoma cell line (A549)	*In vitro* and *in vivo* real time tracking; tumor targeting	The azide groups are incorporated on the surface of the cancer cells via metabolic glycoengineering. Then they are bioorthogonally labeled with DBCO-Cy5 via bioorthogonal click chemistry.	[94]

Table 2. *Summary of the most recent studies reporting the use of click chemistry-based approaches for the functionalization of the EV membrane.*

4.3) Encapsulation of therapeutic agents into EVs: state of the art

EVs can be loaded using two major approaches: active or passive encapsulation [95]. The choice of the best method is related to the physico-chemical properties of the molecule, and especially its hydrophobicity. Passive cargo-loading methods are relatively simple and do not require any particular stimulus or active substances addition; these approaches envisage the co-incubation of the therapeutic molecule with cells, for an endogenous loading, or with isolated

EVs for an exogenous loading. Thanks to the concentration gradient, the agent will passively diffuse through the EV membrane. Incubation is particularly suitable for loading hydrophobic drugs as they can interact with the lipid bilayer [96]–[98]. The active approaches instead aim at enhancing the EV membrane permeability (Table 3). A promising method for loading small molecules, as well as macromolecules, is sonication. Indeed, the treatment with ultrasound compromises the membrane integrity, thus allowing the drug to diffuse into EVs [95]. This method may provide higher loading efficiency compared to simple co-incubation. Sonication can be performed with a water bath or with a probe sonicator [99]. As previously reported [94], [95], a probe sonication can provide higher loading efficiency, but should be used with relatively stable therapeutics, such as the small molecule anticancer agents Paclitaxel and Doxorubicin[100],[101]. Beside the incorporation of small molecules, probe sonication has been used to load macromolecules, such as proteins, enzymes, and growth factors. Electroporation is widely used to load small molecules and nucleic acids, since it generates small pores in the EV membrane through application of an electrical field in a conductive solution. The electrical current disturbs the EV phospholipid bilayer, thus resulting in the formation of temporary pores. Drugs or nucleotides can subsequently diffuse into the interior of the EVs via the pores [95]. Another procedure consists in the application of freeze and thaw cycles during which drugs are incubated with EVs at room temperature for a certain amount of time, and then, the mixture is rapidly frozen at -80 °C or in liquid nitrogen and thawed again at room temperature. This process is repeated for at least 3 cycles to ensure drug encapsulation [95]. Finally, transient permeabilization with saponin (a surfactant molecule) can form complexes with cholesterol in the membranes, thus generating pores after its removal. Saponin turned out to be efficient in assisting the loading into EVs of catalases as well as hydrophilic molecules [97] [102].

Loading Methods	Steps Involved	Advantages	Disadvantages
Electroporation	Phospholipid bilayer of EVs are disorganized by an electric field, creating pores in the membrane which allow the passage of drug to vesicle.	Loading with large molecules is possible	Disrupts integrity of EVs; Low loading efficiency
Sonication	Exosomes derived from donor cells are mixed with drug and sonicated through probe sonicator which permits the drug to flow into exosome	Increased loading efficiency; applicable for small RNAs	Potential deformation of membrane of EVs; Not efficient for hydrophobic drugs.
Freeze/Thaw Method	Exosome are mixed with drug and incubated, subsequently frozen at −80 °C or in liquid nitrogen and are thawed at room temperature.	Medium loading;Fusion of membranespossible	Exosomes may aggregate; Low loading efficiency
Saponin-Assisted Loading	Saponin is incubated with exosomes to generate pores in their membrane by interacting with cholesterol which leads to increased membrane permeability	High drug loading compared to the other methods used in early reports	Generates pores in exosomes; Saponin can cause haemolysis; Toxicity concerns; Saponin concentration control & washing required

Table 3. *Different techniques and their advantages and disadvantages for EV active loading (from: Gaurav I. et al, Molecules 2021, 26, 1544).*

5) The extracellular matrix antigen ED-B fibronectin

The role of the extracellular matrix (ECM) in tumor growth and progression is gaining growing interest [103]. Some ECM proteins (e.g., periostin, hyaluronan, collagens, laminins, perlecan, fibronectin and tenascins) are known to be over-expressed in the tumor microenvironment and so they can potentially represent an ideal target for the development of molecular therapies [104]. Indeed, ECM antigens are generally more stable and abundant than those directly associated with cancer cells, which are genetically more variable, thus representing a better choice for imaging applications and targeted therapy. Over the past two decades, the role of fibronectin (FN) in cancer has been recognized and FN-targeting strategies have been conceived as promising anti-cancer approaches [105]. FN is an abundant, high-molecular weight dimeric glycoprotein expressed in the ECM or body fluids. Each monomer of FN consists of 3 types of homologous repeats termed type I, II and III domains. Alternative splicing variants and post-translational modifications result in the formation of FN isoforms. In particular, one isoform, generated by splicing in the type III repeats, is termed extra domain B-FN (ED-B) and is one of the most investigated FN variants for tumor-targeting strategies [106]. ED-B sequence is composed of 91 amino acids encoded by a single exon ontologically conserved in man, mouse, rat, and rabbit. ED-B is expressed during embryogenesis and its expression is absent in adult normal tissues except in wound healing and cancer, because of which it is called “oncofetal” FN. It has been demonstrated that oncofetal fibronectin (oncFN) plays a key role in tumorigenesis [107], [108] angiogenesis [109], [110], metastasis formation [111], [112] and epithelial-to-mesenchymal transition (EMT) [113].

Targeting an antigen as ED-B, which is expressed by the newly synthesized perivascular areas of the stromal matrix in a wide range of tumor types, will lead to the development of strategies not specifically limited to a single kind of tumor, but potentially exploitable as innovative therapeutic platform easily translatable to different oncological applications. Although EDB-FN-specific antibodies have been developed in the past [114]–[117], they are expensive to manufacture and show poor tissue penetration due to a combination of large size and low affinity. On the other hand, homing peptides are advantageous for what concerns low immunogenicity, versatility in chemical modification, and cost-effective production. They also showed to possess rapid extravasation and high tissue penetrating ability in the context of tumor targeting [118], [119].

An anti-ED-B FN peptide, named PL1, has been identified by Prakash Lingasamy and co-workers [104] as a novel bispecific peptide that recognizes both ED-B FN and TNC-C (tenascin-C domain). In preclinical studies, intravenously injected artificial nanoparticles exposing PL1 showed robust accumulation in a panel of glioblastoma and prostate carcinoma

xenograft models, and the treatment of glioblastoma-bearing mice with PL1-nanoparticles resulted in suppression of tumor growth and extended mice survival [113].

6) Aim of the study

Metastatic disease is the major complication in the clinical management of most types of cancers. The main aim of this thesis was to develop new tools to target metastatic disease by interfering with the tumor microenvironment components, and in particular the tumor extracellular matrix protein ED-B, an oncofetal variant of fibronectin. The research hypothesis behind this project is novel since it implies i) tumor microenvironment targeting, ii) exploiting a highly efficient and specific delivery system, and iii) loading of therapeutic agents able to locally deliver effective drugs potentially lowering systemic toxicity. In this context, natural nanoparticles, and in particular EVs, could represent a valid alternative to synthetic ones for the development of targeted drug delivery systems. Both plasma- and RBC-derived EVs possess highlights. Plasma-EVs own a demonstrated intrinsic homing capacity which makes them a powerful tool for cancer personalized therapy. On the other hand, RBC-EVs would represent a good option for allogeneic therapies. Accordingly, two specific and intermediate aims guided the project. The first one was to set up standardized and reproducible strategies for EV surface functionalization and drug encapsulation using plasma-EVs as prototypic source for autologous therapeutic purposes. The second aim, which evolved after the first two PhD years, was to translate the already developed protocols to nanoerythrosomes (NanoEs), the artificial RBC-derived EVs above described. The whole activities behind this second goal allowed not only to demonstrate that our standardized engineering strategies could be applied to another EV category, but, more importantly, to provide an alternative therapeutic option potentially exploitable in a heterologous context.

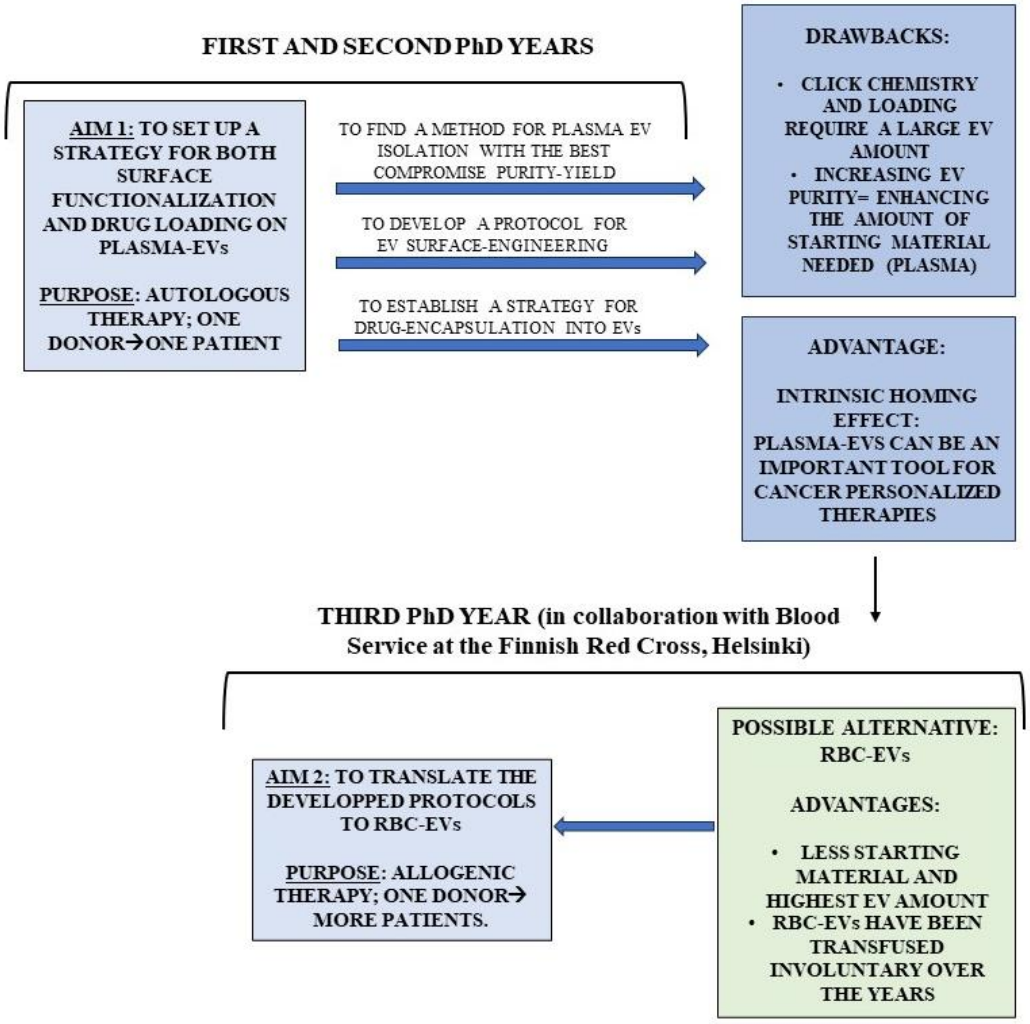

Figure 7*. Schematics of the aims and workflow followed in the thesis.*

MATERIALS AND METHODS

Blood collection and processing

Blood samples were provided by the Institutional Transfusion Center of Ospedale Policlinico San Martino, Genova. Blood was collected from healthy donors in K2E EDTA tubes. Plasma was isolated from blood by serial centrifugation steps, performed at 4°C: 120xg 20 min, 120xg 5 min, 360xg 20 min and 3000xg 10 min. The resulting plasma was stored at –80 °C until EV separation.

RBCs bag collection

Standard erythrocyte concentrates derived from donors with blood type B+ and 0+ were obtained from the Finnish Red Cross Blood Service (Helsinki, Finland). Only concentrates that could not be administered clinically were used in accordance with the Finnish National Supervisory Authority for Welfare and Health (Valvira). The concentrated were used 14-49 days after the blood was donated by healthy volunteers.
Each bag contained RBCs from four different volunteers.

Plasma-EV isolation methods

We compared three different isolation methods: size exclusion chromatography (SEC), a combination of iodixanol density cushion and SEC (IDC+SEC), and sucrose-cushion ultracentrifugation (sUC).

Size exclusion chromatography (SEC): we used IZON smart columns qEV/70 which are recommended for the recovery of particles with diameters ranging from 70nm to 1000nm. qEV isolation columns enable rapid and gentle purification of EVs with almost complete (>97%) removal of contaminating proteins.
According to manufacturer instructions 500µl of plasma has been loaded in the column and the volume of each collected fraction was 500µl. The first 6 fractions represent the void volume; fractions 7, 8, and 9 contain EVs, while “contaminating” proteins are eluted from fraction 10 to fraction 22. PBS-EDTA 2mM was used as an elution buffer to overcome EV aggregation. The elution profile of both EVs and contaminating proteins has been assessed measuring the absorbance at 280nm. EV fractions have been then pooled (1.5mL) and concentrated by ultracentrifugation for 2h at 100 000×g (4°C) (SN985 swinging rotor, Optima TL, Beckman). EV pellet was resuspended in 50µl of PBS-EDTA.

Iodixanol density cushion and SEC: we performed EV isolation by combining OptiPrep cushion gradient and SEC to remove both lipoproteins (IDC) and proteins (SEC). Following the protocol of Nasibeh Karimi et al [56], plasma/serum was layered on top of a 2 mL 50%, 2 mL 30%, and 2 mL 10% OptiPrep cushion. The cushion and sample were centrifuged at 178.000×g for 2 h at 4 °C. The visible band between the 10 and 30% layers was collected (high-density band, 1.06-1.16g/cm³; EV enriched band) and loaded onto a separate SEC column. The low-density band (< 1,025g/cm³) on the top of the tube is enriched in lipoproteins, and therefore it has been discarded. After SEC the EV fractions were then pooled (1.5mL) and concentrated by ultracentrifugation for 2h at 100 000×g (4°C) (SN985 swinging rotor, Optima TL, Beckman). EV pellet was resuspended in 50µl of PBS-EDTA.

Sucrose cushion ultracentrifugation: we applied the protocol proposed by Metka Lenassi's group (with some modifications)[120], with the aim of finding a good compromise between purity (lipoprotein contamination) and yield (sufficient EV quantity to be engineered). Either 1mL or 2.3mL of plasma diluted in PBS-EDTA to a final volume of 11.5mL were loaded on top of 2mL 20% sucrose and centrifuged for 135' at 100 000×g in a SW41Ti swinging rotor. Then, the supernatant was discarded, and the obtained EV pellet was resuspended in 1ml of PBS-EDTA, centrifuged for 10' at 3000×g to remove any co-isolated contaminants (platelets, protein, and lipoprotein aggregates) and concentrated for 2h at 100 000×g (4°C) (SN985 swinging rotor, Optima TL, Beckman). EV pellet was resuspended in 50µl of PBS-EDTA. All the analysis and application of plasma-EVs were performed on freshly isolated EVs.

Nanoerythrosome (NanoE) isolation

NanoEs have been isolated adopting the protocol previously developed by S.Valkonen et al. [121] with some modifications. NanoE production was initiated by separating the erythrocytes from the concentrate: 25 mL of concentrate was diluted with 25 mL cold dPBS and centrifuged at 800×g for 10 min at 4 °C without break. The supernatant was removed, and the pellet was suspended adding an equal volume of cold dPBS, centrifuged at 1560×g for 20 min without brake for two times. In the following step, 15 mL of erythrocytes were sonicated in an ice bath with a Branson digital sonicator 250-D (Branson Ultrasonics, Danbury, CT, USA) equipped with microtip using continuous sonication at maximum power for 30s. After disruption, the suspension containing membrane fragments was diluted with an equal volume of cold dPBS and centrifuged for 1560×g at 20 min and without brake to remove remaining cells and larger fragments. The supernatant was transferred into 6 ultracentrifugation tubes (0.5mL/tube) and, after filling the tubes with cold dPBS, samples were ultracentrifuges at 100,000×g for 60 minutes at 4°C using an MLA-50 fixed rotor (Optima MAX-XP, Beckman). Supernatants were discarded, pellets resuspended and centrifuged (washing step) at 100 000×g for 60 minutes at

4°C. The pellets were then suspended in 1mL dPBS final volume, vortexed for 30s, and centrifuged at 3000×g for 10' to remove any left contaminant. The supernatant was aliquoted and frozen by immerging the vials for 30s in liquid nitrogen before preserving them at -80°C before usage. All the analysis were performed with thawed NanoEs.

EV quantification and characterization by Nanoparticle Tracking Analysis (NTA) ZetaView®

EV size distribution and concentration were analyzed by ZetaView® TWIN-NTA PMX-220 (Particle Metrix GmbH, Inning am Ammersee, Germany), equipped with a sample cell and two lasers (488 nm and 640 nm) and Zetaview 8.05.14_SP7 software. Briefly, after calibration with 100 nm polystyrene beads, samples were diluted in filtered dPBS and injected into the sample cell using a 1 mL syringe. For both size and concentration measurements, the 488 nm laser in scatter mode was used; for the fluorescent NTA, 640 nm laser with a 660 nm filter wavelength was used. Size distribution analyses of 11 different positions were performed for each sample and the reading parameters were set as 80% sensitivity, and shutter speed of 100, minimum brightness of 20. For fluorescent NTA, sensitivity was increased to 90%, minimum brightness of 30.

ELISA

Plasma EV-enriched samples were diluted in dPBS (100 000-times for measurements of ApoA1 in all samples, 3000-times for measurements of ApoB100 in samples after SEC and 80-times for measurements of ApoB100 in samples after sUC) and the concentration (ng/mL) of ApoA1 and ApoB100 measured in duplicates by specific ELISAs (ELISA-ApoA1: #3710-1HP-2, ELISA-ApoB100: #3715-1HP-2, Mabtech, Sweden), according to the manufacturer's instructions. Measured concentrations were normalized to 1 mL of starting plasma and any potential dilution of the samples was accounted for.

Western blot (WB)

Each of the sample analyzed by WB (for plasma-EVs and NanoEs) were resuspended in RIPA buffer (1% NONIDET p-40, 0.1% SDS, 0.1% Sodium deoxycholate, protease inhibitor cocktail 1x, in PBS pH7.5) and protein content was quantified by Bicinchoninic acid (BCA) assay (Thermo Fisher Scientific). Five µg of proteins for each sample were loaded on 4%–12% NuPAGE Bis–Tris gel (Thermo Fisher Scientific). Electrophoresis was performed at 160 V and proteins were blotted on a polyvinylidene fluoride membrane for 1h at 30V with a n XCell Blot Module (Invitrogen). After blocking nonspecific sites with 5% non-fat dry milk (EuroClone, Italy) in Tris Buffered Saline with Tween 20 (TTBS, 20 mM Tris pH 7.5, 500 mM NaCl, 0.05% Tween 20), the membrane was incubated overnight at 4 °C with specific primary antibodies for:

flotillin-1 1:10 000 (ab133497,Abcam), syntenin 1:1000 (ab13326, Abcam), alix 1:1000 (ab186429, Abcam), TSG-101 1:1000 (T5701, Sigma), CD63 1:500 (TS63, Thermo), CD9 1:1000 (ab236620, Abcam) Glycophorin A 1:1000 (ab129024, Abcam), BAND 3/AE 1 1:1000 (ab77236, Abcam) diluted in 2.5% non-fat dry milk/TTBS. After washing three times with TTBS, membranes were incubated with specific HRP-conjugated secondary antibodies anti-mouse (Mouse IgG HRP Linked Whole Ab, GENA931) or anti-rabbit (Rabbit IgG HRP Linked Whole Ab, GENA934). Positivity was highlighted by providing the substrates for the chemiluminescence reaction of HRP (Amersham ECL Prime Western Blotting Detection Reagent, GE Healthcare, Chicago, Illinois, USA) and impressing a photographic sheet by autoradiography (GE Healthcare).

Super resolution microscopy

Super-resolution microscopy analysis of plasma-EVs was performed using Nanoimager S Mark II microscope from ONI (Oxford Nanoimaging, Oxford, UK) equipped with a 100x, 1.4NA oil immersion objective, an XYZ closed-loop piezo 736 stage, and triple emission channels split at 640, 488 and 555 nm. The EV profiler Kit (ONI) was utilized for the experiments following manufacturer's protocol. The Kit comprises fluorescent antibodies anti CD9-488, CD63-568 and CD81-647 and all the buffers and reagents necessary for the experiment. dSTORM mode acquired sequentially in total reflection fluorescence (TIRF) mode was used for the acquisition of images. Single-molecule data was filtered using NimOS software (v.1.18.3, ONI). Data has been processed with the Collaborative Discovery (CODI) online analysis platform www.alto.codi.bio from ONI and the drift correction pipeline version 0.2.3 was used [122].

Transmission Electron Microscopy (TEM)

EVs were resuspended in 20µl dPBS and fixed by adding an equal volume of 2% paraformaldehyde in 0.1 mol/l phosphate buffer (pH 7.4), as previously described [47]. EVs were then adsorbed for 10 min to formvar-carbon coated copper grids by floating the grids on 5µl drops on parafilm. Subsequently, grids with adhered vesicles were rinsed in PBS and negatively stained with 2% uranyl acetate for 5 min at room temperature. Stained grids were embedded in 2.5% methylcellulose for improved preservation and air-dried before examination. Electron micrographs were taken at Hitachi TEM microscope (HT7800 series, Tokyo, Japan) equipped with Megaview 3 digital camera and Radius software (EMSIS, Germany). To visualize EV size distribution, the results were plotted as a colorblind safe scatter dot plot in which each size measured is represented as a point along with lines for the median value and the range.

Anti-EDB fibronectin peptide synthesis

The peptide PL1 (PPRRGLIKLK*TS) [123] that recognizes EDB-Fibronectin (EDB-FN) and a scrambled peptide LKIGPLPK*RTRS that is chemically identical but has a randomized internal sequence, were manually synthesized using the standard method of solid-phase peptide synthesis according to the 9-fluorenyl methoxycarbonyl (Fmoc) strategy with minor modifications [124] [125]. Synthesis was carried on in the prof. Enrico Millo's Lab. Briefly, Rink amide deprotected resin was treated with a coupling reaction mixture of 5 equivalents (eq.) of the appropriate Fmoc-aminoacid, 4.5 eq. of O-benzotriazol-N, N, N', N'-tetramethyluroniumhexafluorophosphate (HBTU), 5 eq. of N, N-diisopropilethylamine (DIPEA), at 0.1 M amino acid final concentration in anhydrous N-methylpyrrolidone (NMP). A solution of 20% (v/v) piperidine in N,N- dimethylformamide (DMF) was used to remove the Fmoc group. The resin was incubated with a cocktail of acetic anhydride, sym-collidine and DMF (0.5:0.5:9 ratio (v/v)) to block the remaining amino groups on the resin. The final peptides (PL1 and the scrambled one) contain an azo group to the N-terminus of the peptide sequence. The azo group was attached via the 6-aminohexanoic acid spacer to the N-terminus of the protected peptide sequence during the solid phase synthesis to avoid the insertion of an azido group in the peptide scaffold that could modify the target specificity. Indeed the final peptides were chemically modified by the introduction of 5 (6) carboxyfluorescein (FAM) on the side chain of the K*. After the incorporation of one orthogonally protected Fmoc-L-Lys (Mtt)-OH the fluorophore was introduced by conjugating to the side chain of the lysine (K*) on the free ε amino group once deprotected from the temporary protection (Mtt).

In particular, after all the peptide coupling steps, the Mtt group was removed by incubating the resin in a cocktail of dichloromethane (DCM) and trifluoroacetic acid 1% (TFA). The resin containing the liberated ε-amino group was then coupled for approximately 2 hours with solutions containing fluorophore. The solution contained 5 eq of FAM, 4.5 eq. of HBTU, 5 eq. of DIPEA at 0.1 M final concentration in anhydrous NMP.

All the resins were then rinsed with dichloromethane and dried. The final cleavage of the peptides from the solid support and removal of all protecting groups were carried out with a trifluoroacetic acid (TFA): tri-isopropylsilane: H_2O (90:5:5) mixture. After the final cleavage from the solid support the peptides will be precipitated in ice cold diethyl ether and then purified by preparative reverse-phase high-performance liquid chromatography (RP-HPLC). The peptides were purified on an Agilent 1260 Infinity preparative HPLC equipped with a Phenomenex C18 Luna column (21.20 x 250 mm). Solvent A was 0.1% formic acid in H_2O and solvent B was 0.1% formic acid in acetonitrile. The gradient was 0–50% B from 5 to 35 min; the flow rate was set to 15 ml /min. The peaks of interest were then collected and evaporated under vacuum, then lyophilized and stored at 4°C to obtain the material for biological assay. The identity and purity of the peptides were verified by mass spectrometry analysis using an

Agilent 1100 series LC/MSD ion trap instrument. m/z = 1862. After purifying the azo-FITC-peptide/scrambled were dissolved in DMSO to a final concentration of 5.9mM.

EV surface functionalization: chemical conjugation by copper-free click chemistry

Before using the anti-EDB-FN peptide, experiments were conducted, as a proof of concept, with a fluorescent azide. EVs (from 10^6 to 5×10^9 for the titration experiments, and in a range between 10^9 to 10^{10} for all the other experiments) were resuspended in 200µL of PBS-EDTA and mixed for 1h at RT with 1µg of DBCO-NHS ester (Dibenzocyclooctyne-N-hydroxy succinimidyl ester, 761524, Sigma). After the first incubation, 1.9µl of a 5.9mM (final concentration 56µM) AlexaFluor647- azide (AZ-647) solution (A10277, ThermoFisher) was added to the reaction and incubated for 4h at RT to obtain AF647-Click-EVs. The fluorescent azide mixed with the EV suspension (without DBCO-NHS ester) was considered a negative control (EV + AZ-647). After the last incubation, AF647-Click EVs were washed by SEC to remove unlabeled chemicals and analyzed by non-conventional flow cytometry. For uptake experiments, AF647-Click-EVs and the negative control were concentrated by ultracentrifugation (3h, 100 000×g, 4°C) and resuspended in 100µL of phenol red-free Dulbecco's modified eagle medium (DMEM). The same procedure was used to conjugate the azo-FITC-peptide/scrambled, synthetized as above described, to both plasma-EV and NanoE surface. The clicked samples were analyzed by non-conventional flow cytometry (Peptide/scrambled-Click EVs) and imaging flow cytometry (Peptide-Click NanoEs).

Non-conventional flow cytometry on plasma-EVs

Plasma-EVs were first characterized by non-conventional flow cytometry, as previously described [126]. Briefly, 1×10^8 EVs in a final volume of 100µL of PBS-EDTA were stained with 10mM CFDA-SE (CFSE) (Vybrant™ CFDA-SE Cell Tracer Kit, Thermo Fisher Scientific, Waltham, MA, USA) (final CFSE concentration: 1µM) at either 4°C or room temperature (RT). The expression of CD9 (APC Mouse Anti-Human CD9, 312108, BioLegend), CD63 (PE-Cy7 Mouse Anti-Human CD63, 561982, BD Biosciences), and CD81 (BV421 Mouse Anti-Human CD81, 740079, BD Biosciences) was evaluated within the CFSE positive events and compared to the corresponding isotype controls. To evaluate AF647-Click EVs 100µL vesicles were stained after click reaction with the same CFSE concentration and AF647 positive events were considered within CFSE positive events. For FITC-peptide/scrambled Click EVs, the same method was applied using an APC-conjugated anti-tetraspanin antibody cocktail, instead of CFSE, containing CD63 (REA1055), CD9 (REA1071) and CD81 (REA513) antibodies (Antibody anti-human, APC, REAffinity (TM), Milteny Biotec). The corresponding isotype control (REA293, REA Control Antibody (S), human IgG1,

APC, REAffinity (TM), Milteny Biotec) has been used as a control to gate the APC positive events. FITC-positive events were considered within APC-positive. Samples were acquired using a CytoFLEX S flow cytometer (Beckman Coulter) and collected data were analyzed using the FlowJo software.

AF647-Clicked plasma EV internalization

The triple negative human breast cancer cell line MDA-MB 231 has been selected as the responder cell line to evaluate the internalization capacity of functionalized EVs. MDA-MB-231 were seeded in a 24-multiwell plate (25.000 cells/well) and cultured in for 1 day, to let them adhere to the plastic support. Cells were then stimulated as follows: i) EVs+AZ647 (negative control, 100µL of sample + 100µL of phenol red-free 2X complete medium); ii) EVs+DBCO+AZ647 (Click-EVs, test group, 100µL of sample + 100µL of red-phenol red-free 2X complete medium). Untreated cells were used as an additional negative control.
After 18h of incubation with either EVs+AZ647 or Click-EVs, cells were detached by Trypsin-EDTA (Gibco), rinsed in sterile PBS, centrifuged, resuspended in 300µL of PBS and analyzed by flow cytometry to evaluate the percentage of AF647 positive cells.
EV internalization was evaluated also by confocal microscopy. Cells were seeded on a glass slide fitting in a 24-multiwell plate (40.000 cells/well) and cultured in a complete medium for 1 day, to let them adhere to the glass support. Cells were then stimulated as above described for different time points (3h, 6h, 10h, 18h), rinsed 3 times with PBS, fixed with PFA 4% for 5 minutes at RT and permeabilized with 0,1% (v/v) Triton X-100 for 5 minutes at RT. Anti-HLA-I (supernatant of the clone W6.32, IgG2a) and anti-Rab5 1:500 (ab218624, Abcam) antibodies were incubated for 1h at RT to stain cell plasma membrane and early endosomes, respectively. Cells were then rinsed 3 times with PBS and incubated with the respective secondary antibodies (Goat anti-Mouse Alexa Fluor 546 and Goat anti-Rabbit Alexa Fluor 488) for 1h at RT and counterstained with DAPI for 20 minutes at RT. Samples were mounted on a glass slide with a water-based mounting medium (Permafluor, Thermo Fisher Scientific) and fluorescence imaged with the TCS SP2-AOBS laser scanning confocal microscope (Leica, Mannheim, Germany) through a plan apochromatic oil immersion objective 40x (1.4 NA). The 488 nm argon laser line was used for Rab5 fluorescence excitation, while the 546 nm and the 633 nm He-Ne lasers were utilized for excitation of HLA class I and Click-EVs fluorescence, respectively. DAPI was excited by a 405 nm diode laser. Leica software was used for image acquisition and analysis.

Fluorimetric assay

A black 96-well plate was coated with 10µg/mL of the target protein Recombinant Human Fibronectin type III EDB protein (ab209886, Abcam) and maintained at 4°C overnight. Parallel

wells were coated with the control proteins superfibronectin from human plasma (S5171, Sigma-Aldrich) and Albumin from human serum (A3782, Sigma-Aldrich). Coated and non-coated wells (here referred as "plastic control") were then rinsed 4 times in PBS and blocked with 2% bovine serum albumin (BSA) for 2 h, RT. After the blocking step, wells were incubated with the primary ligand (peptide or scrambled) diluted at 30μM and 10μM or with only dPBS (Blank). Parallel experiments were conducted evaluating the target specificity of either 1×10^{10} Peptide-Click-EVs or 1×10^{10} Scrambled-Click-EVs. Wells were then extensively rinsed in dPBS before reading the FITC-fluorescence intensity conjugated to the Peptide-Click EVs (wavelength of excitation at 488 nm, emission at 517 nm) using a CLARIOstarPlus fluorimeter (BMG LABTECH).

Fluorimetric analysis for peptide concentration in Peptide-Click EVs

A standard curve of the peptide with five scalar concentrations (14μM, 5.6μM, 2.8μM, 1.4μM and 0.6μM) was produced to obtain a calibration line to be used for estimating the peptide concentration in three different batches of Peptide-Click NanoEs (Tecan, Fluorescent plate reader). The correspondent naïve NanoEs for all batches represented the Blank. From the obtained molar concentration of the peptide, the corresponding mole number was multiplied by the Avogadro number to obtain the molecule number of the peptide. The number of molecules was then normalized to 1mL (peptide molecules/mL of Peptide-Click NanoEs) and compared to the starting amount of peptide (56μM, 3.37×10^{16} peptide molecules/mL) to evaluate the efficiency of the click reaction in terms of peptide molecules conjugated to NanoE surface. By crossing NTA data about Peptide-Click NanoE concentration and these data about peptide concentration we estimated the mean number of peptide molecules/NanoE.

Flow cytometry analysis on MDA MB 231 cells

To evaluate the expression of ED-B FN by cultured MDA-MB-231 cells by flow cytometry, cells were detached with Trypsin-EDTA solution from the plastic support. One million of cells were fixed and permeabilized using the Cell Permeabilization Kit (Thermo Scientific) before staining them with the anti-EDB-FN antibody (ab154210, BC-1, Abcam, Hercules, CA) for 30 min at RT. Cells were then rinsed in PBS, centrifuged and stained for additional 30 minutes with a fluorescein-conjugated anti-mouse secondary antibody (ab97264, Abcam). Cells were then rinsed in PBS, centrifuged, resuspended in 500 μl PBS and analyzed using a CytoFLEX S flow cytometer (Beckman Coulter).

Amnis ImageStreamX MkII analysis

For NanoE characterization, vesicles were stained with 1µM CFSE or 20µM CellTrace Far Red DDAO-SE (CTFR) (C34553, Life Technologies) and double stained with CFSE 1µM and anti-Glycophorin A (CD235a, BD). In both cases samples were incubated for 15' at 37°C and incubation with antibody was performed for 1h at RT. Peptide-Clicked-NanoEs were stained with 20µM CTFR before the click reaction.

For functional studies, cells (MDA-MB-231) were seeded 4 days in advance in 24-well (30000/well) and three wells for each condition were considered. Peptide-Click NanoEs or Not Click NanoEs (both CTFR stained) were added to responder cells in the same amount (1×10^{10}/well) and incubated for 1h,2h,3h,7h,16h and 24h. After incubation, stimuli were removed and cells were detached and fixed with 2% PFA for 7 min at RT. After fixing, PFA was removed, cells were resuspended in cold PBS and maintained at 4°C to be further analyzed. NanoE characterization and their interaction with cells were analyzed using 12 channels Amnis® ImageStream®^{X} Mark II (Cytek Biosciences) imaging flow cytometer and INSPIRE software. Altogether 100 000 EVs or 2000 cells/sample were acquired with High Gain mode at 60 × magnification. Excitation lasers 488, 642, and 785 nm were used with their maximum voltages. Channels Ch1 and Ch09 were used for bright field (BF) detection, and Ch06 as a side scattering signal (SSC). Channels Ch02 and Ch011 were activated for fluorescence emission signal detection. Single colour controls were used for compensation. Both unlabelled NanoEs and cells were used to determine the autofluorescence. Buffer with and without CFSE/CTFR and antibody molecules was used to determine the background noise in NanoEs samples. Compensated data files were analyzed using image-based algorithms available in the IDEAS® statistical analysis software package (Application v 6.2.). The co-localization of the peptide and the specific NanoE marker was determined using the colocalization wizard available in the IDEAS® statistical analysis software package and double-checked by analysing the images by eye. Internalization of EVs was also counted by the mathematical algorithms and masking options available by the IDEAS statistical analysis software package (Application v 6.2.).

EV loading by sonication

Pacific-Blue Paclitaxel (PB-PTX) has been received as a donation from the Division of Medicinal Chemistry and Pharmacology of Ohio State University, Columbus, USA (prof. Blake R. Peterson). We employed a Pacific Blue Paclitaxel (PB-PTX) as a proof of principle, to identify an efficient sonication method that would not affect EV integrity. We examined five different sonication strategies (SONIC 1, SONIC 2, SONIC 3, SONIC 4 and SONIC 5) using EVs in the range 10^{10}-10^{11}, same PB-PTX concentration but varying amplitude, duration and

number of sonication cycles (Fig. 8a). For assessing the sonication method EVs were mixed with PB-PTX in a final volume of 500ul in PBS and sonicated using a probe sonicator (UP 50H, Dr. Hielscher). After that, the suspension was incubated for 1h at 37°C to restore the membrane structure, and the unloaded drug was removed by SEC. The PB-PTX loaded EVs were analyzed by non-conventional flow cytometry after CFSE staining and compared to non-sonicated EVs. Once established the sonication strategy, further experiments were conducted with Paclitaxel (PTX) (Sigma), firstly on plasma-EVs and then on NanoEs, for evaluating the cytotoxic effect and encapsulation efficiency of loaded EVs. For both vesicle types, we adopted the same protocol: 1×10^{11} vesicles in a final volume of 200µL were sonicated with 700µM PTX and then incubated for 1h at 37°C for membrane recovery. After incubation vesicles were washed by SEC to remove the unloaded drug and then concentrated for 1h at 100 000×g (4°C). Pellets were resuspended in PBS and then analyzed by HPLC-MS or used for MTT test. Particle concentration was measured on loaded samples by NTA.

Viability assay (MTT)

MTT assay (3-(4,5-dimethylthiazol-2-yl)-2,5-diphenyltetrazolium bromide) was used to measure the cellular metabolic activity as an indicator of MDA-MB-231 cell viability. After culturing 3500/well in a 96 well plate for 24h cells were incubated for 48h with 10^6, 10^7 and 10^8 loaded vesicles (plasma-EVs or NanoEs), 10^6, 10^7, and 10^8 corresponding empty vesicles and 0.1 µM, 1 µM, and 100 µM free PTX. Samples were analyzed using SPECTROstarNano spectrophotometer (BMG LABTECH) considering the absorbance value at 555 nm of wavelength.

HPLC-MS analysis

Loaded EVs/NanoEs underwent cargo extraction by dilution with acetonitrile (1:1) followed by vortexing for 10', sonicating for 10', and centrifugating at 13300rpm for 10'. The supernatants (8µL) were injected in the HPLC system (Agilent 1100 µHPLC). A 1mm (ID) x 150mm(L) Symmetry C18 column was used (pore size 300Å, particle size 3.5µm) and the eluent phases were represented by water 0.1% (A), formic acid and acetonitrile (B) 0.05% with the following gradient: 0-5min 20% B, 5-30min from 20% to 60% B,30-40min from 60% to 100% B, 40-45min 100% B. Reconditioning at 20% B in 15 minutes. HPLC was coupled to a mass spectrometer with an orthogonal electrospray source (ESI) and trap ionic analyzer with high capacity (Agilent 1100 MSD xct ion trap). Spectrometric parameters were set up through direct infusion analysis (DIA) at 5µl/min using the infusion pump NE1000 (KF Technology, Roma, Italia). The analysis was carry on in ion-changed control mode with a 200 000 target and 300ms accumulation time. The operative parameters were capillary voltage: 4kV; nebulizer pressure: 10 psi; drying gas: 8 L/min; dry temperature: 320°C; rolling averages:3, averages: 5. All the

mass spectra were acquired in positive ion modality in the mass range 300-1200m/z. With the HPLC-MS system, a calibration line has been produced with four different PTX concentrations in triplicate (from 50µM to 0.1µM). The identified peak in the samples was confirmed to be PTX based on the retention time (HPLC) and the mass spectra compared with the standard.

Immunofluorescent analysis of MDA-MB-231 for ED-B expression

Immunofluorescent staining (IF) was performed on fixed and permeabilized MDA-MB- 231 cells: 10.000 cells were seeded in each chamber of an 8-chamber slide (SARSTEDT), fixed with 4% paraformaldehyde (PFA) for 15 min RT, permeabilized with 0.1% (v/v) Triton X-100/dPBS for 10 min. Then, the sample was treated with anti-EDB FN antibody (ab1542210, 1:500, Abcam) and 1% (w/v) BSA/0.1% (v/v) Triton X-100 /dPBS at 4°C overnight and the respective secondary antibody (1:150) APC-conjugated for 60 min at RT. As a further control, nuclei were stained with DAPI. After DAPI staining samples were mounted with a water-based mounting medium (Permafluor, Thermo Fisher Scientific) and fluorescence imaged with the TCS SP2-AOBS laser scanning confocal microscope (Leica, Mannheim, Germany) through a plan apochromatic oil immersion objective 40x (1.4 NA). The 633 nm He-Ne laser were utilized for excitation of EDB-FN and DAPI was excited by a 405 nm diode laser. Leica software was used for image acquisition and analysis.

Internalization of Peptide-Clicked NanoEs by fluorescent microscopy

MDA MB 231 cells were seeded in an 8-chamber slide (Ibidì) (30 000/well) 24h before incubating with clicked-NanoEs. After 3h of incubation (1×10^{10} Peptide-Click NanoEs/well) stimulus was removed and live cells were stained with DAPI for live cell imaging (Thermo). Samples were imaged with a DMi8 Leica microscope through 20x objective.

MDA-MB-231

Cells were cultured in HG DMEM supplemented with 10% Fetal Bovine Serum (FBS) (Gibco, Milan, Italy), 2 mM L-glutamine, and 50 mg/ml penicillin/streptomycin (complete medium) in T75 Flask.

Statistical Analysis

The data were analyzed using unpaired t-test (to compare the percentage of AlexaFluor-647 positive EVs or FITC-positive EVs/NanoEs in negative control and Click-EVs), one-way ANOVA (to evaluate the lipoprotein contaminants, EV characterization by flow cytometry and super resolution microscopy, to compare the EV concentration measured by NTA, to evaluate the AF647-Click EV internalization by flow cytometry) two-way ANOVA (to analyze the

targeting ability of the azo-FITC-peptide and scrambled in their free form and EV-conjugated and the cytotoxic effect of loaded plasma-EVs/NanoEs by MTT assay) and Mann-Whitney Test (to evaluate the differences in terms of EV size by TEM and AF647-Click EV internalization at different time points by confocal microscopy). Data are presented as mean ± SD considering at least three independent replicates for each assay and analyzed by GraphPad Prism 9 (Graph Pad Software, Inc.). For all analyses $p < 0.05$ was considered statistically significant. In all cases: ****$p < 0.0001$, ***$p < 0.001$, **$p < 0.01$, *$p < 0.05$.

RESULTS

Part I. Assessment of a standardized protocol for EV surface functionalization and a drug loading strategy using plasma-derived extracellular vesicles.

1) Sucrose cushion ultracentrifugation represents the isolation method with the best compromise between purity and yield

Plasma is one of the most challenging biofluids to isolate EVs from due to the presence of a massive pattern of contaminants such as proteins and protein aggregates, but especially a large set of lipidic nanoparticles with size or density comparable to EVs [56]. To evaluate the appropriate EV isolation procedure that could guarantee the optimal compromise between yield and purity, we compared three different protocols: size-exclusion chromatography (SEC), a combination of iodixanol density gradient and SEC (IDC+SEC) [56], and a sedimentation rate-based method (sucrose cushion ultracentrifugation, sUC) [120]. The latter has been performed using either 1 or 2.3 ml as the starting volume of plasma.

The concentration of contaminating HDLs and LDLs/VLDLs in plasma-EVs separated by the three different methods has been measured by ELISAs specific for Apolipoprotein A1 (ApoA1) and Apolipoprotein B100 (ApoB100), respectively (Fig. 1a and 1b). While ApoA1 expression increased by 13-fold in SEC-EVs compared to sUC-EVs-1ml, sUC-EVs-2.3ml, and IDC+SEC-EVs, no significant differences were observed among sUC-EVs from 1ml, sUC-EVs from 2.3ml and IDC+SEC-EVs [sUC-1mL: $9.0x10^4 \pm 0.6$ ng/mL; sUC-2.3mL: $8.7x10^4 \pm 0.1$ ng/mL; SEC: $120.2x10^4 \pm 4.9$ ng/mL; IDC+SEC: $8.9x10^4 \pm 0.4$ ng/mL; $p<0.0001$; N=3] (Fig. 1a). Similarly, the concentration of ApoB100 was significantly higher in samples separated by SEC compared to the other considered protocols (Fig. 1b). The concentration of ApoB100 detectable in SEC-EVs was respectively about 110, 88 and 330-fold more compared to sUC-EVs-1ml, sUC-EVs-2.3ml, and IDC+SEC-EVs [sUC-1mL: $3.1 \pm 0.4 \times 10^2$ ng/mL; sUC-2.3mL: $3.9x10^2 \pm 0.6$ ng/mL; SEC: $34.30x10^2 \pm 13.4$ ng/mL; $1.0x10^2 \pm 0.1$ ng/mL, $p<0.0001$; N=3] (Fig. 1b). Based on these data, the combination of IDC+SEC turned out to be the optimal method to eliminate the ApoB100-expressing lipoproteins, while no significant differences in ApoB100 concentration were observed by applying the sUC method to 1 or 2.3 ml of plasma (Fig. 1b). Accordingly, we decided to adopt our modified method (sUC-2.3mL) and we compared by NTA the size distribution and concentration of EVs isolated by SEC, IDC+SEC and sUC-2.3ml (Fig. 1c and 1d). NTA revealed that no significant differences in terms of size distribution were observed among the three analyzed isolation protocols. Indeed, the X50 parameter, indicating the diameter of particles where 50% of the distribution has a smaller and 50% has a larger

particle size, was 130.0±4.5 nm,146.1±12.7 nm and 134.9±10.3 nm for sUC, SEC and IDC+SEC-EVs, respectively (Fig. 1c). Nevertheless, significant differences in terms of EV concentration were observed relating to the separation protocols (Fig. 1d). IDC+SEC was the one resulting in the lowest amount of EVs, being able to isolate 11-fold less EVs than the sUC method and 16-fold less than the SEC method [sUC: 2.5 $\pm$ 0.8 x10^9; SEC: 3.5 $\pm$ 0.7 x10^9; IDC+SEC: 2.2 $\pm$ 0.3 x10^8; sUC vs IDC+SEC: p=0.0014; SEC vs IDC+SEC: p=0.0001; N=4] (Fig. 1d). Taken together, these data indicate that sUC is the ideal method for enrichment of EVs from human plasma, representing the optimal compromise between EV purity and yield compared to the other two considered protocols. In addition, this is still valid when we apply our modified protocol by increasing the plasma starting volume from 1mL to 2.3mL.

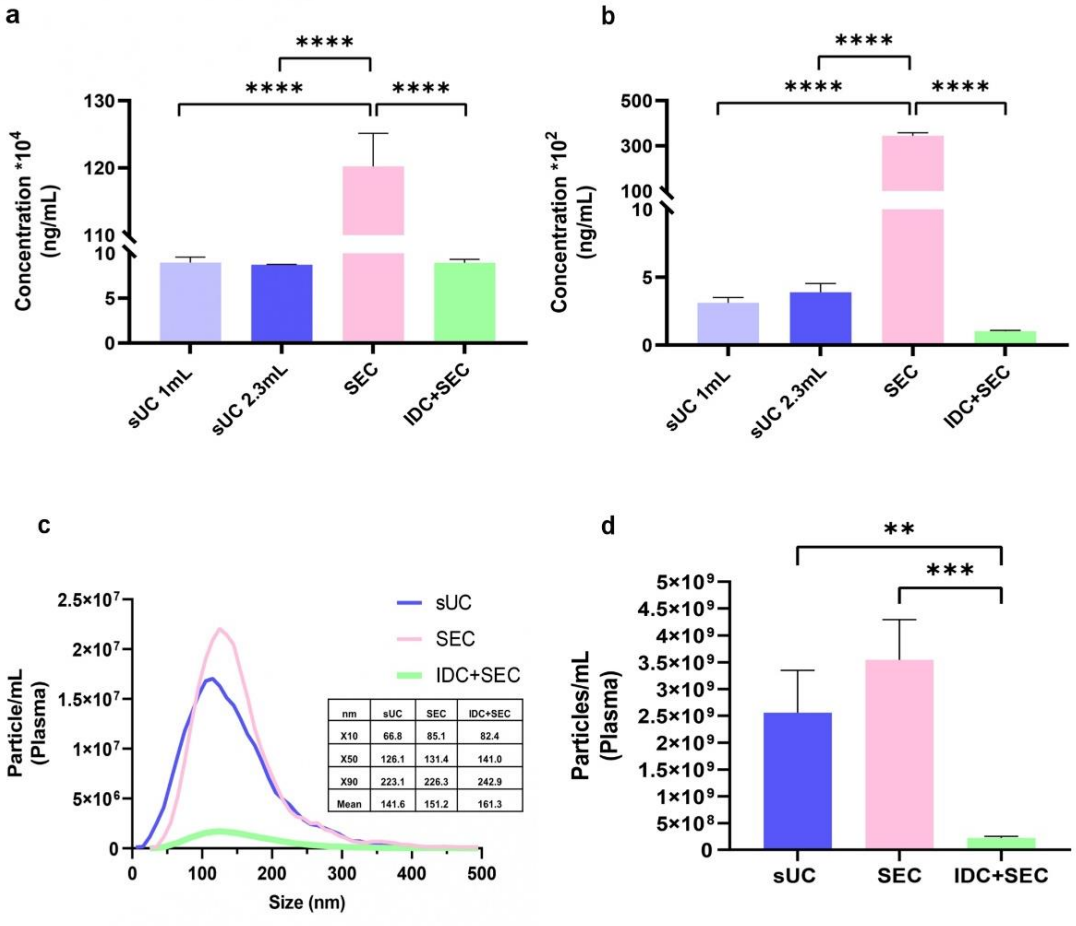

Figure 1: Comparative characterization of plasma-EVs isolated by three different methods.
(**a**, **b**) ApoA1 (**a**) and ApoB100 (**b**) concentration (ng/mL) in sUC- (1mL and 2.3mL), SEC- and IDC+SEC-EVs (N=3). Data are presented as mean ± standard deviation. **** p<0.0001, *** p<0.001, ** p<0.01 (Ordinary one-way ANOVA). (**c**, **d**) Representative size distribution profiles (**c**) and particle concentration (**d**) measured by NTA for sUC-, SEC- and IDC+SEC- EVs (N=3). Data are normalized to 1 ml of starting volume of plasma. Data are presented as mean ± standard deviation (Ordinary one-way ANOVA), ** p<0.01, *** p<0.001.

2) Characterization of sUC-EVs

sUC-EVs were analyzed for their size distribution by NTA which showed the presence of a homogeneous distribution with an average X50 of 130.0±4.5 nm (Fig. 2a). In particular, 10% of the analyzed particles were smaller than 69.1±2.5nm and 90% of them were smaller than 233.3±8.8nm (Fig. 2a). We also evaluated the expression of the typical EV-markers tetraspanin (CD9, CD81 and CD63) by non-conventional flow cytometry [126] (Fig. 2b and c) and by super-resolution microscopy (Fig. 2d and e). Both techniques indicated that CD9 is the most abundant tetraspanin expressed by plasma-EVs (Fig. 2c, histogram and Fig. 2e). Interestingly, the characterization at single EV level revealed a heterogeneous EV population expressing different tetraspanin combinations (Fig. 2d and e), even if CD9 is confirmed as the most expressed one. Moreover, sUC-EVs expressed the typical EV markers Alix, Flotillin-1, TSG-101 and Syntenin, as revealed by western blot analysis (Fig. 2f).

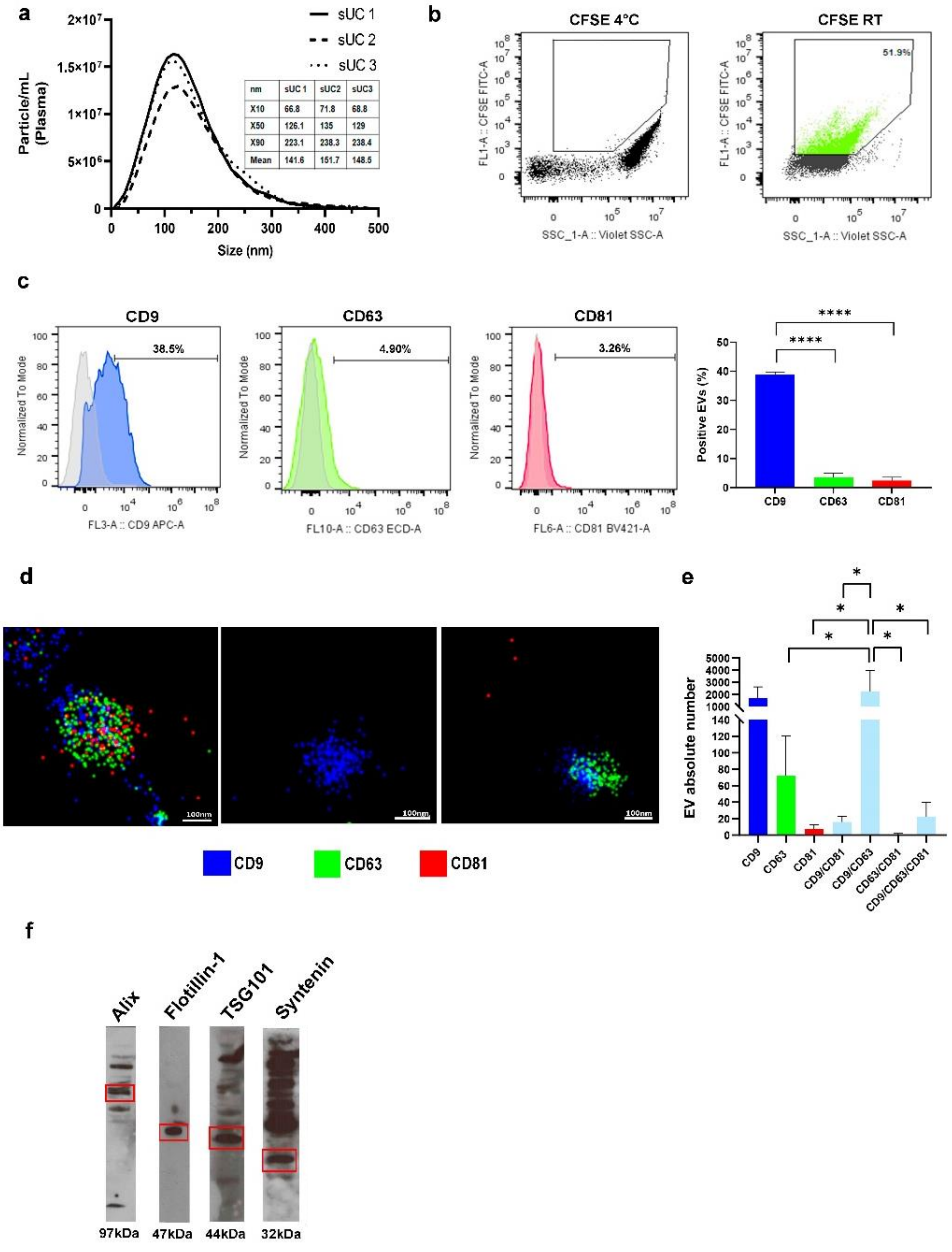

Figure 2: Characterization of sUC-EVs. (**a**) Representative NTA measurements (N=3) showing size distribution (X10, X50, X90 and Mean) and particle concentration. Data have been normalized to 1mL of plasma. (**b**) Flow cytometry strategy used to characterize sUC-EVs. Green dots identify CFDA-SE positive events. EVs were stained with CFDA-SE at 4°C as "blank tube" (left panel) to define the appropriate dimensional gate when considering EVs stained with CFDA-SE at room temperature (right panel). (**c**) Representative flow cytometry showing the expression of CD9 (blue lines), CD63 (green lines) and CD81 (red lines). Areas under the gray lines indicate the expression of the corresponding isotype immunoglobulin. Y-axis scaling: data have been normalized to Mode (Modal setting, FlowJo V10). Histogram indicates the percentage of CD9, CD63 and CD81 positive EVs by flow cytometry. Data are represented as mean ± SD (N=3). **** $p<0.0001$ (Ordinary one-way ANOVA). (**d**) Representative super-resolution microscopy images of EVs stained with CD9 (blue), CD63 (green) and CD81 (red). (**e**) Histogram indicates the absolute number of EVs that were positive for CD9, CD63, CD81 or combinations of them, as evidenced by super resolution microscopy. Data are represented as mean ± SD, *$p<0.05$ (Ordinary one-way ANOVA). (**f**) Western blot analysis of Alix, Flotillin-1, TSG-101 and Syntenin on sUC-EVs.

3) A fluorescent azide (AF647) as a proof of concept: achievement of the click chemistry reaction and its effect on EV identity, size and number

A copper-free click chemistry approach has been used to functionalize the plasma-EV membrane. The method has been set up using, as reagents, the alkyne Dibenzocyclooctyne-N-hydroxy succinimidyl ester (DBCO-NHS) and a fluorescently labeled azide (AZ-647). The latter has been selected as a proof-of-principle molecule to standardize the whole procedure. Firstly, the amino groups of the EV surface proteins reacted with the N-hydroxy succinimidyl (NHS) group of DBCO. The alkyne group of DBCO was then coupled to AZ-647 by copper-free click chemistry. As already reported [89], the highest labeling yield was obtained when EVs were reacted with DBCO-NHS for 1h at RT and then immediately coupled with AZ-647 for 4h at RT. To obtain efficient plasma-EV labeling, the particle number to be used in the click chemistry reaction has been titrated (Fig. 3a-e). AZ-647 mixed with the EV suspension, without DBCO-NHS, served as a negative control. Titration experiments, conducted using five different EV amounts (from 10^6 to 5×10^9) with fixed concentrations of both DBCO-NHS and AZ-647, revealed that the incubation with only AZ-647 induced an irrelevant unspecific EV labeling (Fig. 3a-e, grey histograms) and, more importantly, the reaction was successful when working with at least 10^9 EVs (Fig 3d, 3e, blue histograms). Indeed, experimental replicates conducted with at least 10^9 EVs indicated that the percentage of labeled EVs, ranging from 40 to 60% of total EVs used in the reaction, was significantly higher than the corresponding negative control (Fig. 3f) and these results were confirmed by fluorescent NTA analysis (Fig. 3g). Subsequent analyses were performed to evaluate whether the click chemistry reaction affected the EV identity and integrity. The expression of the vesicle markers Flotillin-1, CD63, and Syntenin did not vary in Click-EVs compared to both naïve EVs and EVs incubated with only AZ-647 (Fig. 3h). These data were confirmed by NTA (Fig. 2i and 3i) and TEM (Fig. 3m) analysis which did

not show any significant variation in EV size among naïve (126.8 ± 64.52nm, Fig. 3m histogram) and corresponding Click-EVs (124.7 ± 44.55nm, Fig. 3m histogram). On the contrary, we observed that click chemistry severely affected EV concentration, with a loss of 80-90% in both negative control and Click-EVs, compared to the starting EV amount (naïve sample) (Fig. 3l).

These results suggest that EV size and identity are not affected by the click reaction, but the final EV number is, and this is probably related to the washing step, necessary after EV labeling to remove the unlabeled reagents. This information explains why it was so important to identify an EV isolation protocol that allows obtaining enough vesicles to be successfully functionalized.

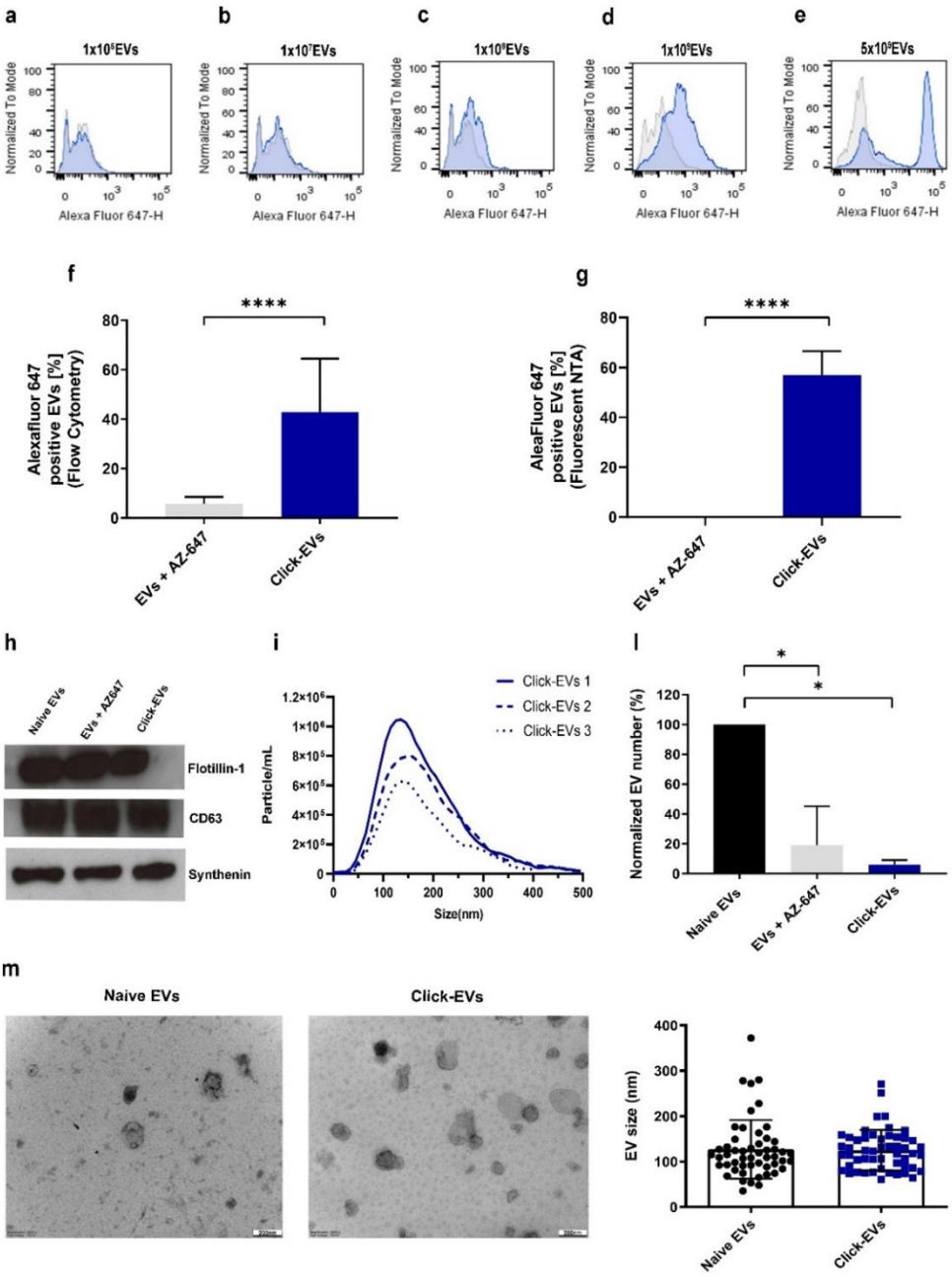

Figure 3: Efficiency of the click chemistry reaction with AF647-AZ and its effect on EV identity, size and concentration. (**a-e**) Titration of EV number from $1x10^6$ to $5x10^9$ with a fixed concentration of both reagents (DBCO-NHS and AZ-647). Areas under the gray lines identify the negative control while the blue one indicates the Click-EVs. Y-axis scaling: data have been normalized to Mode (Modal setting, FlowJo V10). (**f-g**) Histograms represent the percentages of Alexa Fluor 647-positive EVs identified by flow cytometry (f) (N=11) and by fluorescent NTA (g) (N=4) performed using 10^9 EVs. The percentages of Alexa Fluor 647-positive EVs is shown for Click-EVs (blue columns) compared to the negative control (gray columns). Data are indicated as mean ± SD, **** $p<0.0001$ (Unpaired t test). (**h**) Western Blot analysis for the expression of the vesicle markers Flotillin-1, CD63 and Syntenin in the three conditions: naïve EVs, negative control and click-EVs. (**i**) Representative NTA measurements (N=3) showing size distribution (X10, X50, X90 and Mean) and particle concentration of Click-EVs. (**l**) Histogram indicates the EV number variation among the three conditions: naïve EVs, negative control and click-EVs (N=3). Data have been normalized to naïve EVs. Data are indicated as mean ± SD, * $p<0.05$ (Ordinary one-way ANOVA). (**m**) Representative TEM images of naïve EVs (left panel) and click-EVs (middle panel). The right panel represents TEM analysis of EV size distribution. Data are visualized as scatter dot plot showing EV size distribution among naïve and click-EVs. Each size measurement of EVs is showed as a point, whereas lines represent the mean value and the range (N=52). Data are indicated as mean ± SD (Mann-Whitney Test).

4) AF647-Click-EVs are internalized by responder cells in a time-dependent manner and follow an endosomal recycling route

The ability of Click-EVs to be internalized by responder cells (MDA-MB-231 tumor cell line) was evaluated. Responder cells were analyzed by flow cytometry after 18h of co-incubation with either negative control (1×10^9 EVs+AZ-647) or 1×10^9 Click-EVs. Untreated cells were used as an additional negative control. No fluorescence was detected with either untreated cells or cells incubated with EVs+AZ-647 (Fig. 4a, gray and red histogram), confirming the previous results related to the absence of an unspecific EV labeling given by the incubation with the fluorescent azide (Fig. 3f and 3g). Interestingly, 54.6 $\pm$ 22.6% of cells treated with Click-EVs were AF-647 positive, clearly indicating an efficient uptake of Click-EVs (Fig. 4a, left panel blue histogram and right panel). In addition, we evaluated by confocal microscopy the timing and the recycling route of Click-EVs within responder cells at three different time points: 3h, 10h and 18h (Fig. 4b). A few Click-EVs were internalized by responder cells after 3h incubation (Fig. 4b, upper-left panel) and their numbers increased during the time, as determined by the increased fluorescence/cell (Fig. 4b, bottom-right panel). At 10h, the mean fluorescence intensity associated with internalized EVs was almost 20 times higher than the one measured at 3h and augmented even more at 18 h (50 times more than 3h), indicating that Click-EVs internalization progressively increased with time (Fig. 4b, bottom-right panel).

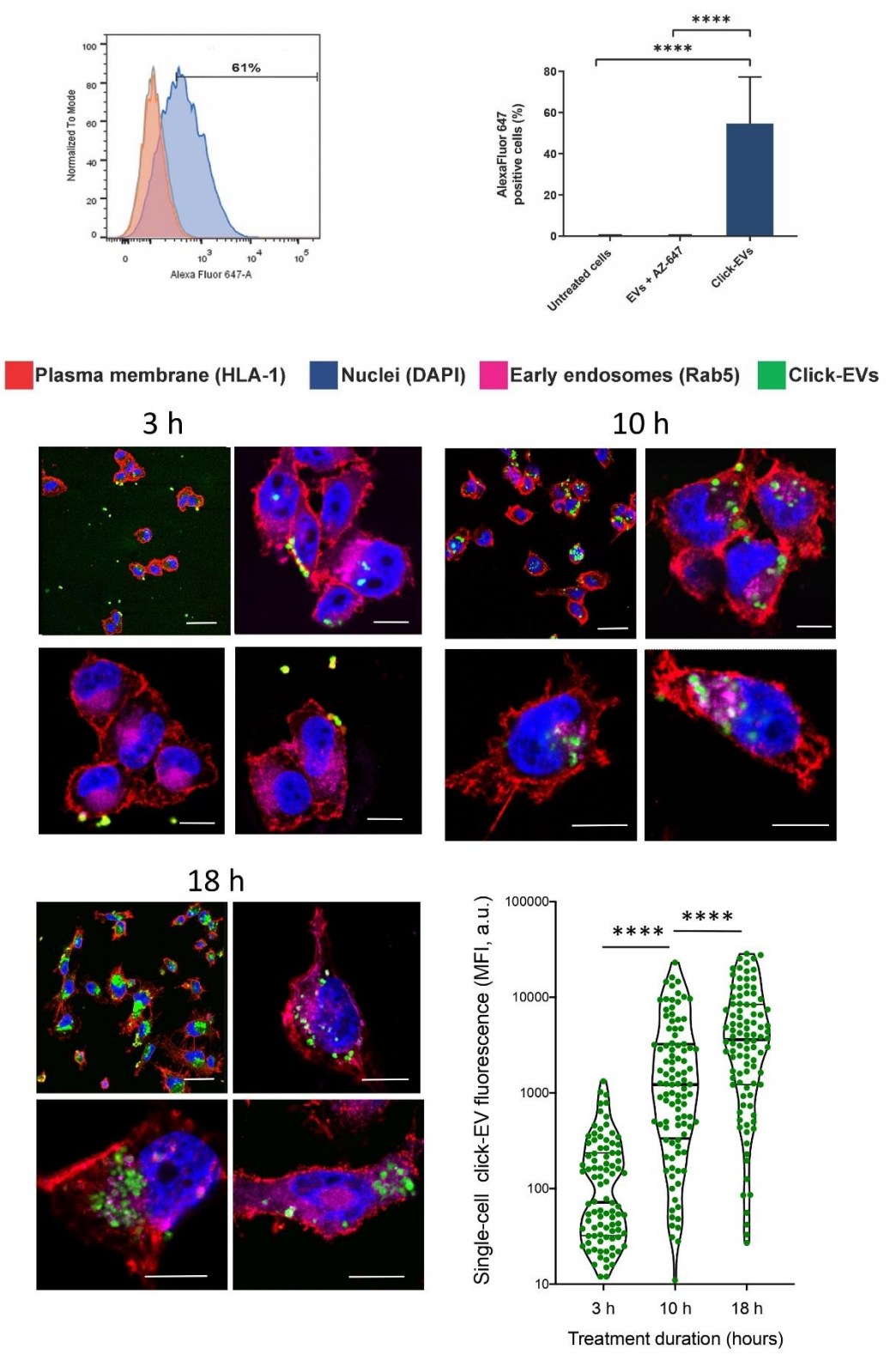

Figure 4. AF-647 Click EV internalization by responder tumor cells. (**a**) Representative overlaid histograms of untreated MDA-MB-231 cells (gray line) or treated as follows: 10^9 EVs+AZ-647 (negative control) (red line) or 10^9 click-EVs (blue line) (left panel). The histogram shown in the right panel indicates the percentage of Alexa Fluor 647-positive cells treated as above described. Data are presented as mean + SD (Ordinary one-way ANOVA),

**** p<0.0001. (**b**) Representative confocal microscopy images of MDA-MB-231 cells treated at different times (as indicated) with click-EVs (green) and stained with anti-HLA class I antibody (red) for plasma membrane identification, anti-Rab5 antibody (pink) and DAPI for nuclear staining. Virtual colors are displayed, which do not conform to fluorescence emission of the various fluorochromes, in order to make the click-EVs better identifiable. For each treatment time, four images are displayed: one at low magnification (upper left, bar = 50 micron) and three at higher magnification (bar = 10 micron) (upper right and bottom panels). The violin graph displays the distribution of Click-EVs fluorescence intensity of the cells at the different treatment times. Dots represent the fluorescence intensity for each cell calculated within Regions of Interest (ROI) defined by the plasma membrane fluorescence. Click-EVs localized on the plasma membrane were considered included in the calculation. Median and quartiles are displayed. Statistical significance of the difference between treatment times are evaluated by non-parametric Mann Whitney test, ****p < 0.0001.

Moreover, analyzing the distribution of Rab5, an early endosome marker, we observed, at longer times, the presence of Rab5 surrounded Click-EVs (Fig. 5). In particular, both the number of cells displaying Click-EVs surrounded by Rab5, and so the number of Rab5-surrounded EVs/cell increased progressively from 10h to 18h (Fig. 5, bottom histogram). Taken together, these data indicate that Click-EVs are efficiently internalized after 10h co-incubation with responder cells, and partially follow the endosomal recycling route.

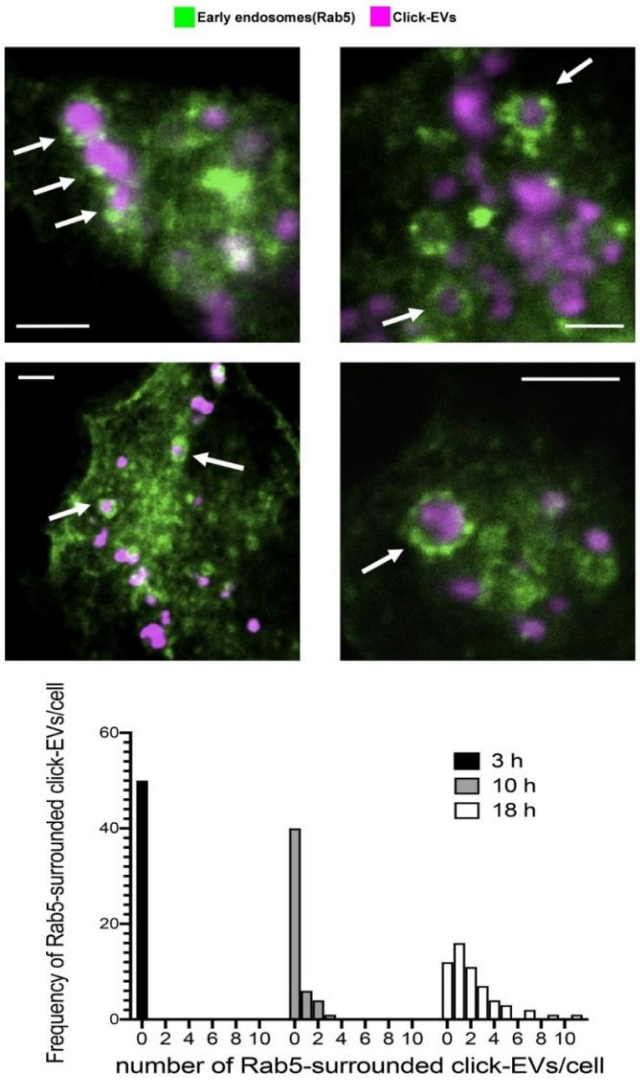

Figure 5. Recycling route of internalized click-EVs. Representative confocal microscopy images displaying Click-EVs (pink) surrounded by Rab5 (green). Virtual colors of the two fluorescence have been changed for image clarity reasons. Arrows indicate the most evident EV structures that are surrounded by Rab5-fluorescence. Bar = 2µM (upper and middle panels). Frequency histogram reporting, in the Y axis, the number of cells containing a given number of Rab5-surrounded click-EVs (shown in the X axis), in MDA-MB-231 cell cultures treated with click-EVs for 3, 10 and 18 hours. These numbers do not account for the entire cell, but only for the cell portion lying in the confocal optical section of the image. Fifty cell sections per treatment condition were evaluated.

5) The synthesized fluorescent peptide can specifically target ED-B fibronectin

An anti-EDB-fibronectin peptide, whose sequence was already described [123], was synthesized adding in its structure an azo molecule and a fluorochrome (FITC) to obtain an "azo-FITC-peptide", useful for the click chemistry application. At the same time, an azo-modified and fluorescent peptide with the same amino acids but arranged in a different order, called "scrambled peptide", was produced as a "control peptide". We performed a fluorometric assay to evaluate the affinity of the azo-FITC-peptide for ED-B Fibronectin, super fibronectin (a plasmatic form of FN), and human albumin, in comparison with the azo-FITC-scrambled. For both the concentrations tested (30µM and 10µM), the azo-FITC-peptide was shown to recognize specifically and significantly EDB-fibronectin compared to super-FN and human albumin (Fig. 6). [ED-B FN coating: Azo-FITC-Peptide 30µM (21446 ± 4225), Azo-FITC-Peptide 10µM (5501 ± 3523), Azo-FITC-scrambled 30µM (0.000 ± 0.000), Azo-FITC-scrambled 10µM (245 ± 478); super fibronectin: Azo-FITC-Peptide 30µm (2579 ± 2602), Azo-FITC-Peptide 10µM (268 ± 535), Azo-FITC-scrambled 30µM (0.000 ± 0.000), Azo-FITC-scrambled 10µM (0.000 ± 0.000); hAlbumin: Azo-FITC-peptide 30µM (690 ± 918), Azo-FITC-peptide 10µM (16 ± 33), Azo-FITC-scrambled 30µM (0.000 ± 0.000), Azo-FITC-scrambled 10µM (2098 ± 2640)]. On the contrary, the azo-FITC-scrambled didn't show any significant bound to all the three proteins challenged (Fig. 6) confirming the high specificity of the sequence and, on the other hand, indicating that our "modified" form of the anti-EDB-FN peptide can still recognize its target.

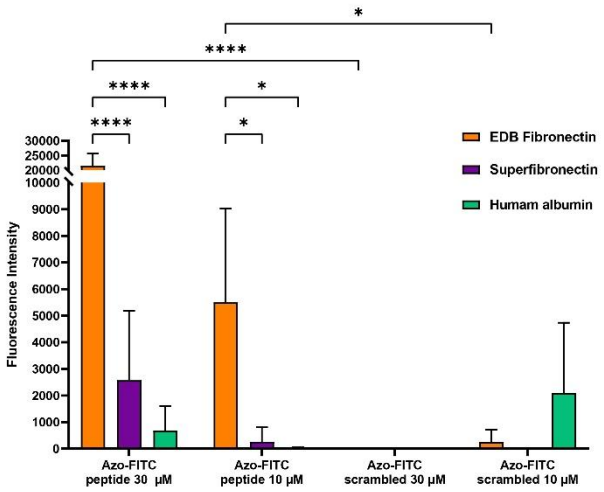

Figure 6. Fluorometric assay for anti-EDB-FN peptide targeting ability

Histogram showing fluorometric assay results measured at 517 nm and subtracted of both blank and corresponding "plastic control" for each coating. The following data represent the fluorescence intensity of the primary ligands on each coating and are presented as mean ± SD, (N = 4). Orange bars represent EDB FN coating, violet bars super fibronectin coating and green bars represent hAlbumin coating, **** $p < 0.0001$, * $p < 0.05$ (Ordinary two-way ANOVA).

6) The click chemistry-based strategy can be applied for EV surface functionalization with the specific anti-ED-B peptide

Once the targeting ability of the peptide has been confirmed, we have applied the click chemistry strategy for EV surface functionalization with both azo-FITC-peptide and azo-FITC-scrambled. In this case, EVs + azo-FITC-peptide/scrambled without DBCO represent the negative control. We used the same non-conventional flow cytometry method previously described to evaluate the achievement of the click chemistry reaction. In this specific experimental set up, Click-EVs were stained with an anti-tetraspanin cocktail antibody conjugated with the fluorochrome APC (Fig. 7a). FITC-positive events falling within the APC gate corresponded to Click EVs (Fig. 7b). The percentage of FITC-positive EVs was significantly higher in the Peptide-Click-EVs (Fig. 7c, left panel) or Scrambled-Click-EVs (Fig. 7c, right panel) in comparison with their corresponding negative controls. These data indicated that the click chemistry approach was able to functionalize the EV-membrane with either peptide or scrambled. As evaluated for AF647-Click-EVs, we also checked the effect of the click chemistry reaction on the identity of Peptide-Click-EVs. Peptide-Click-EVs maintain the expression of the typical EV markers CD63, Flotillin-1, and CD9 when compared to negative control and naïve EVs (Fig. 7d). The same fluorimetric assay described in Figure 6 has been used to confirm whether Peptide-Click-EVs could specifically bind EDB FN, compared to a third-party coating. In this case, only the secreted form of FN (Superfibronectin) was used as negative control. The binding of Peptide-Click-EVs and Scrambled-Click-EVs to EDB FN and Superfibronectin coatings was compared to the binding of free peptides. Peptide-Click-EVs significantly bound EDB FN in comparison to Scrambled-Click-EVs. Neither Peptide-Click-EVs nor Scrambled-Click-EVs bound to Superfibronectin (Fig. 7e). As previously reported (Figure 6), free peptide at both 30 μM and 10 μM concentrations was able to bind only ED-B FN, while the Scrambled peptide did not bind to EDB FN (Fig. 7e).

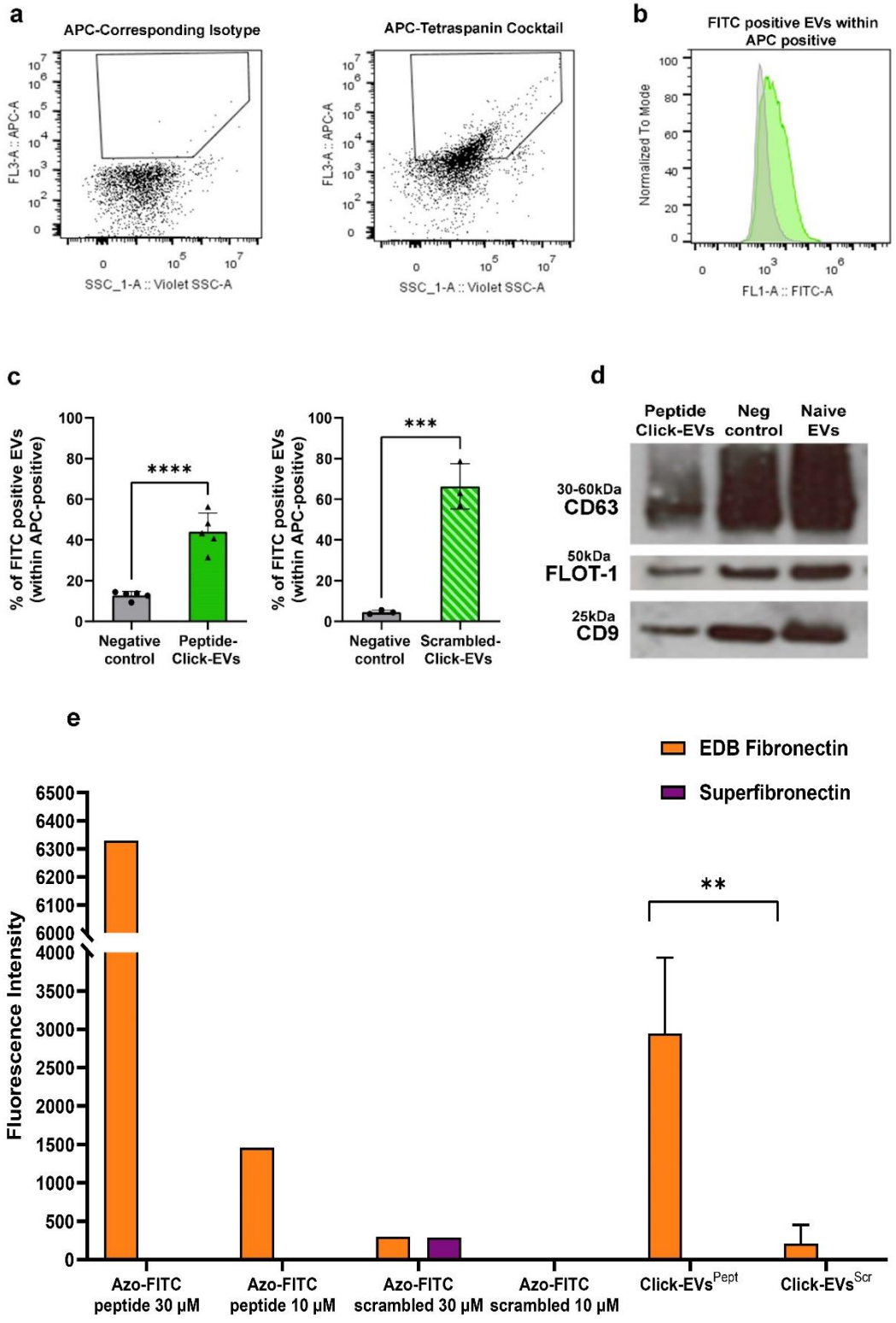

Figure 7. Efficiency of the click chemistry reaction with azo-FITC-peptide/scrambled, its effect on EV identity and targeting ability of Peptide/scrambled-Clicked-EVs. (**a**) Representative dot plot showing flow cytometry strategy used to evaluate the achievement of Peptide/scrambled-clicked EVs. EVs were stained with an APC-anti-tetraspanin cocktail antibodies and the corresponding isotype (left panel) represent the control sample for gating

APC-positive EVs (right panel). (**b**) Representative flow cytometry histogram of FITC-positive EVs within APC-positive events. Gray curve represents the negative control (EVs + azo-FITC-peptide) while the green one shows the Peptide-Click-EVs. (**c**) Histograms representing the percentages of FITC-positive EVs identified by flow cytometry for Peptide-Click EVs (N=5) and Scrambled-Click EVs (N=3). The percentages of FITC positive EVs is shown for Click-EVs (green columns) compared to the negative control (gray columns). Data are indicated as mean ± SD, **** $p < 0.0001$, *** $p < 0.001$ (Unpaired t test). (**d**) Western Blot analysis for the expression of the vesicle markers CD63, Flotillin-1 and CD9 in the three conditions: naïve EVs, negative control and Peptide-Click-EVs. (e)Fluorometric assay showing the fluorescence intensity of the peptide and the scrambled in the free form (10μM and 30μM) and the Peptide/scrambled-Clicked EVs bound to EDB-FN and super-FN. Data are indicated as mean ± SD, ** $p < 0.01$ (Ordinary two-way ANOVA).

7) A fluorescent Paclitaxel is useful for setting up a successful loading-strategy

Since sonication represents one of the most effective technique to load Paclitaxel within vesicles [127], we compared five different sonication protocols (from SONIC 1 to SONIC 5) to identify the one that could guarantee an efficient loading without affecting EV integrity. A fluorescent Paclitaxel (Pacific-Blue Paclitaxel, PB-PTX) was firstly used to evaluate EV loading by non-conventional flow cytometry. In the different sonication protocols, the concentrations of EVs and PB-PTX were the same. They differed in amplitude, type, and number of cycles (Fig. 8a, left panel). Sonicated vesiscles were stained by CFDA-SE and analyzed by FCM to evaluate the optimal sonication protocol (Fig. 8a). Among the others, we selected the method “SONIC 2” since it led to the lowest reduction in CFSE signal on sonicated EVswith around 30% reduction compared to naïve EVs (Fig. 8a, right panel). The efficiency and reproducibility of the selected loading method was evaluated by flow cytometry (Fig. 8b). No significant differences in CFSE signal before and after sonication were evidenced (Fig. 8b, left panel) and 30% of CFSE-positive EVs presented a positivity in the Pacific Blue channel, confirming the accomplishments of the drug loading (Fig. 8b, middle and right panel). To confirm these results, PB-PTX loaded EVs were also analyzed by super-resolution microscopy which revealed the presence of co-localization between CD63 and PB-PTX signals (Fig. 8c). Taken together, these data prove the ability of the selected sonication strategy to efficiently load EVs.

a

Method name	EV number	Amplitude	PB-PTX concentration	Type of cycle	Number of cycles
SONIC 1	10^{10}-10^{11}	20%	1uM	3'' on 3'' off 10' cooling	12
SONIC 2	10^{10}-10^{11}	20%	1uM	30'' on 30'' off 2' cooling	6
SONIC 3	10^{10}-10^{11}	50%	1uM	3'' on 3'' off 10' cooling	12
SONIC 4	10^{10}-10^{11}	50%	1uM	30'' on 30'' off 2' cooling	6
SONIC 5	10^{10}-10^{11}	20%	1uM	30'' on 30'' off 2' cooling	10

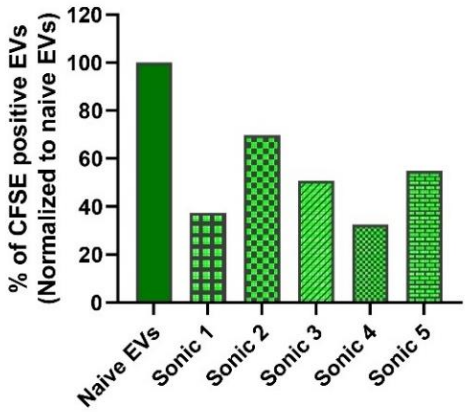

b

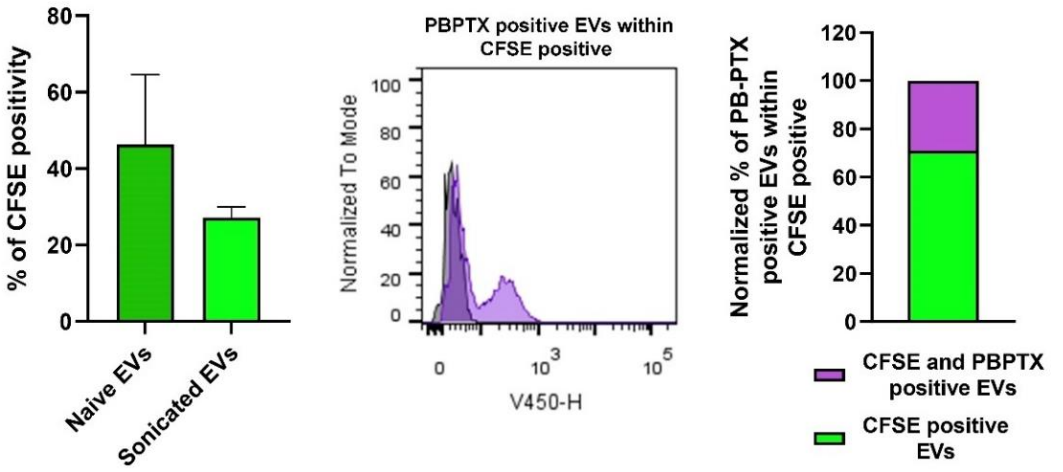

c

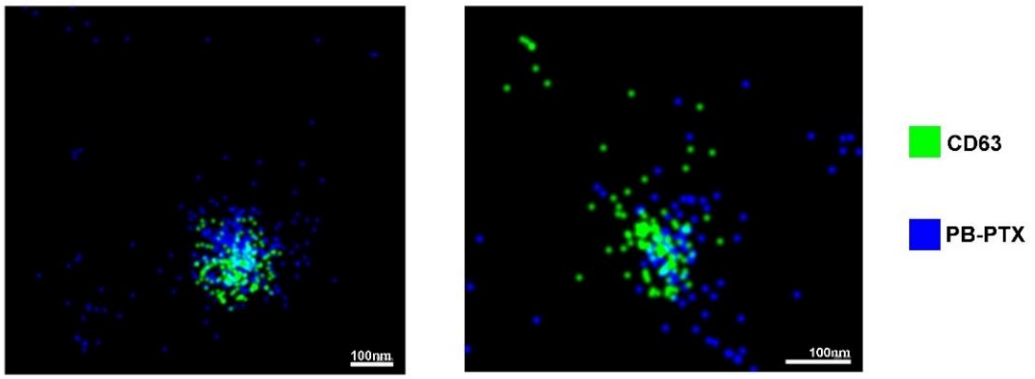

Figure 8. Loading sonication strategy assessment with fluorescent paclitaxel (PB-PTX). (**a**) Parameters applied for the five different sonication strategies (left panel). The histogram on the right panel indicates the variation in the percentage of CFSE-positive EVs after the application of the 5 different sonication methods. (**b**) The left histogram indicates the percentage of CFSE-positive EVs before (naïve EVs) and after sonication with the selected method. Middle panel shows a representative dot plot of PB-PTX positive EVs (purple area) compared to naïve EVs (gray area). The histogram on the right shows the normalized percentage of PB-PTX positive EVs within CFSE-positive

events. Data are indicated as mean ± SD. (c) Representative super resolution microscopy on PB-PTX loaded EVs showing a co-localization with the tetraspanin CD63.

8) Loaded EVs exert a cytotoxic effect on a cancer cell line

As already described in literature, the number of EVs (at least 10^{11}) to be used to obtain a successful and effective drug loading has to be carefully taken into consideration [65]. The loading efficiency was evaluated by a chromatographic technique (HPLC-MS) (Fig. 9a and b). The correct peak, corresponding to paclitaxel, was identified and confirmed through the comparison of the retention times and the mass spectra compared with the reference standard (Fig. 9a). The analysis showed that, compared to the starting Paclitaxel concentration (700uM), loaded EVs presented a concentration of 600nM which corresponds to a 0.1% of loading efficiency (Fig. 9b).

The cytotoxic potential of loaded EVs was then evaluated using a viability assay (MTT on MDA MB 231 cells), comparing the effects of loaded EVs with their naive (empty) counterpart at different concentrations (10^6/well, 10^7/well, and 10^8/well). Untreated cells were used as negative control (Fig. 9c). One-hundred μM, 1μM, and 0.1μM free Paclitaxel was added as an internal control to verify the efficacy of the chemotherapeutic drug. Interestingly, we observed that the highest concentrations of empty EVs (10^8 and 10^7/well) showed a significant intrinsic cytotoxic effect compared to untreated cells (control). However, 10^8 loaded EVs/well induced a significative cytotoxic effect compared to their empty counterpart, with a decrease of 60% in terms of cell viability. The other EV concentrations (10^6/well, 10^7/well) did not induce any cytotoxic effect (Fig. 9c). These results indicate that the loading efficiency is low, but sufficient to exert a cytotoxic effect when 10^8 loaded EVs/well are used.

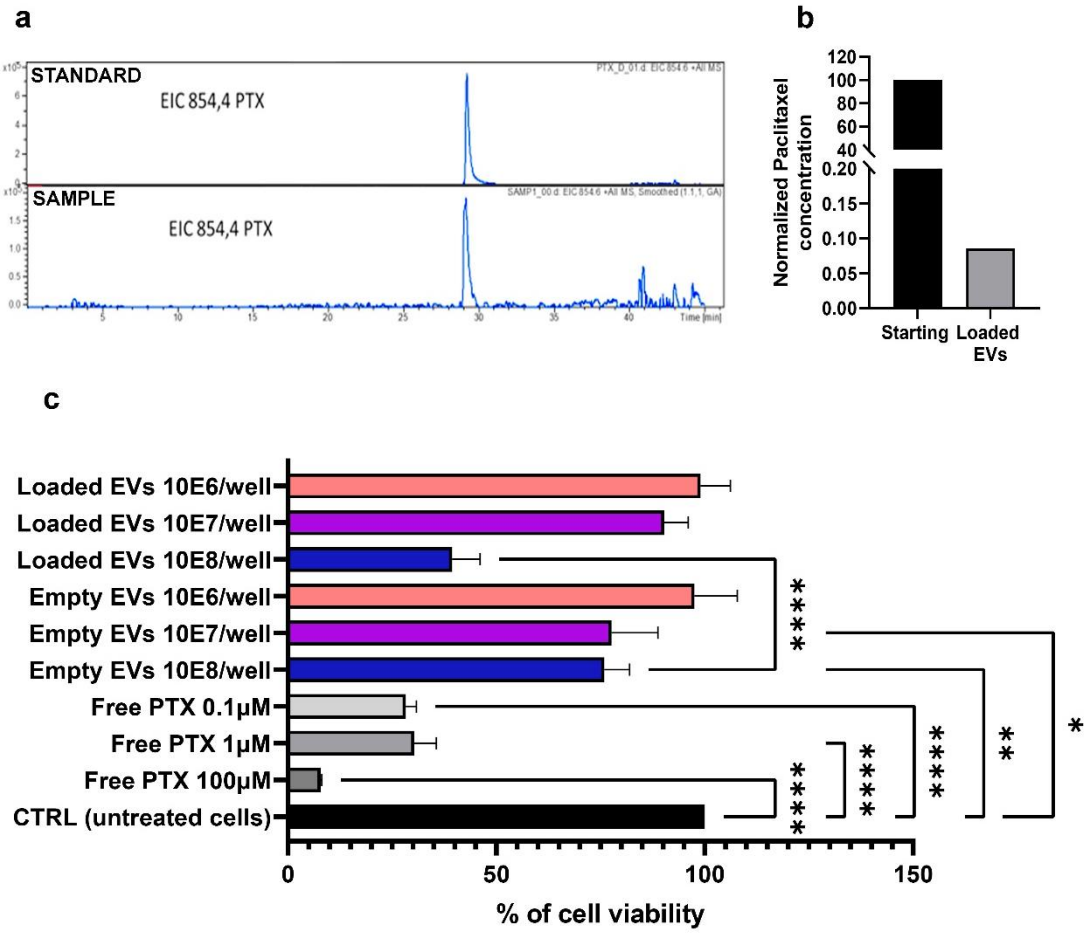

Figure 9. Evaluation of encapsulation efficiency by HPLC-MS and cytotoxic effect by MTT. (**a**) Extracted ion chromatogram (EIC) showing the mass and retention time of the standard (free Paclitaxel) compared to loaded EVs. (**b**) The histogram shows the encapsulation efficiency of loaded EVs normalized to the starting amount of Paclitaxel. (**c**) Effect of PTX-loaded EVs, empty EVs (at the same concentration/well) and free PTX on MDA-MB-231 viability by MTT assay. Data are indicated as mean ± SD, **** $p<0.0001$ ** $p < 0.01$, * $p<0.05$ (Ordinary two-way ANOVA).

Part II. The surface engineering and cargo loading protocols developed with plasma-EVs can be efficiently applied to nanoerythrosomes (NanoEs).

1) NanoE characterization

NanoE concentration and size distribution were analyzed by NTA (Fig. 10a, left panel). The isolation of NanoEs from 6mL of sonicated red blood cells (RBCs) allowed the recovery of 6.2 x 10^{12} ± 1.9 x 10^{12} vesicles (Fig. 10a, middle panel). The size distribution analysis revealed that NanoEs presented an average size (X50) of 145.9 ± 16.42nm, 10% of them were smaller than 76 ± 6.45nm and 90% of them were smaller than 275 ± 11.53nm (Fig. 10a, right panel). We then evaluated the capacity of NanoEs to be efficiently labelled with the luminal dyes CFSE and CTFR (Fig. 10b, c, and d). We firstly excluded the possible autofluorescence signal caused by the presence of hemoglobin on the two considered channels (Ch11 for APC signal, so for CTFR and Ch2 for FITC signal, so for CFSE; Ch6 represents the Side-Scatter) (Fig. 10b and 10c, left panels). Both CFTR and CFSE were able to efficiently stain NanoEs (45 ± 28% and 56 ± 12 % respectively) (Fig. 10b and 10c, right panels and 10d).
In addition, we estimated that 64 ± 22 % of CFSE-positive NanoEs expressed the erythrocyte marker CD235a (Glycophorin A) (Fig. 10e). These data showed that also NanoEs could be efficiently stained with the commonly used EV-dyes and as expected, expressed the typical RBC marker Glycophorin A. Electron microscopy (TEM) was used to evaluate EV size and morphology (Fig. 10f) showing the presence of the usual rounded biconcave EV-shape together with some NanoEs with a “tubular” aspect (Fig. 10f, left panel black arrows). The observed mean size was 247.5 ± 83.19nm (Fig. 10f, right panel).

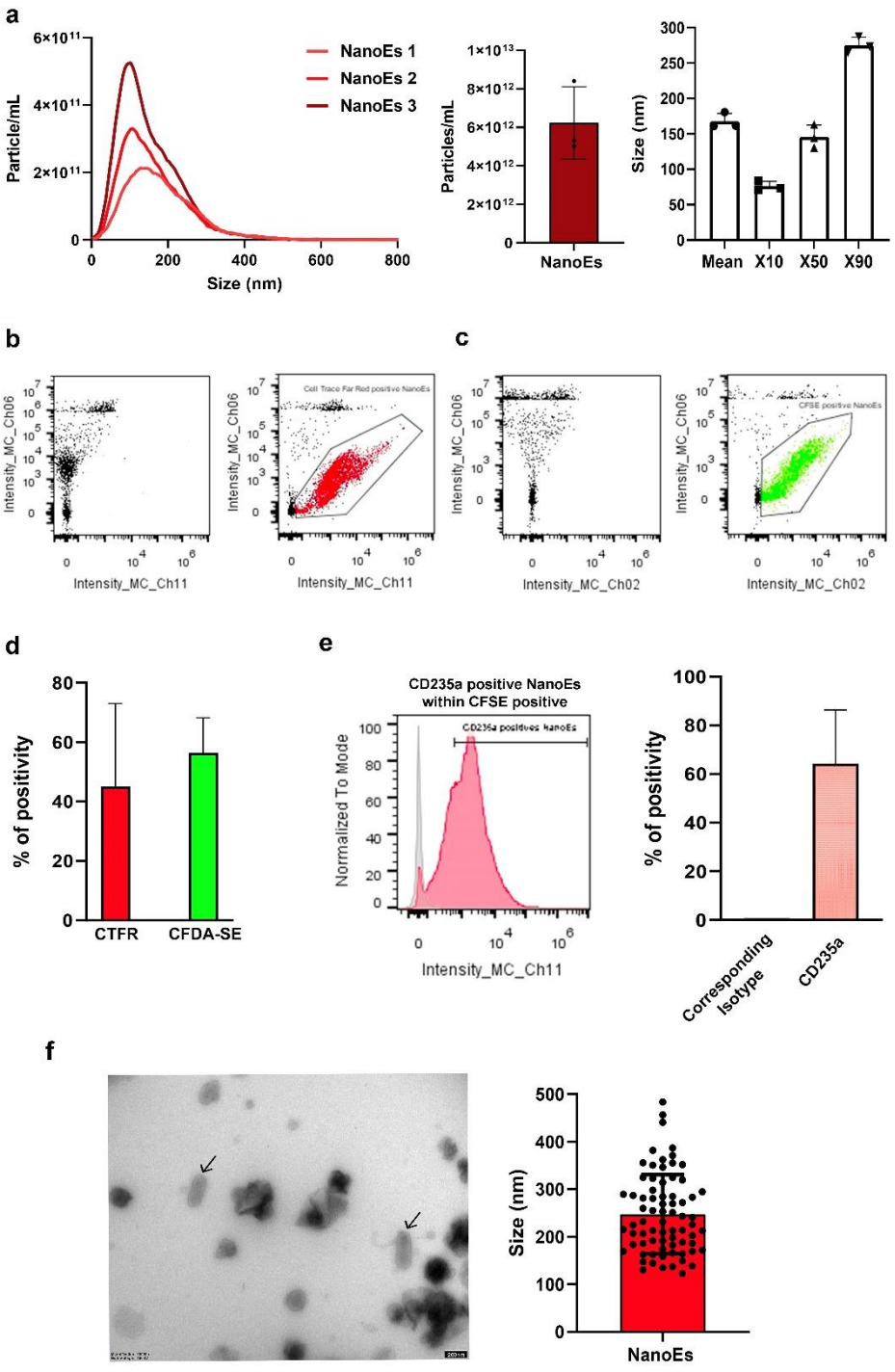

Figure 10. NanoE characterization. (**a**) Representative size distribution (left and right panel) and concentration (middle panel) by NTA (N=3). Data are represented as mean ± SD. (**b**) NanoE staining with CellTrace Far Red DDAO-SE (CTFR) and CFSE (**c**) analyzed by imaging flow cytometry (Amnis). Dot plots show the fluorescent signal (Ch11 for APC and Ch02 for FITC) vs side-scatter (Ch06) for unstained NanoEs (b, left panel; c, left panel), CTFR stained (b, right) and CFSE stained (c, right) NanoEs. (**d**) Histogram representing the percentage of CFSE and CTFR positive NanoEs (N=3). Data are represented as mean ± SD. (**e**) Representative imaging flow cytometry

analysis of CD235a positive NanoEs within CFSE positive (red area) compared to the corresponding control isotype (gray area) (left panel). The histogram on the right shows the percentage of CD235a positive NanoEs within CFSE positive events compared to the corresponding isotype control (N=4) Data are represented as mean ± SD. (**f**) Representative TEM images of NanoEs. Black arrows indicate the "tubular" shape. The mean size in the right panel refers to the diameters for rounded-shaped NanoEs and to the larger diameter for the tubular-shaped NanoEs.

2) NanoE membrane can be efficiently functionalized with the anti-EDB peptide

To functionalize NanoE surface with the fluorescein-conjugated anti-EDB-peptide, the same click chemistry protocol previously described for plasma-EVs has been applied. The click chemistry efficiency has been assessed by imaging flow cytometry. The percentage of FITC-positive clicked-NanoEs falling within the CFTR-positive events (Fig. 11a and 11b) was compared to the corresponding negative control represented by
NanoEs incubated with the peptide, without DBCO. Contrary to plasma-EVs (Fig. 7c), the peptide did not bind unspecifically to NanoEs in the negative control, while about 50% of clicked NanoEs were efficiently functionalized (Fig 11c, left panel).
The stability of Peptide-Click-NanoEs was evaluated by freezing and maintaining them for one week at -80°C. No variation in the FITC signal was observed in the thawed samples compared to the freshly isolated counterpart just described (Fig. 11c, middle panel). Moreover, a comparison, measured by fluorimetry, of the fluorescent signal associated to Peptide-Click-NanoEs with a standard curve constituted by different concentrations of peptide allowed us to evaluate the amount of conjugated peptide, expressed as molecules/mL, in Peptide-Click-NanoEs (Fig. 11d). The starting concentration of peptide used in the click chemistry reaction was 3.37×10^{16} molecules/mL and the peptide effectively conjugated to NanoE surface was $7.59 \times 10^{15} \pm 4.44 \times 10^{15}$ molecules/mL, which correspond to 22% of the total starting concentration (Fig. 11d). By crossing these data with NTA results, we estimated the mean quantity of peptide/NanoE (226 867 ± 84 499 molecules). Peptide-Clicked NanoEs expressed the typical erythrocyte markers BAND 3A and Glycophorin A (Fig. 11e).

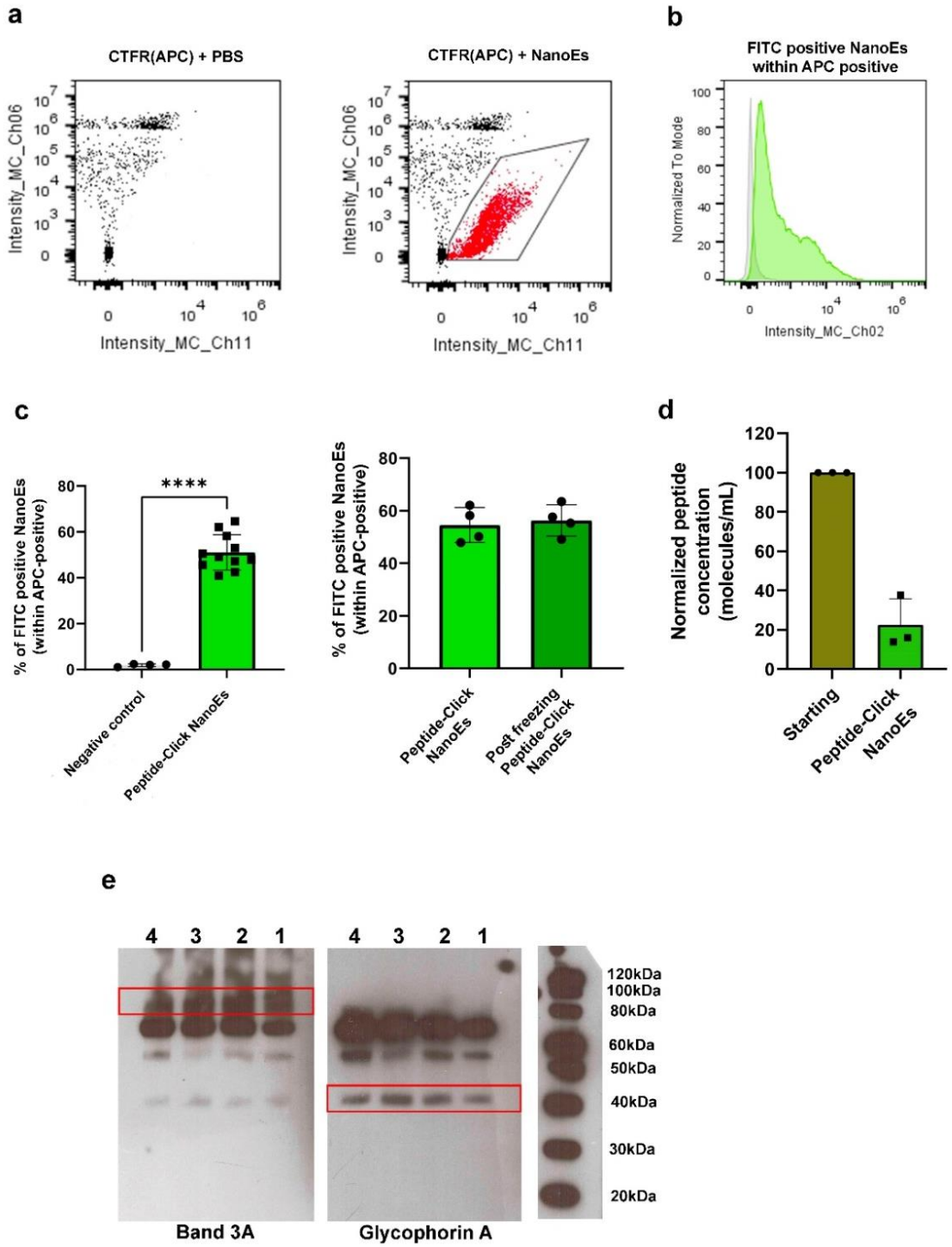

Figure 11. NanoE-surface functionalization with azo-FITC-peptide by click chemistry. (**a**) Imaging flow cytometry strategy for clicked NanoEs; vesicles are stained with CTFR before click chemistry procedures and APC-positive NanoEs (right panel) are gated based on the control represented by the visualization of the dye CTFR without NanoEs (left panel). (**b**) Representative imaging flow cytometry showing the FITC positive NanoEs within the APC-positive events (green area) compared to the negative control represented by NanoEs + azo-FITC-peptide without DBCO-NHS (grey area). (**c**) The percentage of FITC positive NanoEs in the Peptide-Click NanoEs compared to negative control is showed in the left panel (N=11). Data are presented as mean ± SD. ****p<0.0001 (Unpaired t

test). The middle histogram shows the percentage of Peptide-Click NanoEs after one week freezing at -80°C. (**d**) The histogram indicates the normalized peptide concentration (molecules/mL) in the starting mixture (NanoEs + DBCO + peptide) and in the purified Peptide-Click NanoEs. (**e**)Westen Blot showing the expression of Glycophorin A (CD235a) and BAND 3/A in naïve NanoEs (line 1) and Peptide-Click NanoEs in triplicate (line 2-3-4).

3) Peptide-Click NanoEs are successfully internalized by an EDB-FN expressing cancer cell line and showed higher uptake compared to Not-Click NanoEs

Once demonstrated that our click-chemistry protocol could work also on a different vesicle type, we performed in vitro functional studies to evaluate Peptide-Click-NanoE internalization efficiency by responder cells (MDA-MB-231) expressing EDB FN.
Firstly, EDB-FN expression on MDA-MB-231 cells was confirmed by confocal microscopy and flow cytometry (Fig. 12a and 12b). Six different incubation times (1h, 2h, 3h, 7h, 16, 24h) of CTFR-stained Peptide-Click-NanoEs and CTFR-stained Not-Click-NanoEs with the responder cells were considered.
Imaging flow cytometry analysis revealed that both experimental groups started to be internalized by responder cells after 2h incubation (MFI: 12 167.24 ± 8 589.44 and 16 705.87 ± 11 367.98 for Not-Click-NanoEs and Click NanoEs, respectively), reaching the highest MFI levels at 7h (81 653.01 ± 30 936.95 and 95 482 ± 40 275.01 for Not-Click-NanoEs and Click-NanoEs, respectively) with a progressive decrease after this time point up to 24h (35 097.68 ± 6 589.44 and 40 970.46 ± 12 029.39 for Not-Click-NanoEs and Click-NanoEs, respectively) (Fig. 12c, left panel). Interestingly, a higher amount of Peptide-Click-NanoEs was internalized compared to the Not-Clicked ones, especially at the earliest time points (Fig. 12c, left panel), suggesting that NanoE surface functionalization with the anti-EDB-FN peptide could enhance their uptake. In addition, imaging flow cytometry allowed us to appreciate, at single cell level, the co-expression of the APC (from CTFR) and FITC (from peptide) signals in Peptide-Click-NanoEs (Fig 12c, bottom right panels).
The Peptide-Click-NanoEs internalization after 3h incubation with MDA-MB-231 cells was also tested by microscopy, confirming the vesicle uptake evaluating the co-localization of CTFR and FITC signals (Fig. 12d). Taken together, these data indicate that the click chemistry procedure positively affect the NanoE uptake by EDB-expressing cells, being able to enhance their internalization.

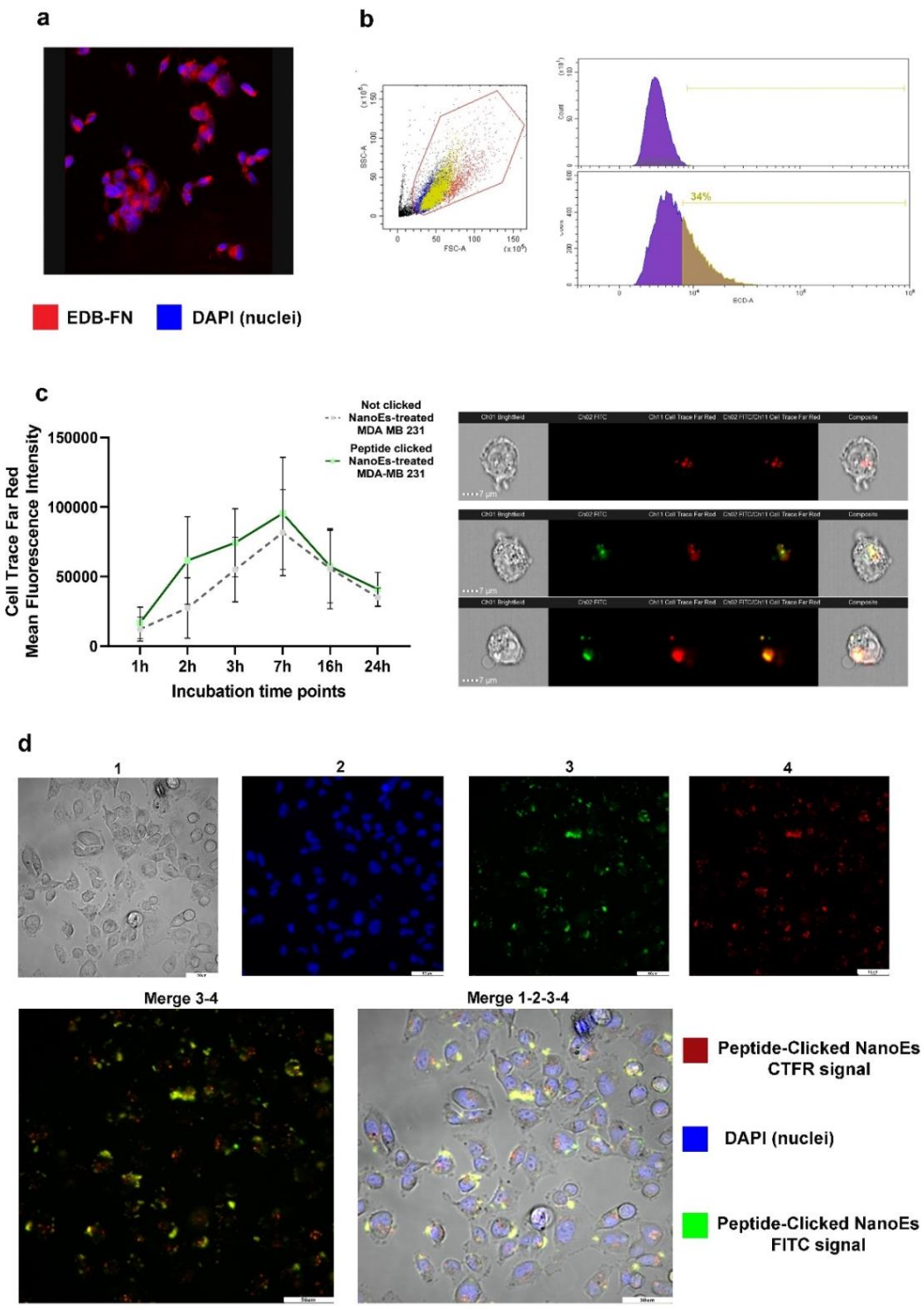

Figure 12. Functional studies for EDB-FN targeting with Peptide-Clicked NanoEs. (**a**) Representative confocal image of MDA-MB-231cells showing the expression of EDB-FN. (**b**) Representative flow cytometry on MDA-MB-231 cells showing EDB-FN expression. (**c**) Imaging flow cytometry on not clicked NanoEs-treated (left panel, gray line) and Peptide-Clicked NanoEs-treated (left panel, green line) MDA-MB-231 at six incubation time points. The x-axis shows the time points, the y-axis shows the Mean Fluorescence Intensity (MFI) on Ch11(APC) of cells after treatments. The right panel shows the representative images (upper panel: Not Clicked NanoEs treated cells; middle and bottom panels: Peptide-Clicked NanoEs treated cells; for both, at 3h incubation) at single cell level in brightfield,

Ch02 (FITC), Ch11 (APC) and the overlay of the three analyzed channels. (**d**) Representative image of MDA-MB-231 incubated for 3h with Peptide-Click NanoEs (live cell imaging). Single channels (1: brightfield, 2: DAPI,3: FITC,4: APC) and the merge of channels 3-4 and 1-2-3-4 are represented.

4) The PTX loading efficiency is higher in NanoEs compared to plasma-EVs and loaded NanoEs exert a cytotoxic effect only due to their therapeutic cargo

HPLC-MS technique was again used to measure. the paclitaxel encapsulation efficiency in NanoEs. Following the same principle above described, the correct peak, corresponding to paclitaxel, was identified and confirmed through the comparison of both, the retention times and the mass spectra with the reference standard (Fig. 12a). When the loading reaction, based on the protocol SONIC 2 previously described, was performed with 1 x 10^{11} NanoEs and 700μM PTX, the concentration of drug within NanoEs was 10.38 ± 9.51 μM (Fig. 13b), representing the 1.5% of the starting PTX concentration.

The cytotoxic effect of loaded NanoEs at different concentrations (10^6/well, 10^7/well, and 10^8/well) has been compared to effect exerted by non-loaded NanoEs at the same concentrations (Empty NanoEs) and by free PTX at three different concentrations (0.1μM, 1μM and 100μM). Untreated cells were used as positive control and normalizing factor. Interestingly, contrary to plasma-EVs, empty NanoEs didn't affect cell viability at any given concentration, and a significant cytotoxic effect was observed when cells were treated with the higher concentration (10^8/well), showing a reduction of cell viability of 54% reduction compared to the corresponding concentration of empty NanoEs (Fig. 13c). These data indicate that NanoEs can be loaded more efficiently than plasma-EVs and they are able to significantly reduce cell viability when used at a specific concentration (10^8/well). Moreover, contrary to plasma-EVs, their cytotoxic effect is completely due to their therapeutic cargo.

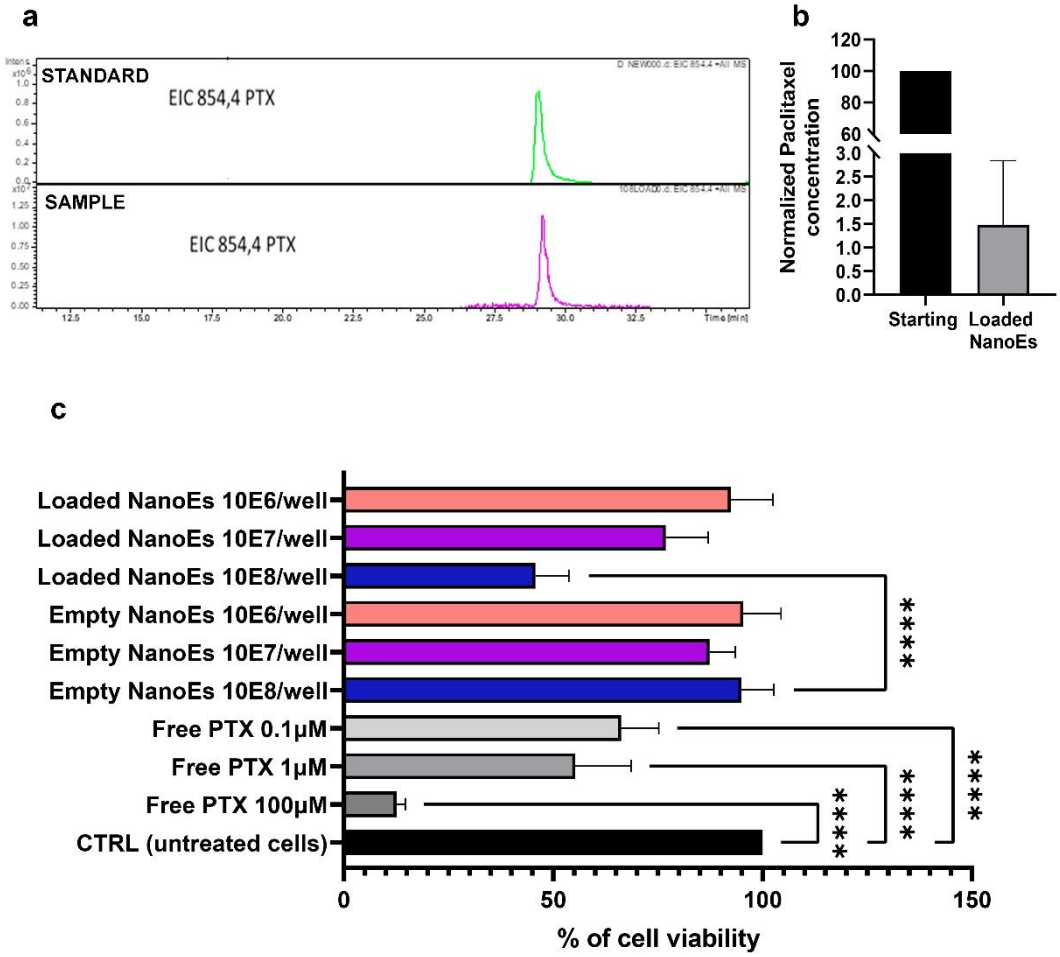

Figure 13. Evaluation of NanoE encapsulation efficiency by HPLC-MS and cytotoxic effect by MTT.
(**a**) Extracted ion chromatogram (EIC) showing the mass and retention time of the standard (free Paclitaxel) compared to loaded EVs. (**b**) The histograms shows the encapsulation efficiency of loaded EVs normalized to the starting Paclitaxel concentration. (**c**) Effect of PTX-loaded EVs, empty EVs (at the same concentration/well) and free PTX on MDA-MB-231 viability by MTT assay. Data are indicated as mean ± SD, **** $p<0.0001$ (Ordinary two-way ANOVA).

DISCUSSION

All cell types possess the universally shared biological property to release extracellular vesicles, that are involved in intercellular communication by transferring bioactive molecules, including proteins, nucleic acids, and lipids [128]. This intrinsic function makes EVs an attractive option for targeted drug delivery, as they can be engineered to carry therapeutic agents to specific target cells or tissues [129]. In comparison with conventional drug-delivery systems, drug administration using natural nanoparticles possesses several advantages, such as an enhanced permeability and retention effect which can allow passive targeting and accumulation at the pathological sites [11], an improved active concentration and bioavailability [12], and a theoretically increased safety and efficacy [13]. In addition, the modification of the EV surface with targeting ligands, such as antibodies or peptides, can enhance their specificity and delivery efficiency, thus potentially reducing adverse side effects [130]. Nowadays, all commercially available nanoparticle-related therapeutics are based on the artificial ones, especially liposomes, with about 14 liposomal products authorized by FDA and EMA [17]. Similarities and differences between liposomes and natural nanoparticles, particularly in protein and lipid composition, are under discussion [24], [25], [98]. Low immunological response [131], targeting potential [132], and ability to cross various biological barriers [19]–[23] emerge as the most considerable advantages of using natural EVs as drug delivery vehicles. It has been demonstrated that cancer-derived EVs show a tissue tropism also at the early stages of neoplastic transformation[29], and that the transplantation of autologous EVs can be used for cancer-specific targeting [30]. It's probably the asymmetrical lipid distribution and specific protein composition of EV membranes the main reason of their peculiar organotropism and homing ability [23][28]. Based on this evidence, biofluids, and in particular blood, would represent an ideal source of EVs to be functionalized for targeted drug delivery or diagnostic purposes. However, it has to be taken into account that plasma is one of the most difficult body fluids to isolate EVs from, due to the presence of a massive pattern of particles [133]. Plasma proteins and protein aggregates, as well as the large set of lipidic nanoparticles, represent the most abundant contaminants [134]. The commonly used methods to separate plasma-EVs are based on size or density. It has been recently observed that combining these two isolation strategies it is possible to remove the great majority of lipoproteins [56]. However, this combined strategy profoundly affects the yield, an important parameter to be considered when EVs have to be applied in downstream procedures which require a high number of vesicles. To adopt the isolation strategy which could allow us to obtain a sufficient amount of pure EVs, we compared three different procedures: a size- (based on size exclusion chromatography, SEC), a sedimentation rate- (sucrose cushion ultracentrifugation, sUC) and a combination of size- and

density- (IDC+SEC) based protocol. The sUC strategy, which has been in the past efficiently used for EV-isolation from conditioned media [61] and, more recently, also successfully applied to isolate EVs from plasma [120] turned out to be the method with the optimal balance between purity and yield.

The main goal of this work was to produce engineered EVs which could reach the tumor microenvironment. In particular, our target is represented by the extracellular matrix oncofetal variant of fibronectin, called ED-B, whose expression, in the adult life, is only associated to wound healing events and cancer. Targeting an antigen as ED-B, which is expressed by the newly synthesized perivascular areas of the stromal matrix in a wide range of tumor types, will lead to the development of strategies not specifically limited to a single kind of tumor, but exploitable as innovative therapeutic platform easily translatable to different oncological applications. In addition, over the past two decades, the role of fibronectin (FN) in cancer has been recognized and FN-targeting strategies have been evaluated as promising anti-cancer approaches.

We adopted a copper-free click chemistry strategy to functionalize the EV membrane, based on the azide-alkyne Huisgen cycloaddition. One of the most notable advantages of employing a copper-free click chemistry approach over traditional methods involving copper ions is the remarkable enhancement in biocompatibility. Copper ions, while effective catalysts, are inherently toxic to cells/EVs and can compromise the integrity of sensitive biological structures. Copper-free click chemistry eliminates this concern, ensuring minimal cytotoxicity and preserving the viability and functionality of the biological systems. Furthermore, copper-free click chemistry methods are highly selective and do not suffer from the non-specific reactions often observed in copper-catalyzed systems. This selectivity is crucial in complex biological environments where a myriad of functional groups coexist. Another advantage lies in the broader scope of clickable substrates achievable with copper-free strategies. Copper-catalyzed methods are limited by the requirement for functional groups that are stable in the presence of copper ions. In contrast, copper-free click chemistry allows for the labeling of a wider array of biomolecules and materials, expanding the possibilities for diverse applications [37] [38] [137] [138]. This enables the precise modification of EV membranes without compromising their native properties, thereby enhancing their therapeutic potential and targeting capabilities. As a proof of concept, a fluorescent azide, has been adopted during the first phase of the study to functionalize the EV membranes, allowing the tracking and easy visualization of the incorporated molecule onto the EV membrane. The use of this proof-of-concept molecule provided a convenient and reliable method to assess the efficiency and homogeneity of the functionalization process. Moreover, the fluorescent azide served as a model molecule, enabling us to validate the applicability and efficacy of our EV membrane functionalization protocol. The whole procedure turned out to be successful without interfering with the EV integrity and

identity. As a drawback, the whole procedure profoundly affected the EV number. This further emphasizes the importance of selecting an isolation protocol that allows the recovery of a sufficient number of vesicles.

There is no consensus regarding the mode of EV uptake, which could be receptor-dependent or not. Moreover, the fate of EV within the recipient cell is not clearly characterized and strictly dependent on both the EV and recipient cell type. Only recently it has been proposed that the EV cargo could be released in the cytosol, degraded within lysosomes or re-secreted through recycling within newly formed EVs, exploiting the endosomal compartment of the target cells [139]. By incubating click-EVs with responder cells, we focused on the analysis of two aspects: the timing of the uptake and their recycling route into cells. We could confirm not only that clicked-EVs were efficiently internalized, transferring their fluorescent signal, by recipient cells, but also that they partially followed the same endosomal recycling route followed by naive EVs. Although EDB-FN-specific antibodies have been developed in the past [114]–[117], they are expensive to manufacture and show poor tissue penetration due to a combination of large size and high affinity. On the other hand, homing peptides are advantageous in terms of low immunogenicity, versatility in chemical modification, and cost-effective production. They also possess rapid extravasation and high tissue penetrating ability in the context of tumor targeting [47] [48]. With this in mind, we synthesized an azo-modified and fluorescent anti-ED-B FN peptide which could be tied to EV membrane by the copper-free click chemistry strategy above described. Furthermore, a scrambled peptide was synthesized to evaluate the target specificity of the anti-ED-B FN peptide and to evaluate whether the functionalization procedures could affect such targeting specificity. We confirmed that the azo-FITC-peptide, either in its free- and EV-conjugated form, was able to specifically target ED-B FN.

The membrane-engineering procedure with the azo-FITC-peptide by click chemistry was firstly applied to plasma-EVs and then successfully translated to artificially produced red blood cell-derived EVs (RBC-EVs), the so-called nanoerythrosomes (NanoEs). The use of RBC-EVs as drug delivery vehicles presents a significant advancement in targeted therapy compared to plasma-EVs. First and foremost, RBC-EVs exhibit enhanced stability and prolonged circulation in the bloodstream due to their natural origin, which significantly reduces the risk of rapid clearance or degradation, common limitations associated with plasma-EVs. Moreover, RBC-EVs have a remarkable biocompatibility profile, minimizing the potential for adverse reactions or immune responses upon administration. Additionally, RBC-EVs offer a customizable surface for functionalization, enabling precise modification with ligands or antibodies that enhance their specificity towards target cells or tissues. This specificity is crucial in achieving targeted drug delivery, minimizing off-target effects, while maximizing therapeutic efficacy. Quality control experiments on NanoE identity and integrity maintenance upon functionalization have been conducted, confirming, as for plasma-EVs, the effectiveness of the proposed methodology.

Interestingly, we observed a lower unspecific binding of the peptide to NanoE surface, compared to plasma-EVs, which make the functionalization more efficient when using NanoEs. As recently demonstrated, this effect can be due to a possible role of the protein corona [92]. The close interaction with the set of proteins and factors inside aqueous phases leads to the formation, in biofluids, of a proteinaceous layer on the EV surface via electrostatic interactions and protein aggregation [140]. This layer has been defined "EV-protein corona". The different production-way of the two examined EV types, one naturally released in the blood stream and the other, artificially derived from purified RBCs, could hypothetically results in the presence of a massive protein corona in plasma-EVs and, on the contrary, in its possible absence, or reduced presence, in NanoEs. Furthermore, after confirming ED-B expression on MDA MB 231 cells, we performed functional studies to evaluate the differences between Peptide-Click-NanoE and not clicked (naïve) NanoE internalization. As already demonstrated for PL1-coupled artificial nanoparticles [141], we observed that the presence of the anti-ED-B peptide on NanoE-membrane enhanced their cellular uptake.

Based on their physico-chemical properties, especially hydrophobicity, therapeutic agents can be loaded into EVs through different methods. They are generally grouped into passive and active encapsulation. Passive loading approaches (mainly co-incubation) are relatively simple and do not require any particular stimulus or addiction of active substances. On the contrary, active strategies, like sonication, electroporation, freeze and thaw cycles and transient permeabilization with saponins, aim to increase EV-membrane permeability [95]. According to literature, sonication is the method that allows a more efficient loading of the chemotherapy drug Paclitaxel [142]. Consequently, we developed a standardized and reproducible sonication-based strategy for Paclitaxel encapsulation onto both plasma-EVs and NanoEs. Thanks to high performance liquid chromatography and mass spectrometry (HPLC-MS) techniques we were able to quantify the encapsulated drug amount. Although we observed that the amount of loaded drug was greater in NanoEs compared to plasma-EVs, in both cases the loading efficiency was not particularly high. However, the amount of drug encapsulated within EVs was sufficient to exert a significant cytotoxic effect against tumor cells.

Taken together, our results indicate that it has been possible to develop standardized methods to engineer natural EVs. Moreover, our study points out that the use of RBC-EVs as targetable drug delivery vehicles represents a promising approach, offering superior stability, biocompatibility, surface customization, and payload capacity when compared to plasma-EVs, thereby revolutionizing the field of targeted drug delivery and advancing the possibilities of precision medicine.

CONCLUSIONS

Targeting a tumor microenvironment antigen as ED-B, which is expressed in a wide range of tumor types, allows the development of therapies not specifically limited to a single kind of tumor, but to different oncological applications. Copper-free click chemistry and sonication have been effective approaches for EV surface functionalization and therapeutic encapsulation, respectively. Although further *in vitro* and *in vivo* experiments need to be performed, the development of these protocols, and especially their standardization, opens the way to possible applications in either an autologous and an heterologous context.

REFERENCES

[1] S. Bayda, M. Adeel, T. Tuccinardi, M. Cordani, and F. Rizzolio, "The History of Nanoscience and Nanotechnology: From Chemical–Physical Applications to Nanomedicine," *Mol. 2020, Vol. 25, Page 112*, vol. 25, no. 1, p. 112, Dec. 2019, doi: 10.3390/MOLECULES25010112.

[2] C. Kinnear, T. L. Moore, L. Rodriguez-Lorenzo, B. Rothen-Rutishauser, and A. Petri-Fink, "Form Follows Function: Nanoparticle Shape and Its Implications for Nanomedicine," *Chem. Rev.*, vol. 117, no. 17, pp. 11476–11521, Sep. 2017, doi: 10.1021/ACS.CHEMREV.7B00194/ASSET/IMAGES/MEDIUM/CR-2017-001946_0019.GIF.

[3] V. Weissig, T. K. Pettinger, and N. Murdock, "Nanopharmaceuticals (part 1): products on the market," *Int. J. Nanomedicine*, vol. 9, no. 1, pp. 4357–4373, Sep. 2014, doi: 10.2147/IJN.S46900.

[4] G. Gregoriadis, "The carrier potential of liposomes in biology and medicine (second of two parts)," *N. Engl. J. Med.*, vol. 295, no. 14, pp. 765–770, Sep. 1976, doi: 10.1056/NEJM197609302951406.

[5] M. Q. Zhang and B. Wilkinson, "Drug discovery beyond the 'rule-of-five,'" *Curr. Opin. Biotechnol.*, vol. 18, no. 6, pp. 478–488, Dec. 2007, doi: 10.1016/J.COPBIO.2007.10.005.

[6] P. P. Ige, R. K. Baria, and S. G. Gattani, "Fabrication of fenofibrate nanocrystals by probe sonication method for enhancement of dissolution rate and oral bioavailability," *Colloids Surfaces B Biointerfaces*, vol. 108, pp. 366–373, Aug. 2013, doi: 10.1016/J.COLSURFB.2013.02.043.

[7] A. D. Bangham, M. M. Standish, and J. C. Watkins, "Diffusion of univalent ions across the lamellae of swollen phospholipids," *J. Mol. Biol.*, vol. 13, no. 1, pp. 238-IN27, Aug.

1965, doi: 10.1016/S0022-2836(65)80093-6.

[8] J. J. Marty, R. C. Oppenheim, and P. Speiser, “Nanoparticles--a new colloidal drug delivery system.,” *Pharm. Acta Helv.*, vol. 53, no. 1, pp. 17–23, 1978.

[9] A. Babu, A. K. Templeton, A. Munshi, and R. Ramesh, “Nanodrug delivery systems: A promising technology for detection, diagnosis, and treatment of cancer,” *AAPS PharmSciTech*, vol. 15, no. 3, pp. 709–721, Feb. 2014, doi: 10.1208/S12249-014-0089-8/METRICS.

[10] F. Farjadian, A. Ghasemi, O. Gohari, A. Roointan, M. Karimi, and M. R. Hamblin, “Nanopharmaceuticals and nanomedicines currently on the market: Challenges and opportunities,” *Nanomedicine*, vol. 14, no. 1, pp. 93–126, Jan. 2019, doi: 10.2217/NNM-2018-0120.

[11] T. C. Yih and M. Al-Fandi, “Engineered nanoparticles as precise drug delivery systems,” *J. Cell. Biochem.*, vol. 97, no. 6, pp. 1184–1190, Apr. 2006, doi: 10.1002/JCB.20796.

[12] K. Balakumar, C. V. Raghavan, N. T. selvan, R. H. prasad, and S. Abdu, “Self nanoemulsifying drug delivery system (SNEDDS) of rosuvastatin calcium: design, formulation, bioavailability and pharmacokinetic evaluation.,” *Colloids Surf. B. Biointerfaces*, vol. 112, pp. 337–343, Aug. 2013, doi: 10.1016/J.COLSURFB.2013.08.025.

[13] M. Karimi, P. Sahandi Zangabad, S. Baghaee-Ravari, M. Ghazadeh, H. Mirshekari, and M. R. Hamblin, “Smart Nanostructures for Cargo Delivery: Uncaging and Activating by Light,” *J. Am. Chem. Soc.*, vol. 139, no. 13, pp. 4584–4610, Apr. 2017, doi: 10.1021/JACS.6B08313.

[14] T. Tian *et al.*, “Surface functionalized exosomes as targeted drug delivery vehicles for cerebral ischemia therapy,” *Biomaterials*, vol. 150, pp. 137–149, Jan. 2018, doi: 10.1016/J.BIOMATERIALS.2017.10.012.

[15] R. S. Kadam, D. W. A. Bourne, and U. B. Kompella, “Nano-advantage in enhanced drug delivery with biodegradable nanoparticles: contribution of reduced clearance,” *Drug Metab. Dispos.*, vol. 40, no. 7, pp. 1380–1388, Jul. 2012, doi: 10.1124/DMD.112.044925.

[16] A. A. Yetisgin, S. Cetinel, M. Zuvin, A. Kosar, and O. Kutlu, “molecules Therapeutic Nanoparticles and Their Targeted Delivery Applications”, doi: 10.3390/molecules25092193.

[17] P. Liu, G. Chen, and J. Zhang, “A Review of Liposomes as a Drug Delivery System: Current Status of Approved Products, Regulatory Environments, and Future Perspectives,” *Mol. 2022, Vol. 27, Page 1372*, vol. 27, no. 4, p. 1372, Feb. 2022, doi: 10.3390/MOLECULES27041372.

[18] X. T. T. Dang, J. M. Kavishka, D. X. Zhang, M. Pirisinu, and M. T. N. Le, “Extracellular

Vesicles as an Efficient and Versatile System for Drug Delivery," *Cells 2020, Vol. 9, Page 2191*, vol. 9, no. 10, p. 2191, Sep. 2020, doi: 10.3390/CELLS9102191.

[19] R. O. Elliott and M. He, "Unlocking the Power of Exosomes for Crossing Biological Barriers in Drug Delivery," *Pharmaceutics*, vol. 13, no. 1, pp. 1–20, 2021, doi: 10.3390/PHARMACEUTICS13010122.

[20] Y. Liu *et al.*, "Targeted exosome-mediated delivery of opioid receptor Mu siRNA for the treatment of morphine relapse," *Sci. Reports 2015 51*, vol. 5, no. 1, pp. 1–10, Dec. 2015, doi: 10.1038/srep17543.

[21] L. Alvarez-Erviti, Y. Seow, H. Yin, C. Betts, S. Lakhal, and M. J. A. Wood, "Delivery of siRNA to the mouse brain by systemic injection of targeted exosomes," *Nat. Biotechnol. 2011 294*, vol. 29, no. 4, pp. 341–345, Mar. 2011, doi: 10.1038/nbt.1807.

[22] H. M. van Dongen, N. Masoumi, K. W. Witwer, and D. M. Pegtel, "Extracellular Vesicles Exploit Viral Entry Routes for Cargo Delivery," *Microbiol. Mol. Biol. Rev.*, vol. 80, no. 2, pp. 369–386, Jun. 2016, doi: 10.1128/MMBR.00063-15/ASSET/E1AA4912-2C3C-4A17-AC61-D7E54B666578/ASSETS/GRAPHIC/ZMR0021624160007.JPEG.

[23] G. Pedrioli, E. Piovesana, E. Vacchi, and C. Balbi, "Extracellular Vesicles as Promising Carriers in Drug Delivery: Considerations from a Cell Biologist's Perspective," *Biology (Basel).*, vol. 10, no. 5, May 2021, doi: 10.3390/BIOLOGY10050376.

[24] L. van der Koog, T. B. Gandek, and A. Nagelkerke, "Liposomes and Extracellular Vesicles as Drug Delivery Systems: A Comparison of Composition, Pharmacokinetics, and Functionalization," *Adv. Healthc. Mater.*, vol. 11, no. 5, p. 2100639, Mar. 2022, doi: 10.1002/ADHM.202100639.

[25] O. M. Elsharkasy *et al.*, "Extracellular vesicles as drug delivery systems: Why and how?," *Adv. Drug Deliv. Rev.*, vol. 159, pp. 332–343, Jan. 2020, doi: 10.1016/J.ADDR.2020.04.004.

[26] I. Gaurav, A. Thakur, A. Iyaswamy, X. Wang, X. Chen, and Z. Yang, "Factors Affecting Extracellular Vesicles Based Drug Delivery Systems," *Mol. 2021, Vol. 26, Page 1544*, vol. 26, no. 6, p. 1544, Mar. 2021, doi: 10.3390/MOLECULES26061544.

[27] O. G. De Jong *et al.*, "Drug Delivery with Extracellular Vesicles: From Imagination to Innovation," *Acc. Chem. Res.*, vol. 52, no. 7, pp. 1761–1770, Jul. 2019, doi: 10.1021/ACS.ACCOUNTS.9B00109/ASSET/IMAGES/LARGE/AR-2019-00109Z_0003.JPEG.

[28] S. G. Antimisiaris, S. Mourtas, and A. Marazioti, "Exosomes and Exosome-Inspired Vesicles for Targeted Drug Delivery," *Pharm. 2018, Vol. 10, Page 218*, vol. 10, no. 4, p. 218, Nov. 2018, doi: 10.3390/PHARMACEUTICS10040218.

[29] M. Garofalo *et al.*, "Cancer-derived EVs show tropism for tissues at early stage of neoplastic transformation," *Nanotheranostics*, vol. 5, no. 1, pp. 1–7, 2021, doi:

10.7150/NTNO.47226.

[30] A. Villa *et al.*, “Transplantation of autologous extracellular vesicles for cancer-specific targeting,” *Theranostics*, vol. 11, no. 5, pp. 2034–2047, Jan. 2021, doi: 10.7150/THNO.51344.

[31] W. Chiangjong, P. Netsirisawan, S. Hongeng, and S. Chutipongtanate, “Red Blood Cell Extracellular Vesicle-Based Drug Delivery: Challenges and Opportunities,” *Front. Med.*, vol. 8, p. 761362, Dec. 2021, doi: 10.3389/FMED.2021.761362.

[32] J. S. Schorey, Y. Cheng, P. P. Singh, and V. L. Smith, “Exosomes and other extracellular vesicles in host-pathogen interactions,” *EMBO Rep.*, vol. 16, no. 1, pp. 24–43, Jan. 2015, doi: 10.15252/EMBR.201439363.

[33] B. L. Deatheragea and B. T. Cooksona, “Membrane vesicle release in bacteria, eukaryotes, and archaea: A conserved yet underappreciated aspect of microbial life,” *Infect. Immun.*, vol. 80, no. 6, pp. 1948–1957, Jun. 2012, doi: 10.1128/IAI.06014-11.

[34] D. G. Robinson, Y. Ding, and L. Jiang, “Unconventional protein secretion in plants: a critical assessment,” *Protoplasma*, vol. 253, no. 1, pp. 31–43, Jan. 2016, doi: 10.1007/S00709-015-0887-1.

[35] E. Chargaff and R. West, “The biological significance of the thromboplastic protein of blood.,” *J. Biol. Chem.*, 1946.

[36] P. Wolf, “The Nature and Significance of Platelet Products in Human Plasma,” *Br. J. Haematol.*, vol. 13, no. 3, pp. 269–288, May 1967, doi: 10.1111/J.1365-2141.1967.TB08741.X.

[37] J. Ratajczak *et al.*, “Embryonic stem cell-derived microvesicles reprogram hematopoietic progenitors: Evidence for horizontal transfer of mRNA and protein delivery,” *Leukemia*, vol. 20, no. 5, pp. 847–856, 2006, doi: 10.1038/SJ.LEU.2404132.

[38] H. Valadi, K. Ekström, A. Bossios, M. Sjöstrand, J. J. Lee, and J. O. Lötvall, “Exosome-mediated transfer of mRNAs and microRNAs is a novel mechanism of genetic exchange between cells,” *Nat. Cell Biol. 2007 96*, vol. 9, no. 6, pp. 654–659, May 2007, doi: 10.1038/ncb1596.

[39] M. Yáñez-Mó *et al.*, “Biological properties of extracellular vesicles and their physiological functions,” *J. Extracell. Vesicles*, vol. 4, no. 2015, pp. 1–60, 2015, doi: 10.3402/JEV.V4.27066.

[40] C. Théry *et al.*, “Minimal information for studies of extracellular vesicles 2018 (MISEV2018): a position statement of the International Society for Extracellular Vesicles and update of the MISEV2014 guidelines,” *J. Extracell. Vesicles*, vol. 7, no. 1, p. 1535750, Dec. 2018, doi: 10.1080/20013078.2018.1535750.

[41] G. Van Niel, G. D’Angelo, and G. Raposo, “Shedding light on the cell biology of extracellular vesicles,” *Nat. Rev. Mol. Cell Biol.*, vol. 19, no. 4, pp. 213–228, Apr. 2018,

doi: 10.1038/NRM.2017.125.

[42] A. Lo Cicero, P. D. Stahl, and G. Raposo, "Extracellular vesicles shuffling intercellular messages: For good or for bad," *Curr. Opin. Cell Biol.*, vol. 35, pp. 69–77, Aug. 2015, doi: 10.1016/j.ceb.2015.04.013.

[43] M. Colombo, G. Raposo, and C. Théry, "Biogenesis, Secretion, and Intercellular Interactions of Exosomes and Other Extracellular Vesicles," *Annu. Rev. Cell Dev. Biol*, vol. 30, pp. 255–289, 2014, doi: 10.1146/annurev-cellbio-101512-122326.

[44] O. Østergaard, C. T. Nielsen, L. V. Iversen, S. Jacobsen, J. T. Tanassi, and N. H. H. Heegaard, "Quantitative proteome profiling of normal human circulating microparticles," *J. Proteome Res.*, vol. 11, no. 4, pp. 2154–2163, Apr. 2012, doi: 10.1021/PR200901P/SUPPL_FILE/PR200901P_SI_003.PDF.

[45] D. K. Jeppesen *et al.*, "Quantitative proteomics of fractionated membrane and lumen exosome proteins from isogenic metastatic and nonmetastatic bladder cancer cells reveal differential expression of EMT factors," *Proteomics*, vol. 14, no. 6, pp. 699–712, Mar. 2014, doi: 10.1002/PMIC.201300452.

[46] P. A. Gonzales *et al.*, "Large-scale proteomics and phosphoproteomics of urinary exosomes," *J. Am. Soc. Nephrol.*, vol. 20, no. 2, pp. 363–379, Feb. 2009, doi: 10.1681/ASN.2008040406.

[47] C. Escrevente, S. Keller, P. Altevogt, and J. Costa, "Interaction and uptake of exosomes by ovarian cancer cells," *BMC Cancer*, vol. 11, Mar. 2011, doi: 10.1186/1471-2407-11-108.

[48] D.-K. Kim *et al.*, "EVpedia: an integrated database of high-throughput data for systemic analyses of extracellular vesicles," 2013, doi: 10.3402/jev.v2i0.20384.

[49] C. Lässer, S. E. O'Neil, L. Ekerljung, K. Ekström, M. Sjöstrand, and J. Lötvall, "RNA-containing Exosomes in Human Nasal Secretions," *https://doi.org/10.2500/ajra.2011.25.3573*, vol. 25, no. 2, pp. 89–93, Mar. 2011, doi: 10.2500/AJRA.2011.25.3573.

[50] A. Poliakov, M. Spilman, T. Dokland, C. L. Amling, and J. A. Mobley, "Structural heterogeneity and protein composition of exosome-like vesicles (prostasomes) in human semen," *Prostate*, vol. 69, no. 2, pp. 159–167, Feb. 2009, doi: 10.1002/PROS.20860.

[51] M. P. Caby, D. Lankar, C. Vincendeau-Scherrer, G. Raposo, and C. Bonnerot, "Exosomal-like vesicles are present in human blood plasma," *Int. Immunol.*, vol. 17, no. 7, pp. 879–887, Jul. 2005, doi: 10.1093/INTIMM/DXH267.

[52] S. Keller, J. Ridinger, A. K. Rupp, J. W. G. Janssen, and P. Altevogt, "Body fluid derived exosomes as a novel template for clinical diagnostics," *J. Transl. Med.*, vol. 9, Jun. 2011, doi: 10.1186/1479-5876-9-86.

[53] C. Lässer, M. Eldh, and J. Lötvall, "Isolation and characterization of RNA-containing

exosomes," *J. Vis. Exp.*, no. 59, pp. 1–6, 2012, doi: 10.3791/3037.

[54] T. Pisitkun, R. F. Shen, and M. A. Knepper, "Identification and proteomic profiling of exosomes in human urine," *Proc. Natl. Acad. Sci. U. S. A.*, vol. 101, no. 36, p. 13368, Sep. 2004, doi: 10.1073/PNAS.0403453101.

[55] S. Perakis and M. R. Speicher, "Emerging concepts in liquid biopsies," *BMC Med.*, vol. 15, no. 1, Apr. 2017, doi: 10.1186/S12916-017-0840-6.

[56] N. Karimi *et al.*, "Detailed analysis of the plasma extracellular vesicle proteome after separation from lipoproteins," *Cell. Mol. Life Sci.*, vol. 75, no. 15, pp. 2873–2886, Aug. 2018, doi: 10.1007/S00018-018-2773-4/FIGURES/6.

[57] K. R. Feingold and C. Grunfeld, "Introduction to Lipids and Lipoproteins," *Endotext*, Jan. 2021, Accessed: Oct. 22, 2023. [Online]. Available: https://www.ncbi.nlm.nih.gov/books/NBK305896/

[58] B. W. Sódar *et al.*, "Low-density lipoprotein mimics blood plasma-derived exosomes and microvesicles during isolation and detection," *Sci. Rep.*, vol. 6, Apr. 2016, doi: 10.1038/SREP24316.

[59] Y. Yuana, J. Levels, A. Grootemaat, A. Sturk, and R. Nieuwland, "Co-isolation of extracellular vesicles and high-density lipoproteins using density gradient ultracentrifugation," *J. Extracell. Vesicles*, vol. 3, no. 1, 2014, doi: 10.3402/JEV.V3.23262.

[60] S. Biagiotti *et al.*, "Extracellular Vesicles as New Players in Drug Delivery: A Focus on Red Blood Cells-Derived EVs," *Pharmaceutics*, vol. 15, no. 2, Feb. 2023, doi: 10.3390/PHARMACEUTICS15020365.

[61] S. Gupta *et al.*, "An improvised one-step sucrose cushion ultracentrifugation method for exosome isolation from culture supernatants of mesenchymal stem cells," *Stem Cell Res. Ther.*, vol. 9, no. 1, Jul. 2018, doi: 10.1186/S13287-018-0923-0.

[62] Z. Onódi *et al.*, "Isolation of High-Purity Extracellular Vesicles by the Combination of Iodixanol Density Gradient Ultracentrifugation and Bind-Elute Chromatography From Blood Plasma," *Front. Physiol.*, vol. 9, no. OCT, Oct. 2018, doi: 10.3389/FPHYS.2018.01479.

[63] J. Shi *et al.*, "Engineered red blood cells as carriers for systemic delivery of a wide array of functional probes," *Proc. Natl. Acad. Sci. U. S. A.*, vol. 111, no. 28, pp. 10131–10136, Jul. 2014, doi: 10.1073/PNAS.1409861111.

[64] R. Sender, S. Fuchs, and R. Milo, "Revised Estimates for the Number of Human and Bacteria Cells in the Body," *PLoS Biol.*, vol. 14, no. 8, Aug. 2016, doi: 10.1371/JOURNAL.PBIO.1002533.

[65] T. C. Pham *et al.*, "Covalent conjugation of extracellular vesicles with peptides and nanobodies for targeted therapeutic delivery," *J. Extracell. Vesicles*, vol. 10, no. 4, Feb.

2021, doi: 10.1002/JEV2.12057.

[66] A. Wannez, B. Devalet, B. Chatelain, C. Chatelain, J. M. Dogné, and F. Mullier, "Extracellular Vesicles in Red Blood Cell Concentrates: An Overview," *Transfus. Med. Rev.*, vol. 33, no. 2, pp. 125–130, Apr. 2019, doi: 10.1016/J.TMRV.2019.02.002.

[67] C. D'Souza-Schorey Crislyn and J. W. Clancy, "Tumor-derived microvesicles: shedding light on novel microenvironment modulators and prospective cancer biomarkers," *Genes Dev.*, vol. 26, no. 12, pp. 1287–1299, Jun. 2012, doi: 10.1101/GAD.192351.112.

[68] D. Gulei, A. I. Irimie, R. Cojocneanu-Petric, J. L. Schultze, and I. Berindan-Neagoe, "Exosomes - Small Players, Big Sound," *Bioconjug. Chem.*, vol. 29, no. 3, pp. 635–648, Mar. 2018, doi: 10.1021/ACS.BIOCONJCHEM.8B00003.

[69] G. R. Monteith, N. Prevarskaya, and S. J. Roberts-Thomson, "The calcium–cancer signalling nexus," *Nat. Rev. Cancer 2017 176*, vol. 17, no. 6, pp. 373–380, Apr. 2017, doi: 10.1038/nrc.2017.18.

[70] L. Christ, E. M. Wenzel, K. Liestøl, C. Raiborg, C. Campsteijn, and H. Stenmark, "ALIX and ESCRT-I/II function as parallel ESCRT-III recruiters in cytokinetic abscission," *J. Cell Biol.*, vol. 212, no. 5, pp. 499–513, 2016, doi: 10.1083/JCB.201507009.

[71] L. Balaj *et al.*, "Tumour microvesicles contain retrotransposon elements and amplified oncogene sequences," *Nat. Commun. 2011 21*, vol. 2, no. 1, pp. 1–9, Feb. 2011, doi: 10.1038/ncomms1180.

[72] S. Crawford, D. Diamond, L. Brustolon, and R. Penarreta, "Effect of increased extracellular Ca++ on microvesicle production and tumor spheroid formation," *Cancer Microenviron.*, vol. 4, no. 1, pp. 93–103, Apr. 2011, doi: 10.1007/S12307-010-0049-0.

[73] F. L. A. Willekens, J. M. Werre, Y. A. M. Groenen-Döpp, B. Roerdinkholder-Stoelwinder, B. De Pauw, and G. J. C. G. M. Bosman, "Erythrocyte vesiculation: a self-protective mechanism?," *Br. J. Haematol.*, vol. 141, no. 4, pp. 549–556, May 2008, doi: 10.1111/J.1365-2141.2008.07055.X.

[74] W. Chiangjong, P. Netsirisawan, S. Hongeng, and S. Chutipongtanate, "Red Blood Cell Extracellular Vesicle-Based Drug Delivery: Challenges and Opportunities," *Front. Med.*, vol. 8, Dec. 2021, doi: 10.3389/FMED.2021.761362.

[75] M. Westerman and J. B. Porter, "Red blood cell-derived microparticles: An overview," *Blood Cells, Mol. Dis.*, vol. 59, pp. 134–139, Jul. 2016, doi: 10.1016/J.BCMD.2016.04.003.

[76] K. Thangaraju, S. N. Neerukonda, U. Katneni, and P. W. Buehler, "Extracellular Vesicles from Red Blood Cells and Their Evolving Roles in Health, Coagulopathy and Therapy," *Int. J. Mol. Sci.*, vol. 22, no. 1, pp. 1–25, Jan. 2020, doi: 10.3390/IJMS22010153.

[77] W. P. Kuo, J. C. Tigges, V. Toxavidis, and I. Ghiran, "Red Blood Cells: A Source of Extracellular Vesicles," *Methods Mol. Biol.*, vol. 1660, pp. 15–22, 2017, doi: 10.1007/978-1-4939-7253-1_2/COVER.

[78] D. X. Zhang, T. Kiomourtzis, C. K. Lam, and M. T. N. Le, "The Biology and Therapeutic Applications of Red Blood Cell Extracellular Vesicles," *Erythrocyte*, Oct. 2019, doi: 10.5772/INTECHOPEN.81758.

[79] A. Khalyfa and D. Sanz-Rubio, "The Mystery of Red Blood Cells Extracellular Vesicles in Sleep Apnea with Metabolic Dysfunction," *Int. J. Mol. Sci.*, vol. 22, no. 9, May 2021, doi: 10.3390/IJMS22094301.

[80] P. Burger, P. Hilarius-Stokman, D. De Korte, T. K. Van Den Berg, and R. Van Bruggen, "CD47 functions as a molecular switch for erythrocyte phagocytosis," *Blood*, vol. 119, no. 23, pp. 5512–5521, Jun. 2012, doi: 10.1182/BLOOD-2011-10-386805.

[81] M. Prudent, D. Crettaz, J. Delobel, J. Seghatchian, J. D. Tissot, and N. Lion, "Differences between calcium-stimulated and storage-induced erythrocyte-derived microvesicles," *Transfus. Apher. Sci.*, vol. 53, no. 2, pp. 153–158, Oct. 2015, doi: 10.1016/j.transci.2015.10.012.

[82] W. M. Usman *et al.*, "Efficient RNA drug delivery using red blood cell extracellular vesicles," *Nat. Commun. 2018 91*, vol. 9, no. 1, pp. 1–15, Jun. 2018, doi: 10.1038/s41467-018-04791-8.

[83] J. Sudnitsyna, E. Skverchinskaya, I. Dobrylko, E. Nikitina, S. Gambaryan, and I. Mindukshev, "Microvesicle Formation Induced by Oxidative Stress in Human Erythrocytes," *Antioxidants (Basel, Switzerland)*, vol. 9, no. 10, pp. 1–23, Oct. 2020, doi: 10.3390/ANTIOX9100929.

[84] M. Richter, P. Vader, and G. Fuhrmann, "Approaches to surface engineering of extracellular vesicles," *Adv. Drug Deliv. Rev.*, vol. 173, pp. 416–426, Jun. 2021, doi: 10.1016/J.ADDR.2021.03.020.

[85] S. Rayamajhi and S. Aryal, "Surface functionalization strategies of extracellular vesicles," *J. Mater. Chem. B*, vol. 8, no. 21, pp. 4552–4569, Jun. 2020, doi: 10.1039/D0TB00744G.

[86] K. Lang and J. W. Chin, "Bioorthogonal reactions for labeling proteins," *ACS Chem. Biol.*, vol. 9, no. 1, pp. 16–20, Jan. 2014, doi: 10.1021/CB4009292/ASSET/CB4009292.FP.PNG_V03.

[87] M. D. Best, "Click chemistry and bioorthogonal reactions: Unprecedented selectivity in the labeling of biological molecules," *Biochemistry*, vol. 48, no. 28, pp. 6571–6584, Jul. 2009, doi: 10.1021/BI9007726/ASSET/IMAGES/MEDIUM/BI-2009-007726_0001.GIF.

[88] C. D. Hein, X. M. Liu, and D. Wang, "Click Chemistry, A Powerful Tool for

Pharmaceutical Sciences," *Pharm. Res. 2008 2510*, vol. 25, no. 10, pp. 2216–2230, May 2008, doi: 10.1007/S11095-008-9616-1.

[89] L. Xu *et al.*, "Design of experiment (DoE)-driven in vitro and in vivo uptake studies of exosomes for pancreatic cancer delivery enabled by copper-free click chemistry-based labelling," *J. Extracell. Vesicles*, vol. 9, no. 1, p. 1779458, Sep. 2020, doi: 10.1080/20013078.2020.1779458.

[90] Y. Wang *et al.*, " Bone-Targeted Extracellular Vesicles from Mesenchymal Stem Cells for Osteoporosis Therapy ," *Int. J. Nanomedicine*, vol. 15, pp. 7967–7977, Oct. 2020, doi: 10.2147/IJN.S263756.

[91] T. Smyth *et al.*, "Surface functionalization of exosomes using click chemistry," *Bioconjug. Chem.*, vol. 25, no. 10, pp. 1777–1784, Oct. 2014, doi: 10.1021/BC500291R/SUPPL_FILE/BC500291R_SI_001.PDF.

[92] A. Musicò *et al.*, "Surface functionalization of extracellular vesicle nanoparticles with antibodies: a first study on the protein corona 'variable,'" *Nanoscale Adv.*, vol. 5, no. 18, pp. 4703–4717, Sep. 2023, doi: 10.1039/D3NA00280B.

[93] G. T. Lim *et al.*, "Bioorthogonally surface-edited extracellular vesicles based on metabolic glycoengineering for CD44-mediated targeting of inflammatory diseases," *J. Extracell. Vesicles*, vol. 10, no. 5, p. e12077, Mar. 2021, doi: 10.1002/JEV2.12077.

[94] S. Song *et al.*, "In Situ One-Step Fluorescence Labeling Strategy of Exosomes via Bioorthogonal Click Chemistry for Real-Time Exosome Tracking in Vitro and in Vivo," *Bioconjug. Chem.*, vol. 31, no. 5, pp. 1562–1574, May 2020, doi: 10.1021/ACS.BIOCONJCHEM.0C00216/SUPPL_FILE/BC0C00216_SI_001.PDF.

[95] X. Luan, K. Sansanaphongpricha, I. Myers, H. Chen, H. Yuan, and D. Sun, "Engineering exosomes as refined biological nanoplatforms for drug delivery," *Acta Pharmacol. Sin. 2017 386*, vol. 38, no. 6, pp. 754–763, Apr. 2017, doi: 10.1038/aps.2017.12.

[96] D. Sun *et al.*, "A Novel Nanoparticle Drug Delivery System: The Anti-inflammatory Activity of Curcumin Is Enhanced When Encapsulated in Exosomes," *Mol. Ther.*, vol. 18, no. 9, p. 1606, 2010, doi: 10.1038/MT.2010.105.

[97] M. J. Haney *et al.*, "Exosomes as drug delivery vehicles for Parkinson's disease therapy," *J. Control. Release*, vol. 207, pp. 18–30, Jun. 2015, doi: 10.1016/J.JCONREL.2015.03.033.

[98] I. Gaurav, A. Thakur, A. Iyaswamy, X. Wang, X. Chen, and Z. Yang, "Factors Affecting Extracellular Vesicles Based Drug Delivery Systems," *Molecules*, vol. 26, no. 6, 2021, doi: 10.3390/MOLECULES26061544.

[99] N. L. Klyachko, C. J. Arzt, S. M. Li, O. A. Gololobova, and E. V. Batrakova, "Extracellular Vesicle-Based Therapeutics: Preclinical and Clinical Investigations," *Pharm. 2020, Vol. 12, Page 1171*, vol. 12, no. 12, p. 1171, Dec. 2020, doi:

10.3390/PHARMACEUTICS12121171.

[100] M. J. Haney *et al.*, "Macrophage-Derived Extracellular Vesicles as Drug Delivery Systems for Triple Negative Breast Cancer (TNBC) Therapy.," *J. Neuroimmune Pharmacol.*, vol. 15, no. 3, pp. 487–500, Nov. 2019, doi: 10.1007/S11481-019-09884-9.

[101] M. S. Kim *et al.*, "Engineering macrophage-derived exosomes for targeted paclitaxel delivery to pulmonary metastases: in vitro and in vivo evaluations," *Nanomedicine Nanotechnology, Biol. Med.*, vol. 14, no. 1, pp. 195–204, Jan. 2018, doi: 10.1016/J.NANO.2017.09.011.

[102] G. Fuhrmann, A. Serio, M. Mazo, R. Nair, and M. M. Stevens, "Active loading into extracellular vesicles significantly improves the cellular uptake and photodynamic effect of porphyrins," *J. Control. Release*, vol. 205, pp. 35–44, May 2015, doi: 10.1016/J.JCONREL.2014.11.029.

[103] G. Chiabotto, E. Ceccotti, M. Tapparo, G. Camussi, and S. Bruno, "Human Liver Stem Cell-Derived Extracellular Vesicles Target Hepatic Stellate Cells and Attenuate Their Pro-fibrotic Phenotype," *Front. Cell Dev. Biol.*, vol. 9, Nov. 2021, doi: 10.3389/FCELL.2021.777462.

[104] P. Lingasamy *et al.*, "Bi-specific tenascin-C and fibronectin targeted peptide for solid tumor delivery," *Biomaterials*, vol. 219, p. 119373, Oct. 2019, doi: 10.1016/J.BIOMATERIALS.2019.119373.

[105] S. Bruno *et al.*, "HLSC-Derived Extracellular Vesicles Attenuate Liver Fibrosis and Inflammation in a Murine Model of Non-alcoholic Steatohepatitis," *Mol. Ther.*, vol. 28, no. 2, pp. 479–489, Feb. 2020, doi: 10.1016/J.YMTHE.2019.10.016.

[106] M. Tapparo *et al.*, "Renal Regenerative Potential of Extracellular Vesicles Derived from miRNA-Engineered Mesenchymal Stromal Cells," *Int. J. Mol. Sci. 2019, Vol. 20, Page 2381*, vol. 20, no. 10, p. 2381, May 2019, doi: 10.3390/IJMS20102381.

[107] N. R. Ayat *et al.*, "Optimization of ZD2 Peptide Targeted Gd(HP-DO3A) for Detection and Risk-Stratification of Prostate Cancer with MRI," *ACS Med. Chem. Lett.*, vol. 9, no. 7, pp. 730–735, Jul. 2018, doi: 10.1021/ACSMEDCHEMLETT.8B00172/SUPPL_FILE/ML8B00172_SI_001.PDF.

[108] Z. Han *et al.*, "Extradomain-B fibronectin-targeted dextran-based chemical exchange saturation transfer magnetic resonance imaging probe for detecting pancreatic cancer," *Bioconjug. Chem.*, vol. 30, no. 5, pp. 1425–1433, May 2019, doi: 10.1021/ACS.BIOCONJCHEM.9B00161/SUPPL_FILE/BC9B00161_SI_001.PDF.

[109] X. X. Ye *et al.*, "EDB Fibronectin-Specific SPECT Probe 99mTc-HYNIC-ZD2 for Breast Cancer Detection," *ACS Omega*, vol. 2, no. 6, pp. 2459–2468, Jun. 2017, doi: 10.1021/ACSOMEGA.7B00226/ASSET/IMAGES/LARGE/AO-2017-00226H_0002.JPEG.

[110] Y. Li *et al.*, "Synthesis and Assessment of Peptide Gd-DOTA Conjugates Targeting Extradomain B Fibronectin for Magnetic Resonance Molecular Imaging of Prostate Cancer," *Mol. Pharm.*, vol. 14, no. 11, pp. 3906–3915, Nov. 2017, doi: 10.1021/ACS.MOLPHARMACEUT.7B00619/SUPPL_FILE/MP7B00619_SI_001.PDF .

[111] Y. Li *et al.*, "Evaluation of Physicochemical Properties, Pharmacokinetics, Biodistribution, Toxicity, and Contrast-Enhanced Cancer MRI of a Cancer-Targeting Contrast Agent, MT218," *Invest. Radiol.*, vol. 57, no. 10, pp. 639–654, Oct. 2022, doi: 10.1097/RLI.0000000000000881.

[112] Z. Han *et al.*, "Targeted Contrast Agent Specific to an Oncoprotein in Tumor Microenvironment with the Potential for Detection and Risk Stratification of Prostate Cancer with MRI," *Bioconjug. Chem.*, vol. 28, no. 4, pp. 1031–1040, Apr. 2017, doi: 10.1021/ACS.BIOCONJCHEM.6B00719/ASSET/IMAGES/MEDIUM/BC-2016-00719M_0008.GIF.

[113] Z. Han *et al.*, "EDB fibronectin specific peptide for prostate cancer targeting," *Bioconjug. Chem.*, vol. 26, no. 5, pp. 830–838, May 2015, doi: 10.1021/ACS.BIOCONJCHEM.5B00178/ASSET/IMAGES/MEDIUM/BC-2015-00178P_0009.GIF.

[114] T. K. Eigentler *et al.*, "A dose-escalation and signal-generating study of the immunocytokine L19-IL2 in combination with dacarbazine for the therapy of patients with metastatic melanoma," *Clin. Cancer Res.*, vol. 17, no. 24, pp. 7732–7742, Dec. 2011, doi: 10.1158/1078-0432.CCR-11-1203/84447/AM/A-DOSE-ESCALATION-AND-SIGNAL-GENERATING-STUDY-OF.

[115] B. Weide *et al.*, "Intralesional treatment of stage III metastatic melanoma patients with L19-IL2 results in sustained clinical and systemic immunologic responses," *Cancer Immunol. Res.*, vol. 2, no. 7, pp. 668–678, Jul. 2014, doi: 10.1158/2326-6066.CIR-13-0206/466982/AM/INTRALESIONAL-TREATMENT-OF-STAGE-III-METASTATIC.

[116] K. Wagner, P. Schulz, A. Scholz, B. Wiedenmann, and A. Menrad, "The Targeted Immunocytokine L19-IL2 Efficiently Inhibits the Growth of Orthotopic Pancreatic Cancer," *Clin. Cancer Res.*, vol. 14, no. 15, pp. 4951–4960, Aug. 2008, doi: 10.1158/1078-0432.CCR-08-0157.

[117] C. Schliemann *et al.*, "Complete eradication of human B-cell lymphoma xenografts using rituximab in combination with the immunocytokine L19-IL2," *Blood*, vol. 113, no. 10, pp. 2275–2283, Mar. 2009, doi: 10.1182/BLOOD-2008-05-160747.

[118] C. Zahnd *et al.*, "Efficient tumor targeting with high-affinity designed ankyrin repeat proteins: Effects of affinity and molecular size," *Cancer Res.*, vol. 70, no. 4, pp. 1595–1605, Feb. 2010, doi: 10.1158/0008-5472.CAN-09-2724.

[119] Z. Han and Z. R. Lu, “Targeting fibronectin for cancer imaging and therapy,” *J. Mater. Chem. B*, vol. 5, no. 4, pp. 639–654, 2017, doi: 10.1039/C6TB02008A.

[120] M. Holcar *et al.*, “Enrichment of plasma extracellular vesicles for reliable quantification of their size and concentration for biomarker discovery,” *Sci. Reports 2020 101*, vol. 10, no. 1, pp. 1–13, Dec. 2020, doi: 10.1038/s41598-020-78422-y.

[121] S. Valkonen *et al.*, “Biological reference materials for extracellular vesicle studies,” *Eur. J. Pharm. Sci.*, vol. 98, pp. 4–16, Feb. 2017, doi: 10.1016/J.EJPS.2016.09.008.

[122] R. Skovronova, C. Grange, V. Dimuccio, M. C. Deregibus, G. Camussi, and B. Bussolati, “Surface marker expression in small and medium/large mesenchymal stromal cell-derived extracellular vesicles in naive or apoptotic condition using orthogonal techniques,” *Cells*, vol. 10, no. 11, p. 2948, Nov. 2021, doi: 10.3390/CELLS10112948/S1.

[123] P. Lingasamy *et al.*, “Bi-specific tenascin-C and fibronectin targeted peptide for solid tumor delivery,” 2019, doi: 10.1016/j.biomaterials.2019.119373.

[124] B. Cardinali *et al.*, “Trastuzumab quantification in serum: a new, rapid, robust ELISA assay based on a mimetic peptide that specifically recognizes trastuzumab,” *Anal. Bioanal. Chem.*, vol. 406, no. 18, pp. 4557–4561, 2014, doi: 10.1007/S00216-014-7842-4.

[125] G. Sociali *et al.*, “Differential modulation of SIRT6 deacetylase and deacylase activities by lysine-based small molecules,” *Mol. Divers.*, vol. 24, no. 3, pp. 655–671, Aug. 2020, doi: 10.1007/S11030-019-09971-2.

[126] C. Gorgun, D. Reverberi, G. Rotta, F. Villa, R. Quarto, and R. Tasso, “Isolation and Flow Cytometry Characterization of Extracellular-Vesicle Subpopulations Derived from Human Mesenchymal Stromal Cells,” *Curr. Protoc. Stem Cell Biol.*, vol. 48, no. 1, p. e76, Feb. 2019, doi: 10.1002/CPSC.76.

[127] S. Salarpour, H. Forootanfar, M. Pournamdari, M. Ahmadi-Zeidabadi, M. Esmaeeli, and A. Pardakhty, “Paclitaxel incorporated exosomes derived from glioblastoma cells: comparative study of two loading techniques,” *Daru*, vol. 27, no. 2, pp. 533–539, Dec. 2019, doi: 10.1007/S40199-019-00280-5.

[128] L. M. Doyle and M. Z. Wang, “Overview of extracellular vesicles, their origin, composition, purpose, and methods for exosome isolation and analysis,” *Cells*, vol. 8, no. 7, Jul. 2019, doi: 10.3390/CELLS8070727.

[129] S. Walker *et al.*, “Extracellular vesicle-based drug delivery systems for cancer treatment,” *Theranostics*, vol. 9, no. 26, pp. 8001–8017, Oct. 2019, doi: 10.7150/THNO.37097.

[130] “Comprehensive Biotechnology - 2nd Edition.” https://shop.elsevier.com/books/comprehensive-biotechnology/moo-young/978-0-444-

53352-4 (accessed May 31, 2023).

[131] X. Zhu *et al.*, "Comprehensive toxicity and immunogenicity studies reveal minimal effects in mice following sustained dosing of extracellular vesicles derived from HEK293T cells," *J. Extracell. Vesicles*, vol. 6, no. 1, p. 1324730, Dec. 2017, doi: 10.1080/20013078.2017.1324730.

[132] S. A. A. Kooijmans, R. M. Schiffelers, N. Zarovni, and R. Vago, "Modulation of tissue tropism and biological activity of exosomes and other extracellular vesicles: New nanotools for cancer treatment," *Pharmacol. Res.*, vol. 111, pp. 487–500, Sep. 2016, doi: 10.1016/J.PHRS.2016.07.006.

[133] M. Tsamchoe, S. Petrillo, A. Lazaris, and P. Metrakos, "Isolation of extracellular vesicles from human plasma samples: The importance of controls," *Biotechnol. J.*, vol. 18, no. 6, p. 2200575, Jun. 2023, doi: 10.1002/BIOT.202200575.

[134] S. Reymond, L. Gruaz, and J. C. Sanchez, "Depletion of abundant plasma proteins for extracellular vesicle proteome characterization: benefits and pitfalls," *Anal. Bioanal. Chem.*, vol. 415, no. 16, pp. 3177–3187, Jul. 2023, doi: 10.1007/S00216-023-04684-W/FIGURES/6.

[135] J. C. Jewett and C. R. Bertozzi, "Cu-free click cycloaddition reactions in chemical biology," *Chem. Soc. Rev.*, vol. 39, no. 4, pp. 1272–1279, Mar. 2010, doi: 10.1039/B901970G.

[136] C. G. Gordon, J. L. MacKey, J. C. Jewett, E. M. Sletten, K. N. Houk, and C. R. Bertozzi, "Reactivity of biarylazacyclooctynones in copper-free click chemistry," *J. Am. Chem. Soc.*, vol. 134, no. 22, pp. 9199–9208, Jun. 2012, doi: 10.1021/JA3000936/SUPPL_FILE/JA3000936_SI_005.CIF.

[137] A. Bernardin *et al.*, "Copper-Free Click Chemistry for Highly Luminescent Quantum Dot Conjugates: Application to in Vivo Metabolic Imaging," *Bioconjug. Chem.*, vol. 21, no. 4, pp. 583–588, Apr. 2010, doi: 10.1021/BC900564W.

[138] R. E. Bird, S. A. Lemmel, X. Yu, and Q. A. Zhou, "Bioorthogonal Chemistry and Its Applications," *Bioconjug. Chem.*, vol. 32, no. 12, pp. 2457–2479, Dec. 2021, doi: 10.1021/ACS.BIOCONJCHEM.1C00461/ASSET/IMAGES/LARGE/BC1C00461_0012.JPEG.

[139] E. Bonsergent, E. Grisard, J. Buchrieser, O. Schwartz, C. Théry, and G. Lavieu, "Quantitative characterization of extracellular vesicle uptake and content delivery within mammalian cells", doi: 10.1038/s41467-021-22126-y.

[140] M. Heidarzadeh, A. Zarebkohan, R. Rahbarghazi, and E. Sokullu, "Protein corona and exosomes: new challenges and prospects," *Cell Commun. Signal. 2023 211*, vol. 21, no. 1, pp. 1–15, Mar. 2023, doi: 10.1186/S12964-023-01089-1.

[141] P. Lingasamy *et al.*, "Pl1 peptide engages acidic surfaces on tumor-associated

fibronectin and tenascin isoforms to trigger cellular uptake," *Pharmaceutics*, vol. 13, no. 12, p. 1998, Dec. 2021, doi: 10.3390/PHARMACEUTICS13121998/S1.

[142] S. Salarpour, H. Forootanfar, M. Pournamdari, M. Ahmadi-Zeidabadi, M. Esmaeeli, and A. Pardakhty, "Paclitaxel incorporated exosomes derived from glioblastoma cells: comparative study of two loading techniques," *DARU, J. Pharm. Sci.*, vol. 27, no. 2, pp. 533–539, Dec. 2019, doi: 10.1007/S40199-019-00280-5.

ACKNOWLEDGMENTS

I would like to express my deepest gratitude to my supervisor, Roberta, for leading me with kindness and patience passing me her knowledge and passion for the research.
I am also grateful to Prof. Rodolfo Quarto for welcoming me to the U.O. of "Oncologia Cellulare" and for his precious feedback and suggestions.
A special thanks to Daniele Reverberi, whose collaboration and total availability have been essential during the early phases of this project, and Silvia Bruno who kindly spent time helping me to approach for the first time to the fluorescent microscopy analysis.
I owe a lot to Cansu Gorgun for her willingness, contribution, and expertise which enriched the quality of my work.
Finally, I would like to express thanksgiving to Saara Laitinen and her team, Ulla, Petra, Reetta, Kai, and Juha for welcoming me with enthusiasm, supporting me, and dedicating their time for helping me to progress in this project during the time I spent in their Lab at the Finnish Red Cross (Helsinki).